THREE DIMENSIONAL FRACTURE ANALYSIS
OF
FILLET WELDS

A THESIS SUBMITTED TO
THE GRADUATE SCHOOL OF NATURAL AND APPLIED SCIENCES
OF
MIDDLE EAST TECHNICAL UNIVERSITY

BY

FERHAN FIÇICI

IN PARTIAL FULFILLMENT OF THE REQUIREMENTS
FOR
THE DEGREE OF MASTER OF SCIENCE
IN
MECHANICAL ENGINEERING

MAY 2007

Approval of the Graduate School of Natural and Applied Sciences

_____

Prof. Dr. Canan ÖZGEN
Director

I certify that this thesis satisfies all the requirements as a thesis for the degree of Master of Science

_____

Prof. Dr. Kemal İDER
Head of Department

This is to certify that we have read this thesis and that in our opinion it is fully adequate, in scope and quality, as a thesis for the degree of Master of Science

_____

Asst. Prof. Dr. Serkan DAĞ
Supervisor

Examining Committee Members

Prof. Dr. Eres SÖYLEMEZ (METU, ME) _____

Asst. Prof. Dr. Serkan DAĞ (METU, ME) _____

Assoc. Prof. Dr. Suat KADIOĞLU (METU, ME) _____

Prof. Dr. Mehmet ÇALIŞKAN (METU, ME) _____

Kadir GENİŞ (M.S.) (HİDROMEK LTD) _____

I hereby declare that all information in this document has been obtained and presented in accordance with academic rules and ethical conduct. I also declare that, as required by these rules and conduct, I have fully cited and referenced all material and results that are not original to this work.

Name, Last name: Ferhan FIÇICI

Signature :

ABSTRACT

THREE DIMENSIONAL FRACTURE ANALYSIS OF FILLET WELDS

FIÇICI, Ferhan

M.S, Department of Mechanical Engineering

Supervisor: Asst. Prof. Dr. Serkan DAĞ

May 2007, 124 pages

The aim of this study is to model three dimensional surface crack problems in fillet welds. It is assumed that weld material has the same material properties with the sheet metals. The surface crack is considered to occur at two regions; one at the weld root and the other at the weld toe. The surface crack is assumed to have a semi – elliptical crack front profile. The surface crack problem is analyzed under mechanical loading and the models are built up by three dimensional finite elements. Around the crack front, strain singularity is taken into account by using degenerated 20 – node quarter – point solid elements. The main results of this work are the stress intensity factors around the crack front for the test specimen model subjected to axial and bending loads.

Keywords: Stress intensity factors, displacement correlation technique, semi – elliptical surface crack, mixed mode, parametric modeling

ÖZ

KÖŞE KAYNAKLARININ ÜÇ BOYUTLU KIRILMA ANALİZİ

FIÇICI, Ferhan

Yüksek Lisans, Makine Mühendisliği Bölümü

Tez Yöneticisi: Y. Doç. Dr. Serkan DAĞ

Mayıs 2007, 124 sayfa

Bu çalışmanın amacı, köşe kaynaklarında üç boyutlu yüzey çatlak problemlerinin modellenmesidir. Kaynak malzemesinin, sac metaller ile aynı malzeme özelliklerine sahip olduğu varsayılmıştır. Yüzey çatlağının iki bölgede olduğu düşünülmüştür; biri kaynak kökündedir, diğeri kaynak ucundadır. Yüzey çatlağının yarı eliptik çatlak yüzü görüntüsüne sahip olduğu varsayılmıştır. Yüzey çatlağı problemi, mekanik yükleme altında incelenmiştir ve modeller üç boyutlu sonlu elemanlar ile oluşturulmuştur. Çatlak yüzü çevresinde, bozulmuş 20 düğümlü çeyrek noktalı katı elemanlar kullanılarak gerinim tekilliği hesaba katılmıştır. Bu çalışmanın temel sonuçları, çekmeye ve eğmeye maruz kalmış test numunesi için çatlak yüzü çevresinde gerilme şiddeti faktörleridir.

Anahtar kelimeler: Gerilme şiddeti faktörleri, yer değiştirme ilgileşim teknikleri, yarı eliptik yüzey çatlağı, karışık usul, parametrik modelleme

To My Whole Family

ACKNOWLEDGMENTS

The author expresses sincere appreciation to Asst Prof. Dr. Serkan DAĞ for his guidance, advice, criticism, systematic supervision, encouragement, and insight throughout the study.

The author sends his special thanks to Mr. Cevdet Can UZER, Mr. Taner KARAGÖZ and Mr. Erkal ÖZBAYRAMOĞLU for their technical assistance and spiritual support throughout the study.

The author appreciates the continuous morale support from his friends Mr. Alper YALÇINKAYA, Mr. Ayhun ÜNAL, and Mr. Murat SOYSAL. The author is also regardful to Mr. Recep Kaya GÖKTAŞ and Mr. Mehmet Çağatay TARHAN for spiritual supports from abroad.

The author offers very special thanks to his sweetheart for encouragements and spiritual support during the study.

And lastly, the author extends his special thanks to his parents, Aynur and Mehmet FIÇICI and his brother Erhan FIÇICI, for their encouragement and faith in him.

TABLE OF CONTENTS

LIST OF TABLES

TABLES

LIST OF FIGURES

FIGURES

NOMENCLATURE

K	: Stress Intensity Factor
Y	: Geometrical Parameter
K_{IC}	: The Critical Mode I Stress Intensity Factor
K_I	: Mode I Stress Intensity Factor
r	: Distance from the Crack Tip
σ_{ij}	: The Components of the Stresses
θ	: Angle from the Crack Plane
u	: Displacement Component in x-direction
v	: Displacement Component in y-direction
μ	: Shear Modulus
κ	: Shear Parameter
ν	: Poisson's Ratio
E	: Young's Modulus
a	: Radius of the Circular Crack Length
K_{II}	: Mode II Stress Intensity Factor
K_{III}	: Mode III Stress Intensity Factor
w	: Displacement Component in z-direction
s	: Arc Length of the Crack Front
t	: Tangential Direction on the Crack Front
n	: Normal Direction on the Crack Front
b	: Binormal Direction on the Crack Front
σ_{bb}	: Normal Stress Component on the Crack Front
u_{bb}	: Normal Displacement Component on the Crack Front
G	: Energy Release Rate
$t1$	: Thickness of the Base Sheet Metal

t2	: Thickness of the Upper Sheet Metal
B	: Width of the Specimen
Ψ	: Angle of the crack with respect to base sheet metal
a	: Depth of Crack in the finite elements model
c	: Length of Crack in the Finite Elements Model
K_v	: Vertical Leg of the Fillet Weld
K_h	: Horizontal Leg of the Fillet Weld
U_i	: Displacement Component in i-direction
f	: Non-dimensional value of Stress Intensity Factor
E (Φ)	: Elliptical Integral
Φ, β	: Parametric Angle
$\frac{K_I}{K_O}$	: Normalized Mode I Stress Intensity Factor
$\frac{K_{II}}{K_O}$	: Normalized Mode II Stress Intensity Factor
$\frac{K_{III}}{K_O}$	: Normalized Mode III Stress Intensity Factor
$\frac{G_I}{G_O}$	: Normalized Energy Release rate

CHAPTER 1

INTRODUCTION

1.1 Introduction

Earth-moving machines are heavy-duty vehicles used for engineering applications such as construction tasks, mining, trenching, moving large amount of bulk materials – sand, earth, and stone – and road construction. Backhoe loaders, bulldozers, cranes, drilling machines, excavators, graders and telehandlers are the main types of the earth-moving machines. Each of these machines is working in rough conditions and all of the earth-moving machines are faced with the enormous loadings during their applications. These loadings can cause harmful malfunctions to the structures of the machines.

Backhoe loader is the most common earth-moving machine which consists of a tractor, front shovel/bucket and small backhoe in the rear (figure 1.1). Due to its small size, compared to the other machines, the backhoe loaders have widespread use in life. As the name implies, it has a loader assembly on the front and a backhoe on the back, and with these two mechanisms, backhoe-loaders are very common and can be used for a wide variety of tasks: construction, small demolitions, light transportation of building materials, powering building equipment, digging holes/excavating, breaking asphalt, and paving roads. The movements of the mechanisms are satisfied by means of hydraulic cylinders.

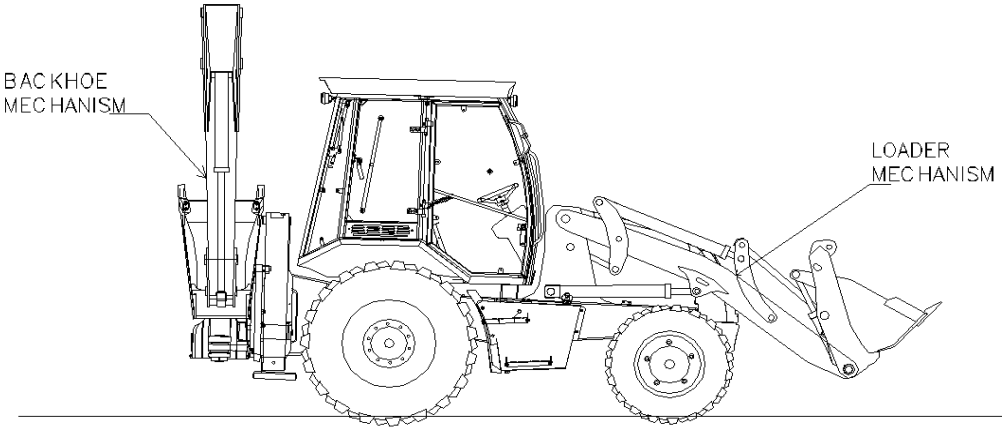

Figure 1.1 General View of a backhoe loader

Excavator, which is also called a 360-degree excavator or digger, is one of the earth-moving machines consisting of a backhoe and cab mounted on a pivot (a rotating platform). It is a mobile machine that is moved by means of either crawler track or rubber-tired undercarriage [1] (figure 1.2). Owing to these specifications, excavator has a wide working range. As a result of the structure, it is commonly used for digging applications, compared to elevating and carrying. Its digging mechanism is composed of boom, arm, bucket/shovel and the hydraulic cylinders, and the movements of these machines are carried by these hydraulic components.

Both excavators' and backhoe loaders' attachments are manufactured by means of mostly welding operations. With respect to their weights and structural constructions, excavators and backhoe loaders are working in severe working conditions. As a result of the working conditions, some defects can occur at the welding areas or very close regions to them. Also, at the end of the welding process, an initial defect can be formed inside the weld material. Fatigue life of the attachments is determinative for the disposal time of the earth-moving machineries. Therefore, it can be easily understood that weld regions are very important for fatigue life of the structure and the

manufacture and the design processes must be performed considering these points.

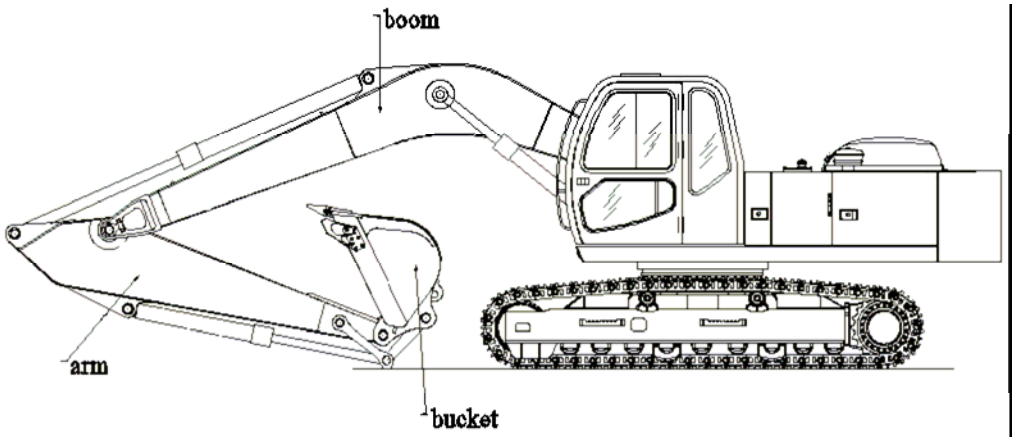

Figure 1.2 General View of an excavator

In the previous studies, the effects of the defects were examined by empirical approaches and numerical approaches for possible defect regions near the weld areas. The empirical work was performed for the relevant standards, such as BS7910, BS7608, BS5400, by the methods, four-point-bending test and three-point-bending test. In these studies, T-welded joints, butt-weld joints were used [2] [3] [4] [5]. In these work, fatigue life predictions were made by using the 'Paris-Erdoğan equation' according to the tests results.

Moreover, stress intensity factor calculations for modes I, II and III were made by placing different crack shape into finite element models and boundary element models, generated with various software, in different studies [6] [7] [8]. In these studies, 3-D models were created, axi-symmetric

boundary conditions were defined and the stress intensity factors were calculated by means of various techniques.

In the present study, three-dimensional surface crack problem in a welded joint is examined using a three dimensional finite element technique. As software, MSC.Mentat-Marc is used. The crack problem is analyzed when the mechanical loading is applied to a T-weld shaped specimen. Full model of the specimen is generated and the crack is placed inside the model. The stress intensity factors for modes I, II and III loading are calculated by means of displacement correlation technique.

1.2 Literature Survey

The aim of this study is to model the three dimensional semi-elliptical surface crack for a construction with fillet weld and to calculate the modes I, II and III stress intensity factors around the crack front under mechanical loading by using the finite element method (FEM). This construction is called as a T-weld joint. Three-dimensional crack problems are examined by various scientists in the past. Scientists have made important amount of progressions about the three-dimensional crack problems since 1950's [9]. The present work contributes in the sense that fracture mechanics analyses are conducted by creating full three dimensional models of T – weld joints.

In the study by Gray et al. [11] (2002), the stress intensity factors for different types of crack fronts were found by means of the displacement correlation technique in order to examine the effects of quarter-point elements. Calculations were made for two dimensional models. It is shown that as the number of the crack front elements increases, more accurate results can be obtained. Element number between 10 and 20 is enough to have correct results. Furthermore, the quarter-point elements make the calculations exact compared to the standard elements.

In the paper by Hou et al. [12] in 2001, the finite element method and crack growth laws in fracture mechanics were combined. The main approach was that the stress intensity factors for general three-dimensional cracks were calculated by means of the finite element method and the crack growth behavior was observed by using the crack growth principles in 3-D cases. In order to satisfy the stress and strain singularity at a crack front, collapsed brick elements with 20 nodes mid-side nodes at the quarter points were used. Firstly, three-dimensional model was formed and then a crack front was placed to this model in desired shape (semi-circular, semi-elliptical or longitudinal) and based on this model, the stress intensity factor could be calculated at each node along the crack front using *J*-integral method.

In other paper published by Guo et al. [13] (2006), the stress intensity factor for a crack, which was placed at the weld toe of T-plate, was examined by means of the weight function together with the stress distribution on the crack plane. The validity of the weight function was examined by comparison to the numerical data obtained by the finite element method. The loading condition was pure tensile and the mode I stress intensity factor was calculated by *J*-integral. The results showed that the stress intensity factor for a cracked padded plate can be obtained using the weight function of a T-plate together with the actual stress distribution on the crack plane.

In another paper by Kuok et al. [14], three-dimensional finite element method was used to investigate the stress intensity factors of a semi-elliptical surface crack in a plate with finite thickness. The nodal displacement method was chosen to calculate the stress intensity factor. To maintain the singularity at the crack front, 20 nodes collapsed brick elements were placed and because of the symmetry condition, only the quarter of the plate was modeled. It is shown that as the crack depth is increased, *J*-integral gives more accurate results compared to the nodal displacement method.

In the paper by Muktepavel et al. [16], the fatigue test was applied to T-weld joints from steel weldox 420 by means of four-point-bending test method. Various types of weld treatments, such as shot-peening, etc, were used in order to avoid defects occurring during tests. For all types of treatment, a crack was formed at the crack toe of the specimen.

Fatigue tests were conducted for fillet weld regions of two stainless steel grades: ferritic – martensitic EN1.4003 and austenitic EN1.4310 by means of three-point-bending method in the study by Lathi et al. [17] (2000). The test results were shown a good agreement with suggested fatigue classes in the Eurocode3 design standard. Nevertheless, if the size of the fillet weld was increased, the failure location was moved to the weld toe instead of weld root. According to the Eurpcode3, crack formation has a tendency of occurring at the weld root.

In the paper by Fricke et al. [18] in 2005, the locations of the crack at fillet welds due to mechanical loading were mentioned. According to the test results, two different types of fatigue cracks are possible, starting from the weld toe and from the non – welded root gap. Even though the crack initiation site is dependent on the weld throat thickness and the axial misalignments, the common weld crack initiation region is the weld toe region, where the hot – spot stress occurs. A crack can be initiated if a non – welded root gap formed during welding process.

In the research by Jia et al. [20], three dimensional static and dynamic stress intensity factor computations using ANSYS was searched. As it was mentioned, element formation at the crack tip for various crack problems was easily applicable with the capability of automatic meshing. The singularity of stresses near the crack tip was satisfied by the quarter – point elements giving the possibility of computing the stress intensity factors near the crack tip for three – dimensional crack problems. In this study, it was finally stated

that stress intensity factor calculations using the displacement correlation technique gave precise and reliable results.

Inan (2004) [10] considered the three – dimensional surface cracking problem in functionally graded material (FGM) coatings bonded to homogeneous substrates by using three – dimensional finite element modeling. In this work, it was assumed that the surface crack front had a semi – circular profile. As loading cases, both mechanical and transient thermal loading types were considered. During the finite element analyses, the strain singularities were ensured by using 20 nodes quarter – point wedge elements at the crack front. Mode I stress intensity factor was derived by three – dimensional displacement correlation technique. For analyzing the accuracy of the stress intensity factor derivations, comparisons were made between calculated stress intensity factors and the stress intensity factors given by Newman and Raju [21] for different crack problems under various types of loadings. As a result of his study, the difference between these two groups of stress intensity factor calculations was smaller than 5%. This results show that calculations of mode I stress intensity factor by means of displacement correlation technique using finite element analysis was sufficiently accurate.

In the thesis study of Sabuncuoglu [22], fatigue crack growth analysis was performed for functionally graded materials (FGM's) by using finite element analysis method. A parametric modeling code for test specimen given in ASTM E399 was prepared for mode I stress intensity factor calculations by using ANSYS software. All the parametric modeling stages were carried out by APDL codes [22]. Because of the symmetrical properties of the crack, it was formed as one forth of the model, and 20 nodes brick elements were used in order to satisfy the strain singularity at the crack front. As a control point, a sample model was formed and after the analysis, results coming from displacement correlation technique calculations were compared to the values from the studies Kadioglu et al. [23] and Guo et al. [24]. As can be

seen from this work, displacement correlation technique is a reliable approach for finding out stress intensity factors in three – dimensional analysis.

1.3 Scope of the Study

The purpose of this study is to model semi – elliptical and quarter – elliptical surface cracks in a test specimen. The specimen, whose material is *st37*, is declared in the standard ISO/DIS 14345 [25]. The specimen is examined by considering axial and bending types of loading. All parts of the model including the semi-elliptical and quarter-elliptical with respect to the crack location surface crack are generated in the finite element software MSC.MENTAT – MARC [26] and the crack profile can be placed at the weld toe or at the weld root depending on the user's choice. Its profile is semi elliptic when the crack is inside the thickness of the specimen. When the crack is located at edge of the structure, crack profile is in the shape of quarter elliptic. In this study, 20 node quarter-point collapsed brick elements- called as wedge elements- are used in order to maintain the strain singularity along the crack front profile. Displacement correlation technique is derived for computing modes I, II and III stress intensity factors under mechanical loading. The main goal is to prepare a parametric model with user interface which makes all of the stages – including modeling the specimen, placing the crack, loading, post-processing and computing the mixed-mode stress intensity factors – automatically. In order to check out the accuracy of the calculations and the software MSC.MENTAT – MARC, a sample model is generated with an embedded circular crack front (penny-shaped crack geometry) under tension load. The results of calculated mode I stress intensity factor are compared to the values, which are found according to the equation extracted from Sneddon's solution [27]. Also, a comparison is performed for mixed-mode stress intensity factor with the study of Noda et al. [37]

This thesis is composed of five chapters. In this chapter, the introduction, the literature survey and the scope of the study are stated. Theory of fracture mechanics and three dimensional fracture analyses are mentioned in chapter 2. The problem description is stated in chapter 3. In chapter 4, the finite element modeling and the displacement correlation technique for mode I, mode II and mode III stress intensity factors are given full details. All of the results and the comparisons are given in chapter 5. Finally, discussions and conclusions are presented in chapter 6.

CHAPTER 2

THEORY OF FRACTURE MECHANICS

2.1 Introduction

In modern materials science, fracture mechanics is an important tool in improving the mechanical performance of materials and components. It applies the physics of stress and strain, in particular the theories of elasticity and plasticity, to the microscopic crystallographic defects found in real materials in order to predict the macroscopic mechanical failure of bodies. Fracture mechanics is a method for predicting failure of a structure containing crack. It uses methods of analytical solid mechanics in order to calculate the driving force on a crack and those of experimental solid mechanics in order to characterize the material's resistance to failure. Fracture mechanics is based on the principle that all materials contain initial defects in the form of cracks or voids which can affect the load carrying capacity of engineering structures. Propagation of the cracks under repeated loading can be studied in fracture mechanics by two approaches:

- Stress Analysis (Focusing the stress fields in crack region; Stress Intensity Factor)

- Energy Balance (Energy Release Rate)

2.2 Three Dimensional Fracture Analysis

Stress Intensity Factor, *K*, is used in fracture mechanics to more accurately predict the stress state ("stress intensity") near the tip of a crack caused by a remote load or residual stresses. When this stress state becomes critical a small crack grows ("extends") and the material fails. The load at which this failure occurs is referred to as the fracture strength. The experimental fracture strength of solid materials is 10 to 1000 times below the theoretical strength values, where tiny internal and external surface cracks create higher stresses near, hence lowering the theoretical value of strength. Stress intensity factor is a measure of the strength of the singular fields at the crack tip under different loading modes. Unlike "stress concentration", Stress Intensity, *K*, as the name implies, is a parameter that governs the magnitude of the applied stress that includes the geometrical parameter *Y* (load type). These load types are categorized as Mode I, II, or III. The critical Mode I stress intensity factor, K_{IC} is the most often used engineering design parameter in fracture mechanics and hence must be understood if we are to design fracture tolerant materials used in bridges, buildings, aircraft, or even bells. Polishing just will not do if we detect a crack. Typically for most materials if a crack can be seen it is very close to the critical stress state predicted by the "Stress Intensity Factor" [33].

2.2.1 Modes of Loading

There are three possible modes of crack extension in linear elastic fracture mechanics; the opening mode, sliding mode, and tearing mode.

- Mode I: The opening mode is defined by the symmetric separation of the crack surfaces with respect to the plane, prior to extension.

- Mode II: The sliding mode is defined by displacements in which the crack surfaces slide over one another perpendicular to the leading edge of the crack.

- Mode III: The tearing mode finds the crack surfaces sliding with respect to one another parallel to the leading edge.

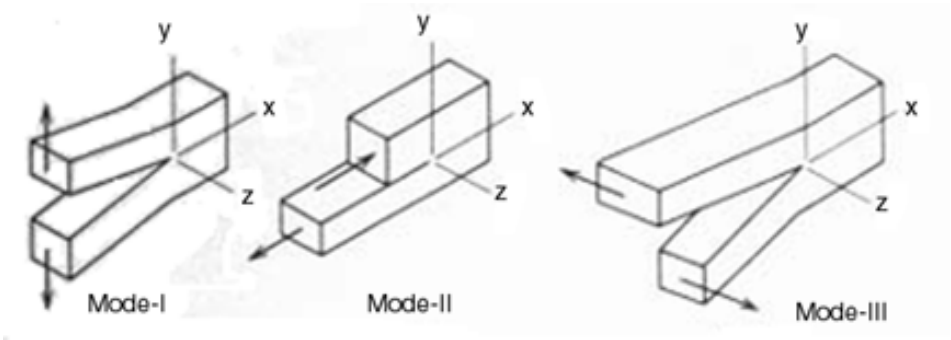

Figure 2.1 Modes of loading

2.2.2 Fracture Toughness of the Material

When the stress intensity factor (such as K_I) reaches a critical value (K_{IC}), the crack begins to grow. This critical value of the stress intensity factor is known as fracture toughness of the material, which depends on the thickness of the specimen and the temperature. The fracture toughness can be considered as the limiting value of the stress intensity just as the yield stress might be considered as the limiting value of the applied stress. Mode I plane strain fracture toughness is denoted as K_{IC}. K_C which is the plane stress fracture toughness is used to measure a material's fracture toughness in a sample that has a thickness that is less than some critical value, *B*. When the

material's thickness is less than *B*, and stress is applied, the material is in a state called plane stress. A material's thickness is related to its fracture toughness graphically in Figure 2.2. If a stress is applied to a sample with a thickness greater than *B*, it is in a state called plane strain [10].

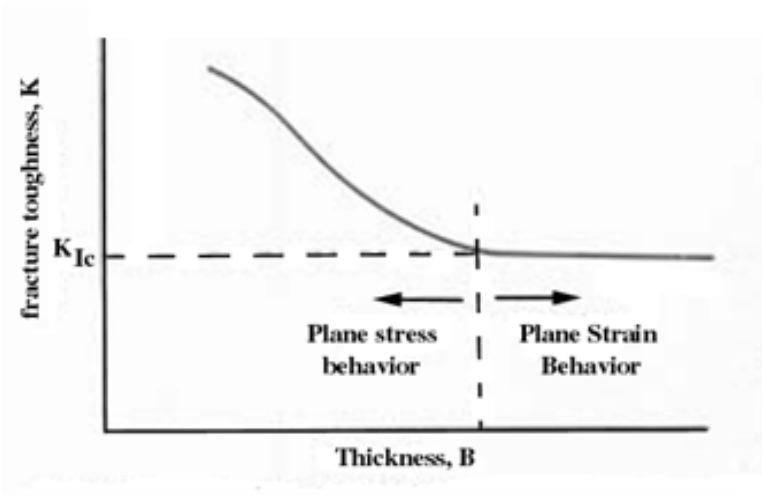

Figure 2.2 The effect of thickness on fracture toughness

2.2.3 Stress Fields and Asymptotic Expressions for a Crack

The stresses and strains at any point near a crack tip (Figure 2.3) can be derived from the theory of elasticity. Stresses and strains within the interior of a solid body subjected to external load and/or displacement conditions are known to satisfy a set of fundamental differential equations resulting from equilibrium, compatibility conditions and physical properties of the material which constitutes the solid body.

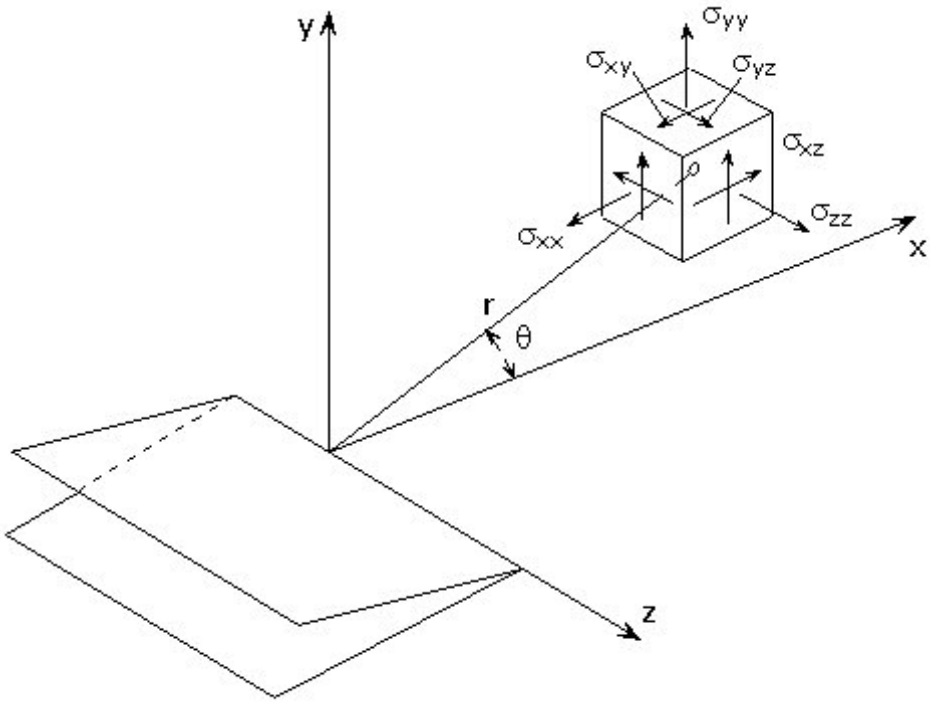

Figure 2.3 Stress field near a crack tip

Asymptotic stress and displacement fields at the crack tip are of critical importance in fracture analysis and also, an important quantity in fracture mechanics is the stress intensity factor which gives the strength of the singular fields for small values of "*r*". The distribution of stresses and displacements in small region around a crack tip given by asymptotic expressions are always the same for any cracked body. Although the asymptotic expressions are universal, the stress intensity factor depends on the geometry and the loading conditions. In other words, the stress intensity factor is a function of the size and position of the crack in the geometry and the applied stress.

In figure 2.4, polar coordinate system for a two dimensional crack is shown.

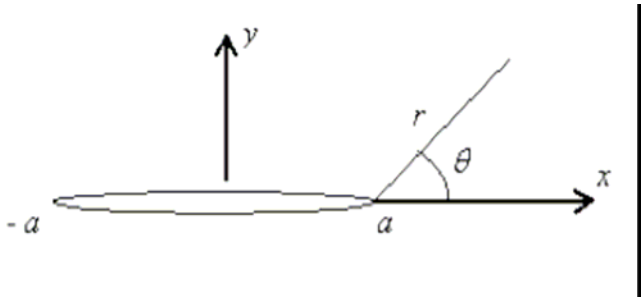

Figure 2.4 A two-dimensional crack configuration

For each loading mode (mode I, II and III), two dimensional linear elastic crack tip fields and definitions of stress intensity factors are cited below. [39]

Mode I Crack:

$$\sigma_{yy}(r,\theta) = \frac{K_I}{\sqrt{2\pi r}}\cos\left(\frac{\theta}{2}\right)\left\{1+\sin\left(\frac{\theta}{2}\right)\sin\left(\frac{3\theta}{2}\right)\right\} \tag{2.1}$$

$$\sigma_{xx}(r,\theta) = \frac{K_I}{\sqrt{2\pi r}}\cos\left(\frac{\theta}{2}\right)\left\{1-\sin\left(\frac{\theta}{2}\right)\sin\left(\frac{3\theta}{2}\right)\right\} \tag{2.2}$$

$$\sigma_{xy}(r,\theta) = \frac{K_I}{\sqrt{2\pi r}}\cos\left(\frac{\theta}{2}\right)\sin\left(\frac{\theta}{2}\right)\sin\left(\frac{3\theta}{2}\right) \tag{2.3}$$

$$u(r,\theta) = \frac{K_I}{2\mu}\sqrt{\frac{r}{2\pi}}\cos\left(\frac{\theta}{2}\right)\left\{\kappa-1+2\sin^2\left(\frac{\theta}{2}\right)\right\} \tag{2.4}$$

$$v(r,\theta) = \frac{K_I}{2\mu}\sqrt{\frac{r}{2\pi}}\sin\left(\frac{\theta}{2}\right)\left\{\kappa+1-2\cos^2\left(\frac{\theta}{2}\right)\right\} \tag{2.5}$$

where K_I is the mode I stress intensity factor and σ_{xx}, σ_{yy} and σ_{xy} are the components of stress with the distance r from the crack front and with angle θ from the crack plane. In equations 2.4 and 2.5, u and v are the displacements in x and y directions. μ is the shear modulus and κ is

$\left(\frac{3-\nu}{1+\nu}\right)$ for plane stress and $(3-4\nu)$ for plane strain where ν is the Poisson's ratio. There is a relationship between shear modulus (μ) and Young's modulus (E) such that:

$$\mu = \frac{E}{2(1+\nu)} \tag{2.6}$$

Definition of the mode I stress intensity factors can be expressed as:

$$K_I(a) = \lim_{x \to a^+} \sqrt{2\pi(x-a)}\sigma_{yy}(x,0) \tag{2.7}$$

$$K_I(-a) = \lim_{x \to -a^-} \sqrt{2\pi(-x-a)}\sigma_{yy}(x,0) \tag{2.8}$$

where crack length is equal to *2a*.

Mode II Crack:

$$\sigma_{yy}(r,\theta) = \frac{K_{II}}{\sqrt{2\pi r}} \sin\left(\frac{\theta}{2}\right)\cos\left(\frac{\theta}{2}\right)\cos\left(\frac{3\theta}{2}\right) \tag{2.9}$$

$$\sigma_{xx}(r,\theta) = -\frac{K_{II}}{\sqrt{2\pi r}} \sin\left(\frac{\theta}{2}\right)\left\{2+\cos\left(\frac{\theta}{2}\right)\cos\left(\frac{3\theta}{2}\right)\right\} \tag{2.10}$$

$$\sigma_{xy}(r,\theta) = \frac{K_{II}}{\sqrt{2\pi r}} \cos\left(\frac{\theta}{2}\right)\left\{1-\sin\left(\frac{\theta}{2}\right)\sin\left(\frac{3\theta}{2}\right)\right\} \tag{2.11}$$

$$u(r,\theta) = \frac{K_{II}}{2\mu}\sqrt{\frac{r}{2\pi}} \sin\left(\frac{\theta}{2}\right)\left\{\kappa+1+2\cos^2\left(\frac{\theta}{2}\right)\right\} \tag{2.12}$$

$$v(r,\theta) = -\frac{K_{II}}{2\mu}\sqrt{\frac{r}{2\pi}} \cos\left(\frac{\theta}{2}\right)\left\{\kappa-1-2\sin^2\left(\frac{\theta}{2}\right)\right\} \tag{2.13}$$

Definition of the mode II stress intensity factors are:

$$K_{II}(a) = \lim_{x \to a^+} \sqrt{2\pi(x-a)}\sigma_{xy}(x,0) \tag{2.14}$$

$$K_{II}(-a) = \lim_{x \to -a^-} \sqrt{2\pi(-x-a)}\sigma_{xy}(x,0) \tag{2.15}$$

Mode III Crack:

$$\sigma_{xz}(r,\theta) = -\frac{K_{III}}{\sqrt{2\pi r}}\sin\left(\frac{\theta}{2}\right) \tag{2.16}$$

$$\sigma_{yz}(r,\theta) = \frac{K_{III}}{\sqrt{2\pi r}}\cos\left(\frac{\theta}{2}\right) \tag{2.17}$$

$$\sigma_{xx}(r,\theta) = \sigma_{yy}(r,\theta) = \sigma_{zz}(r,\theta) = 0 \tag{2.18}$$

$$w(r,\theta) = \frac{K_{III}}{\mu}\sqrt{\frac{r}{2\pi}}\sin\left(\frac{\theta}{2}\right) \tag{2.19}$$

$$u(r,\theta) = v(r,\theta) = 0 \tag{2.20}$$

where w is displacement in z direction and K_{III} is mode III stress intensity factor whose definition is given as:

$$K_{III}(a) = \lim_{x \to a^+} \sqrt{2\pi(x-a)}\sigma_{yz}(x,0) \tag{2.21}$$

$$K_{III}(-a) = \lim_{x \to -a^-} \sqrt{2\pi(-x-a)}\sigma_{yz}(x,0) \tag{2.22}$$

In figure 2.5, a three dimensional crack front is shown. The parameter *s* in this figure is the arc length of the crack front and *t, n, b* is a local coordinate system located at point *P* composed of the tangential (*t*), normal (*n*) and binormal (*b*) directions, *n* pointing into the material side. (*r,* θ) are the polar coordinates in the normal plane (*n, b*) [34]. Three dimensional linear elastic crack tip fields are given below:

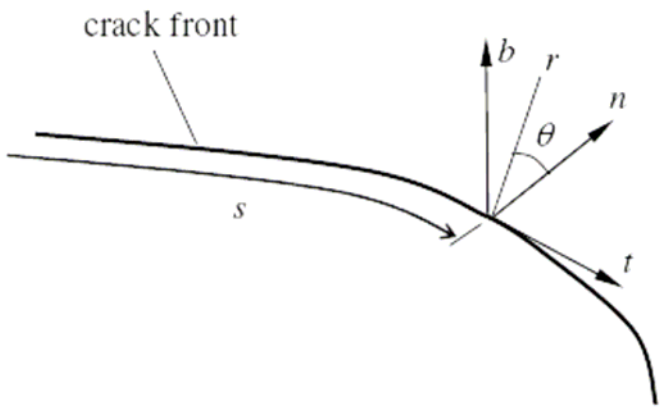

Figure 2.5 Three dimensional crack front

$$\sigma_{nn} = \frac{K_I(s)}{\sqrt{2\pi r}}\cos\left(\frac{\theta}{2}\right)\left[1-\sin\left(\frac{\theta}{2}\right)\sin\left(\frac{3\theta}{2}\right)\right] - \frac{K_{II}(s)}{\sqrt{2\pi r}}\sin\left(\frac{\theta}{2}\right)\left[2+\cos\left(\frac{\theta}{2}\right)\cos\left(\frac{3\theta}{2}\right)\right] \tag{2.23}$$

$$\sigma_{bb} = \frac{K_I(s)}{\sqrt{2\pi r}}\cos\left(\frac{\theta}{2}\right)\left[1+\sin\left(\frac{\theta}{2}\right)\sin\left(\frac{3\theta}{2}\right)\right] + \frac{K_{II}(s)}{\sqrt{2\pi r}}\sin\left(\frac{\theta}{2}\right)\cos\left(\frac{\theta}{2}\right)\cos\left(\frac{3\theta}{2}\right) \tag{2.24}$$

$$\sigma_{tt} = 2\nu\left[\frac{K_I(s)}{\sqrt{2\pi r}}\cos\left(\frac{\theta}{2}\right) - \frac{K_{II}(s)}{\sqrt{2\pi r}}\sin\left(\frac{\theta}{2}\right)\right] \tag{2.25}$$

$$\sigma_{nb} = \frac{K_I(s)}{\sqrt{2\pi r}}\sin\left(\frac{\theta}{2}\right)\cos\left(\frac{\theta}{2}\right)\cos\left(\frac{3\theta}{2}\right) + \frac{K_{II}(s)}{\sqrt{2\pi r}}\cos\left(\frac{\theta}{2}\right)\left[1-\sin\left(\frac{\theta}{2}\right)\sin\left(\frac{3\theta}{2}\right)\right] \tag{2.26}$$

$$\sigma_{nt} = -\frac{K_{III}(s)}{\sqrt{2\pi r}}\sin\left(\frac{\theta}{2}\right) \tag{2.27}$$

$$\sigma_{bt} = \frac{K_{III}(s)}{\sqrt{2\pi r}}\cos\left(\frac{\theta}{2}\right) \tag{2.28}$$

$$\begin{aligned} u_n = \frac{1+\nu}{E}\sqrt{\frac{2r}{E}}\Bigg\{ & K_I(s)\cos\left(\frac{\theta}{2}\right)\left[(1-2\nu)+\sin^2\left(\frac{\theta}{2}\right)\right] \\ & + K_{II}(s)\sin\left(\frac{\theta}{2}\right)\left[2(1-\nu)+\cos^2\left(\frac{\theta}{2}\right)\right]\Bigg\} \end{aligned} \tag{2.29}$$

$$\begin{aligned} u_b = \frac{1+\nu}{E}\sqrt{\frac{2r}{\pi}}\Bigg\{ & K_I(s)\sin\left(\frac{\theta}{2}\right)\left[2(1-\nu)-\cos^2\left(\frac{\theta}{2}\right)\right] \\ & - K_{II}(s)\cos\left(\frac{\theta}{2}\right)\left[(1-2\nu)-\sin^2\left(\frac{\theta}{2}\right)\right] \end{aligned} \tag{2.30}$$

$$u_t = 2\frac{1+\nu}{E}\sqrt{\frac{2r}{\pi}}K_{III}(s)\sin\left(\frac{\theta}{2}\right) \tag{2.31}$$

where K_I, K_{II} and K_{III} are the stress intensity factors and these are defined as:

$$K_I = \lim_{r\to 0}\sqrt{2\pi r}\,\sigma_{bb}(r,0) \tag{2.32}$$

$$K_{II} = \lim_{r\to 0}\sqrt{2\pi r}\,\sigma_{nb}(r,0) \tag{2.33}$$

$$K_{III} = \lim_{r\to 0}\sqrt{2\pi r}\,\sigma_{bt}(r,0) \tag{2.34}$$

2.2.4 Energy Release Rate

The energy release rate often denoted by *G* is the amount of energy, per unit length along the crack edge, which is supplied by the elastic energy in the body and by the loading system in creating the new fracture surface area. In terms of the stress intensity factor, there is relationship called the Irwin relationship. Note that there are our two models for the stress intensity factor one for plane stress and plane strain [40].

$$G = \left(\frac{1-\nu^2}{E}\right) \cdot K^2 \text{ (For plane strain)} \tag{2.35}$$

$$G = \frac{K^2}{E} \text{ (For plane stress)} \tag{2.36}$$

The total energy release rate in combined mode cracking can be obtained by adding the energies from the different modes.

$$G = G_I + G_{II} + G_{III} = \frac{1-\nu^2}{E} \cdot \left(K_I{}^2 + K_{II}{}^2 + \frac{K_{III}{}^2}{(1-\nu)} \right) \tag{2.37}$$

In this study, three dimensional semi – elliptical surface cracks in a welded joint under mechanical loading are examined. Therefore, the cracks are assumed to be exposed to mode I, II and III loading. The stress intensity factors and energy release rate are derived and displacement correlation technique (DCT) is used with respect to relevant asymptotic expressions. Material properties of the weld connection are assumed to have the same with main structure, such as Poisson’s ratio and modulus of elasticity.

CHAPTER 3

DESCRIPTION OF THE PROBLEM

3.1 General Survey of Earth-Moving Machines

Back-hoe loaders and excavators are the earth – moving machines which are composed of hydraulic cylinders, bucket or shovel, boom, arm and chassis as well as powerful engine and hydraulic units, pumps, valves, hoses. All of the digging and loading parts of these machines, except hydraulic cylinders, are manufactured by means of welding operations. As welding process, butt welding and fillet welding are usually performed with the methods of metal inert gas (MIG) and tungsten inert gas (TIG). In the welded construction, approximately 80% of the welds are fillet welds and 15% are butt welds. The remaining 5% are plug, slot and spot welds [29]. A butt weld is a type of weld joint that it is made by welding together the flat ends, or edges, of piece of iron or steel, or of separate pieces, without having them overlap [28] (Figure 3.1). A fillet weld is a weld of approximately triangular cross-section applied to the surface profile of the plates. According to the relative positions of the welded components, three types of fillet weld applications exist:

(a) Lap joint,
(b) Tee or cruciform joint,
(c) Corner joint (Figure 3.2) [29].

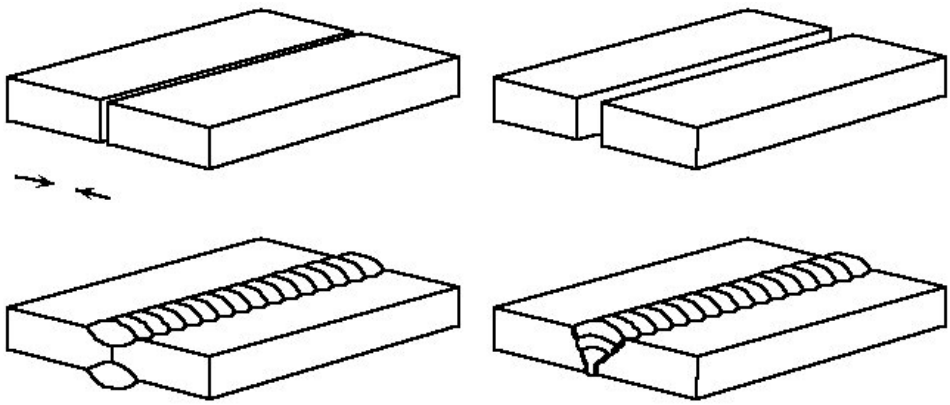

Figure 3.1 Samples of butt weld [29]

As it has been mentioned in the previous chapter, excavators and back-hoe loaders are used in hazardous areas, such as marble quarries, stone quarries, construction sites, etc. and during their applications, they face enormous cyclic loadings (figure 3.3, figure 3.4). These types of loadings cause fatigue problems and strength properties become more important regarding the life prediction. Besides the poor strength properties, fracture behavior of the structure is also important. These machines must be designed so that they can be used, adjusted, and maintained without putting people around in danger when these operations are performed under the conditions anticipated by the manufacturer. Measures must be taken to minimize any possibility of accident throughout the predicted lifetimes of the machines, including the phases of assembly and dismantling. In order to maintain the safety and the reliability, all of the processes beginning from design to the end of the manufacture must be conducted with respect to working conditions of the machines.

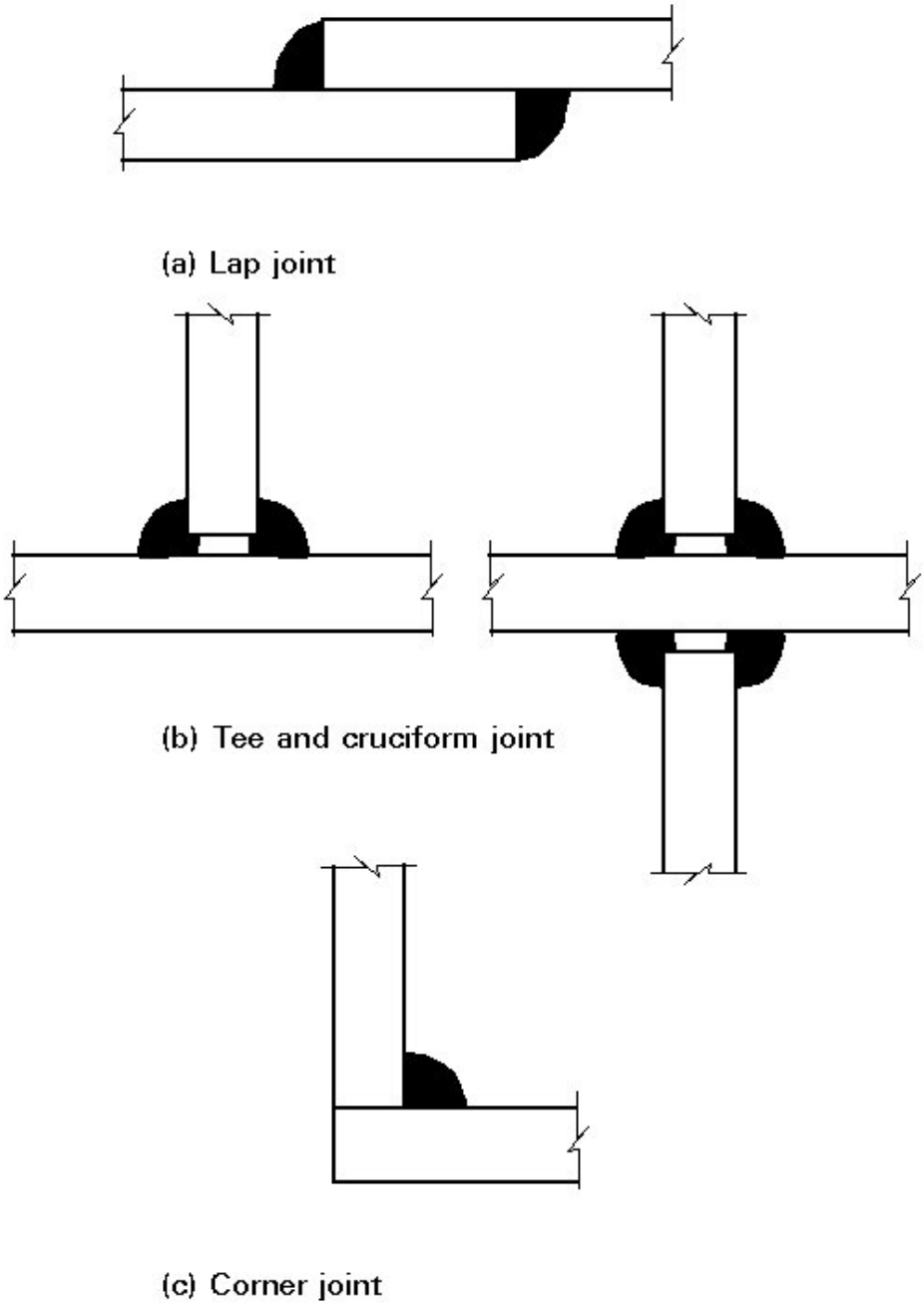

Figure 3.2 Fillet welds

Figure 3.3 Excavator working at stone quarry

Figure 3.4 Excavator working at construction site

3.2 Defects that occur during applications

Excavators and back-hoe loaders are exposed to high repeated loads during their operations and under these repeated loads; random defects are formed in the high stress regions of the structures. This phenomenon is called as fatigue. Most of these high stress regions are placed very close to the welding areas. In these areas, three types of behavior can be observed: 1) Crack initiation, 2) Crack propagation from initial crack. 3) Failure.

3.2.1 Crack initiation

In reality, a small crack occurs at the end of the welding process. This small crack cannot be seen with naked eye. Also, it cannot be observed with non-destructive testing methods like ultrasonic flaw detectors, magnetic-particle inspection or so on. It occurs in the structure of the material and measurement devices' tolerances do not let the operator detect the crack. It is possible to fix the flaw with only electron microscope, therefore, in earth-moving machinery sector, this type of defects is ignored and structure with weld process is called as welding with full penetration. In structural work, the composition of the electrode is usually chosen so that the resultant weld metal is stronger than the connected elements. Although butt weld or fillet weld is formed with full penetration, residual stresses are caused in heat affected zone (HAZ) [30]. These regions become possible cracking regions. During operation of excavators and back-hoe loaders, some flaws occur at these regions due to cyclic and high loads and in the course of time they can be seen by naked eye because of crack propagation. In figure 3.5, an excavator boom with flaws at the fillet weld region is shown. Detail of this crack can be seen in figure 3.6. In this figure, it is noted that reinforcement and bottom sheet are welded at both sides of the reinforcement. However, during welding process, a small crack occurs initially at the weld toe and in operation period crack growth occurs.

Figure 3.5 Flaw in excavator structure

Figure 3.6 Detail of the flaw

3.2.2 Crack propagation from initial crack

In welding process, full penetration cannot be satisfied. In this situation, an undesirable weld gap is formed at the end of the manufacture process. This opening behaves like an initial crack. Because of high repeated loads, this crack continues to grow and structure fails by means of crack propagation.

Figure 3.7 Crack propagation due to weld gap

In figure 3.7, it is seen that reinforcement and bottom sheet are welded at only one side. At the end of welding, a weld gap occurs because weld does not penetrate to the other side of reinforcement. This weld gap behaves like initial crack. Crack propagates at the weld root of the junction.

In figure 3.8, a tee joint without edge preparation is shown. For this model, partial penetration occurred and for this reason, an initial crack was formed between the sheet metals.

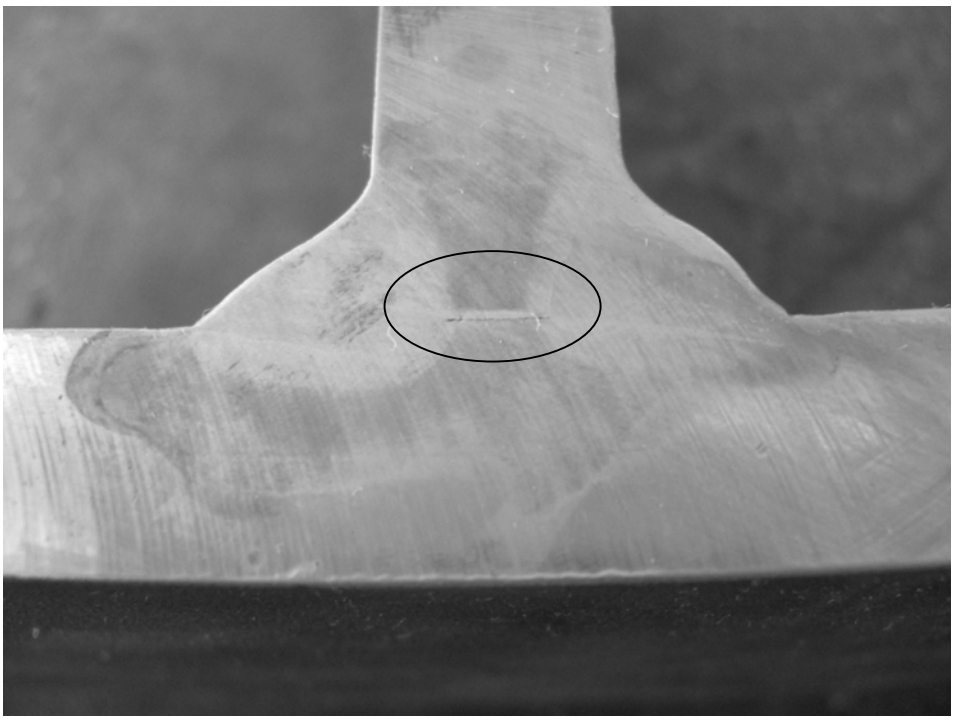

Figure 3.8 Tee joint with weld gap

3.2.3 Failure

Failure occurs when the material that has not been affected by the crack cannot withstand the applied stress. This stage happens very quickly. The rate at which a crack grows has considerable importance in determining the life of a material. The propagation of a crack occurs during the second step of fatigue failure. As a crack begins to propagate, the size of the crack also

begins to grow. The rate at which the crack continues to grow depends on the stress level applied [31]. In figure 3.9, failure of part from an excavator boom at the time of operation can be seen. Dark grey region in the figure is the place of the initial crack and it makes the structure fail at that point.

Figure 3.9 Failed parts of an excavator boom

3.3 Crack Map of the Excavator Boom

For an excavator boom, it is observed from test results and operation feedbacks that there are five possible defect regions. All of these are due to weld gaps or weld toes. These regions can be seen in figure 3.10.

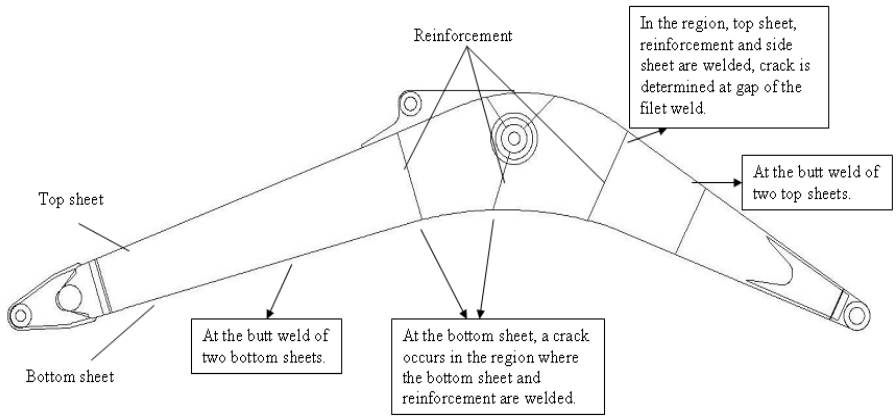

Figure 3.10 Crack Map of the Excavator Boom

3.4 Boom Structural Analysis by Finite Element Method

In the thesis study of Yener [32], design of a computer interface for automatic finite element analysis of an excavator boom is carried out. This work lets the user model the excavator boom by setting the parameters. All of the stress concentration regions can be observed during the post-processing application. However, effects of weld areas cannot be determined in this study, because, when modeling process is performed, any type of welding (fillet or butt welds) is not formed. It is known that the stress intensity factors of a material are important to predict its life-span; therefore, a new model including welding connections with weld gaps is needed. Nevertheless, if full model of an excavator boom is formed with weld connection including weld gap, it is very difficult to conduct the finite element analysis as there are too many finite elements and nodes in the model. Instead of this, a new model containing the same deformation characteristics is needed. When the stress concentration regions of the full model are investigated, it is seen that a T-shaped specimen is suitable in order to find out the stress intensity factors of the material.

CHAPTER 4

FINITE ELEMENT MODELING AND DISPLACEMENT CORRELATION TECHNIQUE

4.1 Finite Element Modeling

Finite Element Analysis (FEA) consists of a computer model of a material or design that is stressed and analyzed for specific results. It is used in new product design, and existing product refinement. A company is able to verify a proposed design will be able to perform to the client's specifications prior to manufacturing or construction. Modifying an existing product or structure is utilized to qualify the product or structure for a new service condition. In case of structural failure, FEA may be used to help determine the design modifications to meet the new condition.

Finite elements resemble fragments of the structure. Nodes appear on element boundaries and all elements that share a node have the same displacement components at that node. Nodes are assigned at a certain density throughout the material depending on the anticipated stress levels of a particular area. Regions which will receive large amounts of stress usually have a higher node density than those which experience little or no stress. Points of interest may consist of: fracture point of previously tested material, fillets, corners, complex detail, and high stress areas. Mesh structure is programmed to contain the material and structural properties, which define how the structure will react to certain loading conditions and it acts like a

spider web in that from each node, there extends a mesh element to each of the adjacent nodes. [35].

T-shaped specimen with a fillet weld is modeled in MSC.MENTAT – MARC 2005 (Figure 4.1). Different from the previous work, full model is created in order to find out the modes I, II and III stress intensity factors at the crack front. The close-up view is shown in the figure 4.2.

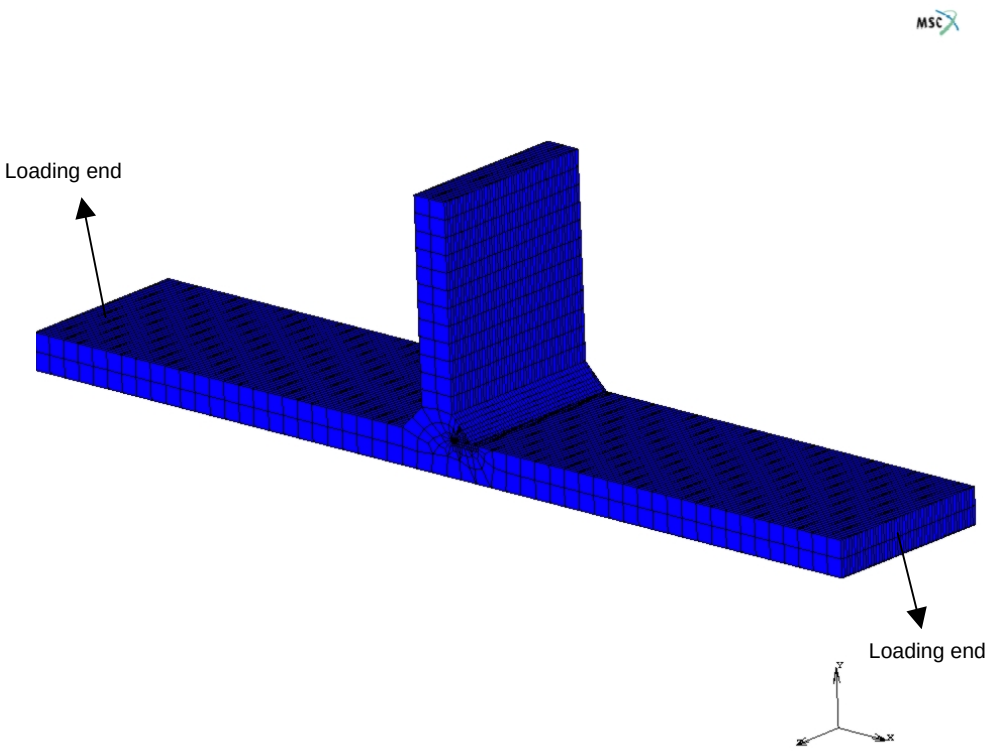

Figure 4.1 Full model of the specimen

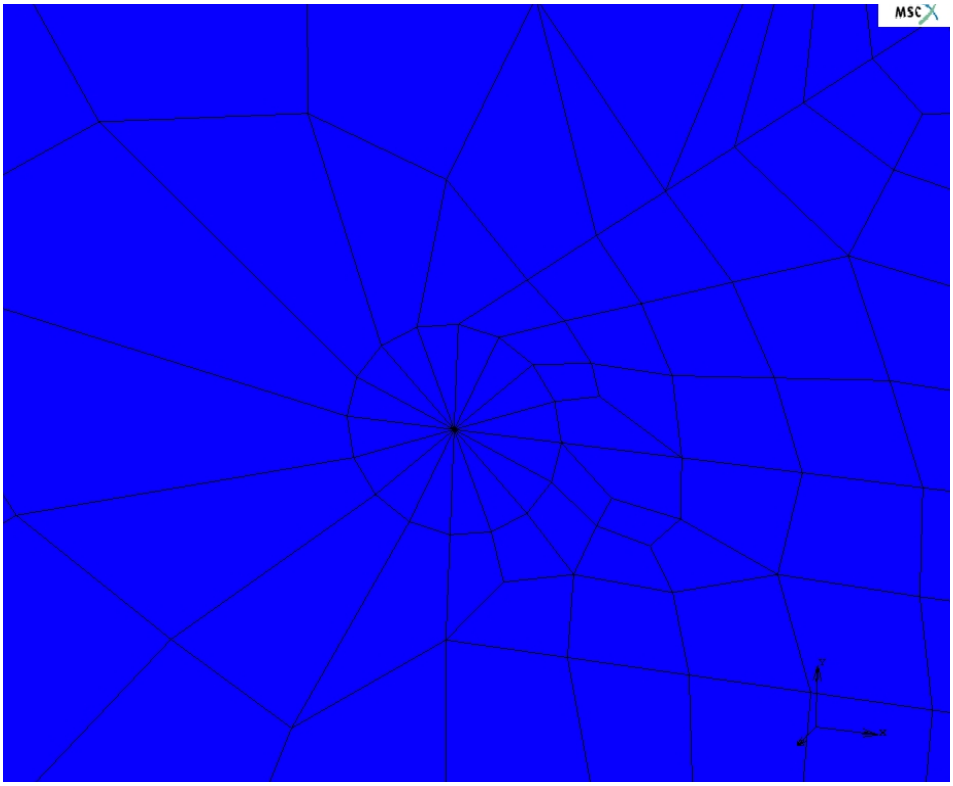

Figure 4.2 Close-up view of the wedge elements

In a conventional type of finite element modeling, all the geometric, material and boundary condition parameters are put in separately by user. In this study, however, all of these input data are formed automatically by the PYTHON code, which is a software code that lets the user to configure the parametric model of a structure.

In the finite element model of the specimen, there are nearly 16000 elements and 60000 nodes. At the crack front, the elements are 20 node collapsed brick elements (wedge elements), which are seen in figure 4.3. These elements are used to satisfy the strain singularity around the crack front. In the remaining part of the model, 10 node tetrahedral elements (figure 4.4) are placed for the model with semi-elliptical type of crack front. For the wedge

elements, mid-point nodes are moved to the quarter points to provide the singularity.

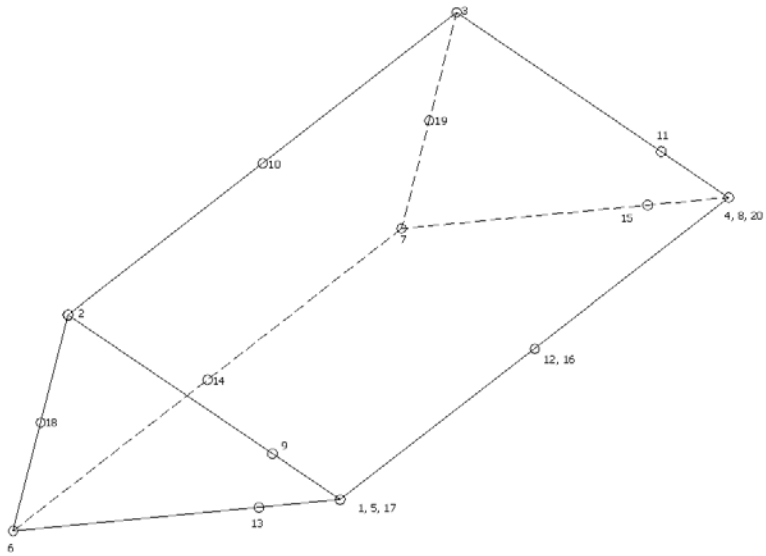

Figure 4.3 20 node collapsed brick element

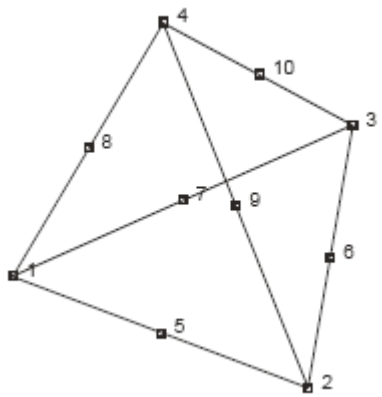

Figure 4.4 10 node tetrahedral elements

Some analyses are performed related to radius and number of the 20 node collapsed brick elements. Consequently, analyses, having one over twenty-five of the crack depth (*a*) for the radius of the wedge elements and sixteen for number of the wedge elements along the crack front have the sufficient accuracy compared to the theoretical solutions. The circular crack and singular elements with quarter point nodes are given in figures 4.5 and 4.6.

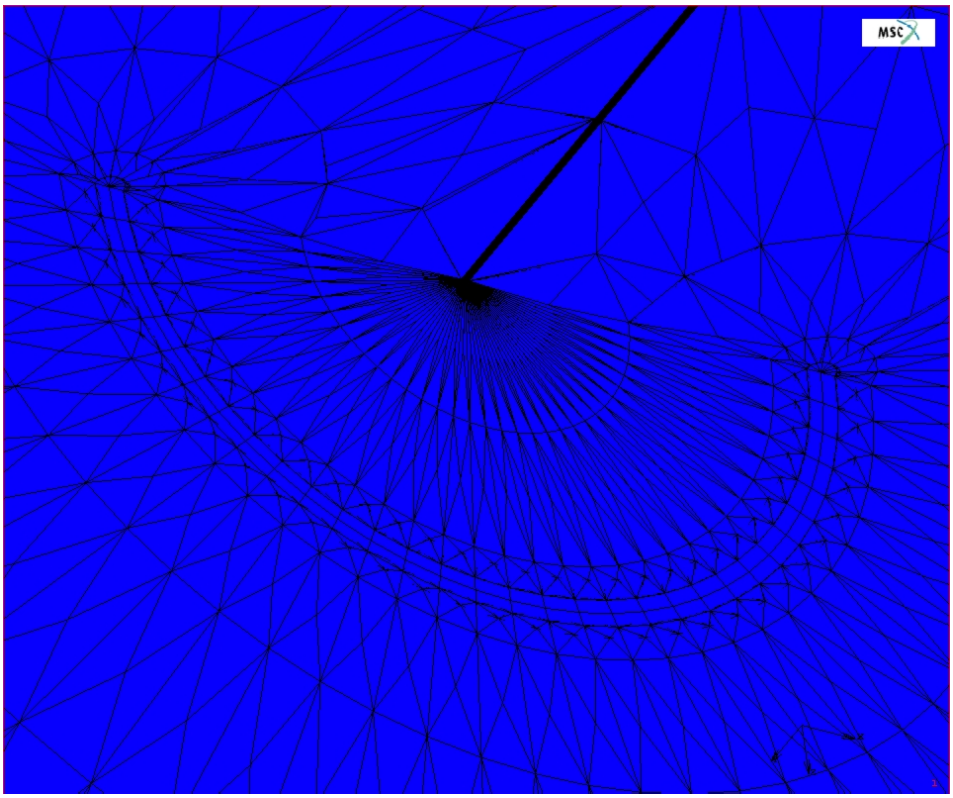

Figure 4.5 Circular crack

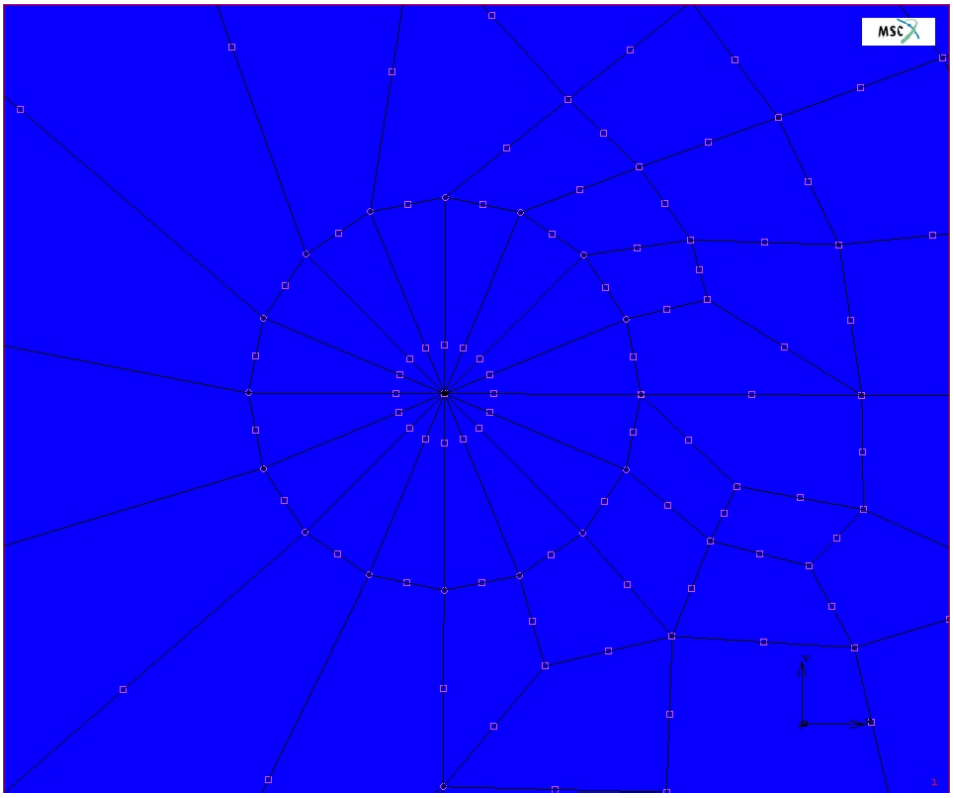

Figure 4.6 Singular elements with quarter point nodes

The stages of the modeling T-shaped specimen with a fillet weld in finite element analysis software MSC. MENTAT – MARC are described below:

- User enters the geometric (Figure 4.7) and material properties of the specimen by using an interface.

    - Crack place
    - Material type
    - Thickness of the base sheet metal (*t1*)
    - Thickness of the upper sheet metal (*t2*)
    - Width of the specimen (*B*)
    - Angle of the crack with respect to base sheet metal (ψ)

- Depth of crack (*a*)
- Length of crack (*c*)
- Vertical leg of the fillet weld (K_v)
- Horizontal leg of the fillet weld (K_h)
- If necessary, distance of the crack center from front surface
- Whether weld is double sided or single sided

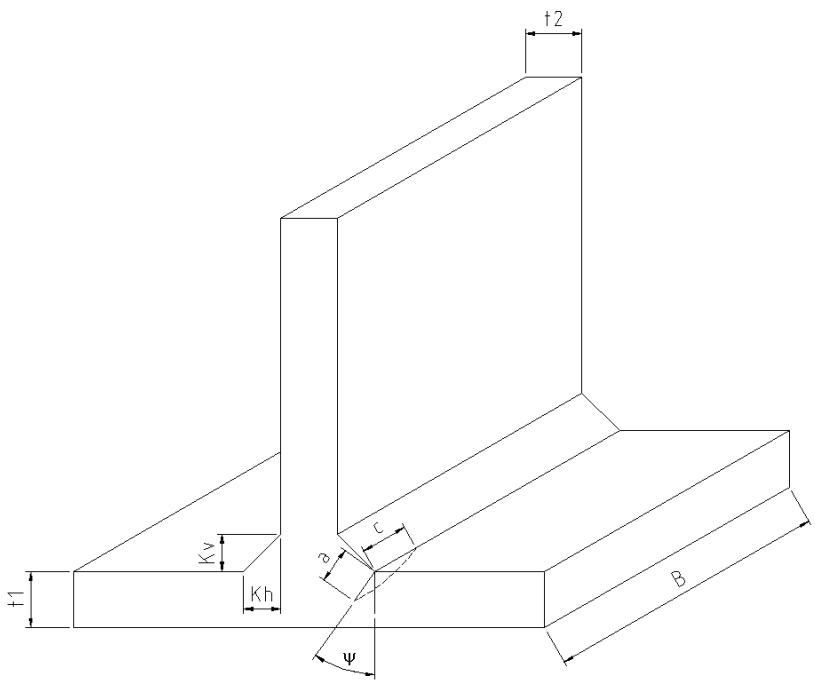

Figure 4.7 Parameters of the model

- Boundary points and curves are created with respect to parameters.
- Wedge elements with quarter points' nodes are formed.
- Nodes of wedge elements are taken into memory in order to use these for calculations of stress intensity factors.

- Remaining parts of the specimen are modeled.
- Boundary nodes are swept to satisfy the integrity of the model.
- Boundary conditions are applied.
- Material properties are defined.
- Analysis is performed.
- Wedge elements' displacements are taken from the result file as a post-processing application.
- By using displacement correlation technique, stress intensity factors are determined at the crack front.

Now, displacement correlation technique and its derivations for this type of problem are outlined.

4.2 Displacement Correlation Technique

Displacement correlation technique is used in order to calculate the modes I, II and III stress intensity factors for the T-shaped specimen. As a starting point of these derivations, equations for three dimensional crack fronts, which are mentioned in chapter 2, are used.

4.2.1 K_I Calculation

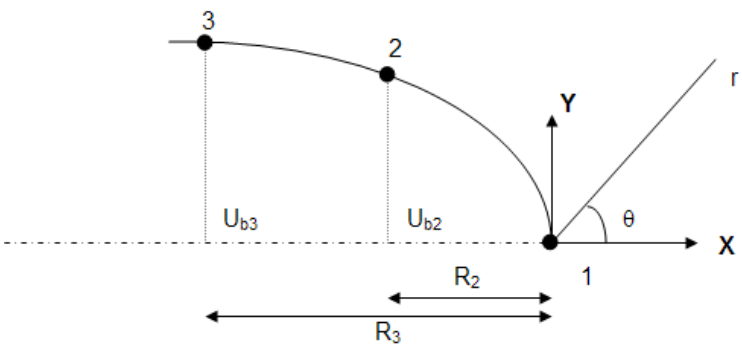

Figure 4.8 Deformed shape of the crack surface

Normal displacement is given as;

$$U_b = \left(\frac{1+\nu}{E}\right)\times\left(\sqrt{\frac{2r}{\pi}}\right)\times K_I \times sin\left(\frac{\theta}{2}\right)\times\left[2(1-\nu)-\cos^2\left(\frac{\theta}{2}\right)\right] \qquad (4.1)$$

For figure 4.7 ($\theta = \pi$);

$$U_b\,(r,\pi) = \left(\frac{1+\nu}{E}\right)\times\left(\sqrt{\frac{2r}{\pi}}\right)\times K_I \times \left[2(1-\nu)\right] \qquad (4.2)$$

$$U_b\,(r,\pi) = \frac{2(1-\nu^2)}{E}\times\left(\sqrt{\frac{2r}{\pi}}\right)\times K_I \qquad (4.3)$$

From the equation (4.3);

$$U_b\,(r,\pi) = \frac{4(1-\nu^2)}{E}\times\left(\sqrt{\frac{r}{2\pi}}\right)\times K_I \qquad (4.4)$$

Stress Intensity Factor obtained from equation (4.4) is given as;

$$K_I = \left[\lim_{r\to 0}\left\{\frac{U_b\,(r,\pi)}{\sqrt{r}}\right\}\right]\times\frac{\sqrt{2\pi}\times E}{4(1-\nu^2)} \qquad (4.5)$$

Asymptotically, $\frac{U_b\,(r,\pi)}{\sqrt{r}}$ is linear, so that

$$\frac{U_b\,(r,\pi)}{\sqrt{r}} = Ar + B \qquad (4.6)$$

We have 2 conditions. These are

Point 2: when $r = R_2$, then $U_b = U_{b2}$

Point 3: when $r = R_3$, then $U_b = U_{b3}$

$$r = R_2 \longrightarrow \frac{U_b(R_2, \pi)}{\sqrt{R_2}} = \frac{U_{b2}}{\sqrt{R_2}} = AR_2 + B \tag{4.7}$$

$$r = R_3 \longrightarrow \frac{U_b(R_3, \pi)}{\sqrt{R_3}} = \frac{U_{b3}}{\sqrt{R_3}} = AR_3 + B \tag{4.8}$$

We have two unknowns "*A*" and "*B*", from equations (4.7) and (4.8);

$$B = \frac{R_2^{\frac{3}{2}} \times U_{b3} - R_3^{\frac{3}{2}} \times U_{b2}}{\sqrt{R_2 \times R_3} \times (R_2 - R_3)} \tag{4.9}$$

At the crack tip, SIF is equal to

$$K_I = B \times \frac{\sqrt{2\pi} \times E}{4(1-\nu^2)} \tag{4.10}$$

Therefore;

$$K_I = \frac{\sqrt{2\pi} \times E}{4(1-\nu^2)} \times \left\{ \frac{R_2^{\frac{3}{2}} \times U_{b3} - R_3^{\frac{3}{2}} \times U_{b2}}{\sqrt{R_2 \times R_3} \times (R_2 - R_3)} \right\} \tag{4.11}$$

The above equations are derived by considering a single crack surface. We can extend this derivation by considering both of the crack surfaces.

Recalling equations (4.1) and (4.2);

$$U_b = \left(\frac{1+\nu}{E}\right) \times \left(\sqrt{\frac{2r}{\pi}}\right) \times K_I \times \sin\left(\frac{\theta}{2}\right) \times \left[2(1-\nu) - \cos^2\left(\frac{\theta}{2}\right)\right] \tag{4.1}$$

$$U_b\,(r,\pi) = \left(\frac{1+\nu}{E}\right)\times\left(\sqrt{\frac{2r}{\pi}}\right)\times K_I\times\left[2(1-\nu)\right] \qquad (4.2)$$

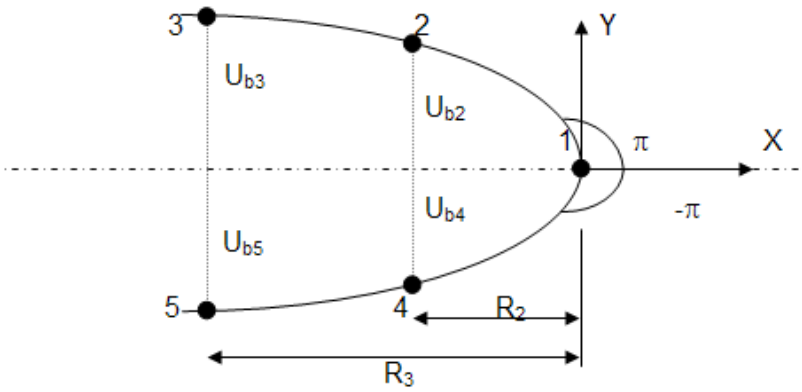

Figure 4.9 Schematic view of the crack surfaces

Also, applying equation (4.1) for the angle $\theta = -\pi$, we obtain

$$U_b\,(r,-\pi) = -\left(\frac{1+\nu}{E}\right)\times\left(\sqrt{\frac{2r}{\pi}}\right)\times K_I\times\left[2(1-\nu)\right] \qquad (4.12)$$

Subtracting these two equation from each other, then

$$U_b(r,\pi) - U_b(r,-\pi) = \frac{8(1-\nu^2)}{E}\times\sqrt{\frac{r}{2\pi}}\times K_I \qquad (4.13)$$

Stress Intensity Factor obtained from equation (4.4) is that;

$$K_I = \left[\lim_{r\to 0}\left\{\frac{U_b(r,\pi)-U_b(r,-\pi)}{\sqrt{r}}\right\}\right]\times\frac{\sqrt{2\pi}\times E}{8(1-\nu^2)} \qquad (4.14)$$

Considering the linearity of $\frac{U_b(r,\pi)-U_b(r,-\pi)}{\sqrt{r}}$, then

$$\frac{U_b(r,\pi)-U_b(r,-\pi)}{\sqrt{r}} = Ar + B \qquad (4.15)$$

Two conditions (for $r = R_2$ and $r = R_3$) will be applied to equation (4.15), then

$$r = R_2 \longrightarrow \frac{U_b(R_2,\pi)-U_b(R_2,-\pi)}{\sqrt{R_2}} = \frac{U_{b2}-U_{b4}}{\sqrt{R_2}} = AR_2 + B \qquad (4.16)$$

$$r = R_3 \longrightarrow \frac{U_b(R_3,\pi)-U_b(R_3,-\pi)}{\sqrt{R_3}} = \frac{U_{b3}-U_{b5}}{\sqrt{R_3}} = AR_3 + B \qquad (4.17)$$

From these two equations, "*B*" will be obtained. In equation (4.14), as "*r*" goes to zero, then $\frac{U_b(r,\pi)-U_b(r,-\pi)}{\sqrt{r}}$ is equal to "*B*".

All derived equations show that Stress Intensity Factor Mode I at the crack tip ($r = 0$) is

$$K_I = \frac{\sqrt{2\pi}\times E}{8(1-\nu^2)}\times\left\{\frac{R_2^{\frac{3}{2}}\times(U_{b3}-U_{b5})-R_3^{\frac{3}{2}}\times(U_{b2}-U_{b4})}{\sqrt{R_2}\times\sqrt{R_3}\times(R_2-R_3)}\right\} \qquad (4.18)$$

4.2.2 K_{II} Calculation

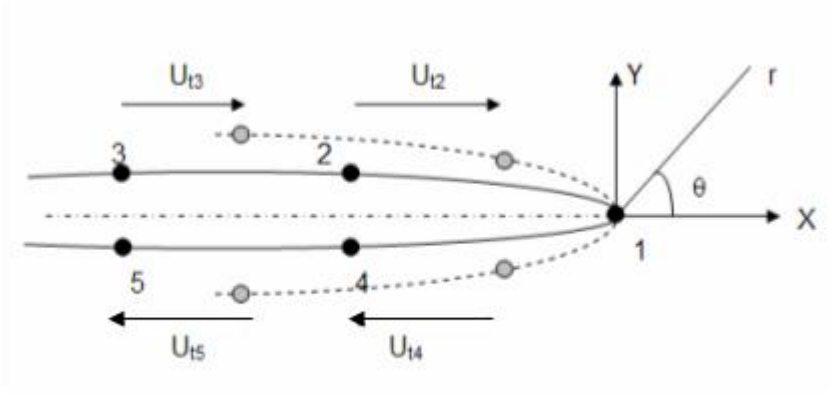

Figure 4.10 Schematic view of the crack surfaces for mode II loading

Firstly, let's calculate mode II stress intensity factor for anti-symmetric displacements;

$$U_t(r,\theta) = \frac{K_{II}}{2\mu} \times \sqrt{\frac{r}{2\pi}} \times \sin\left(\frac{\theta}{2}\right) \times \left\{\kappa + 1 + 2\cos^2\left(\frac{\theta}{2}\right)\right\} \qquad (4.19)$$

Considering plane strain,

$$\kappa = 3 - 4\nu \qquad (4.20).$$

And also

$$\mu = \frac{E}{2(1+\nu)} \qquad (4.21)$$

Using equations (4.20) and (4.21) into equation (4.19), then

$$U_t(r,\theta) = \frac{1+\nu}{E} \times K_{II} \times \sqrt{\frac{r}{2\pi}} \times \sin\left(\frac{\theta}{2}\right) \times \left\{3 - 4\nu + 1 + 2\cos^2\left(\frac{\theta}{2}\right)\right\} \quad (4.22)$$

The displacement equation becomes

$$u_t(r,\theta) = \frac{1+\nu}{E}\sqrt{\frac{2r}{E}}\left\{K_I(s)\cos\left(\frac{\theta}{2}\right)\left[(1-2\nu)+\sin^2\left(\frac{\theta}{2}\right)\right]\right.$$
$$\left. + K_{II}(s)\sin\left(\frac{\theta}{2}\right)\left[2(1-\nu)+\cos^2\left(\frac{\theta}{2}\right)\right]\right\} \quad (4.23)$$

For $\theta = \pi$:

$$U_t(r,\pi) = \frac{4(1-\nu^2)}{E} \times K_{II} \times \sqrt{\frac{r}{2\pi}} \quad (4.24)$$

This derived equation is the same with equation (4), so no need to make the same calculations for mode II SIF. Then, we can easily express that K_{II} equal to (like eq. (4.18))

$$K_{II} = \frac{\sqrt{2\pi} \times E}{8(1-\nu^2)} \times \left\{\frac{R_2^{\frac{3}{2}} \times (U_{t3} - U_{t5}) - R_3^{\frac{3}{2}} \times (U_{t2} - U_{t4})}{\sqrt{R_2} \times \sqrt{R_3} \times (R_2 - R_3)}\right\} \quad (4.25)$$

4.2.3 K_{III} Calculation

For stress intensity factor mode III; equation (4.26) coming from equations for three dimensional crack front is used.

$$U(r,\theta) = \frac{K_{III}}{\mu}\sqrt{\frac{r}{2\pi}}\sin\left(\frac{\theta}{2}\right) \quad (4.26)$$

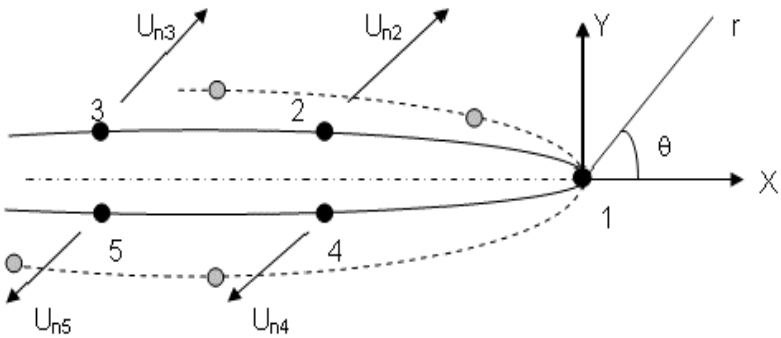

Figure 4.11 Schematic view of the crack surfaces for mode III loading

For $\theta = \pi$:

$$U_n(r,\pi) = 2 \cdot \frac{(1+\nu)}{E} \cdot K_{III} \sqrt{\frac{r}{2 \cdot \pi}} \tag{4.27}$$

Like K_I and K_{II}, stress intensity factor K_{III} is calculated with the same manner. It can be expressed that;

$$K_{III} = \frac{\sqrt{2\pi} \times E}{4(1+\nu)} \times \left\{ \frac{R_2^{\frac{3}{2}} \times (U_{n3} - U_{n5}) - R_3^{\frac{3}{2}} \times (U_{n2} - U_{n4})}{\sqrt{R_2} \times \sqrt{R_3} \times (R_2 - R_3)} \right\} \tag{4.28}$$

4.3 Verification of the Displacement Correlation Technique for embedded cracks and surface cracks

In this section, stress intensity factors obtained by using MARC are verified by making comparison to the results given by Sneddon [27], Irwin [38] and Noda et al. [37]

Firstly, the results of the model are confirmed by comparing them with the results along crack front obtained by using the solution for the embedded crack in an infinite medium.

Then the results of the model are compared with stress intensity factor calculations along a crack front of a 3D inclined semi – elliptical surface crack in a semi – infinite body under tension.

4.3.1 Verification by using Sneddon's Solution

The solution for the embedded circular crack is given by Sneddon [27]. This problem is known as *penny shaped crack problem* in the literature. This problem is shown in figure 4.12.

By the linear elastic fracture mechanics aspects, the stress intensity factor was found for this type of problem. For penny-shaped crack problem, stress intensity factor is found as

$$K = \frac{2}{\pi} \cdot \sigma \cdot \sqrt{\pi \cdot a} = 0.64 \cdot \sigma \cdot \sqrt{\pi \cdot a} \tag{4.29}$$

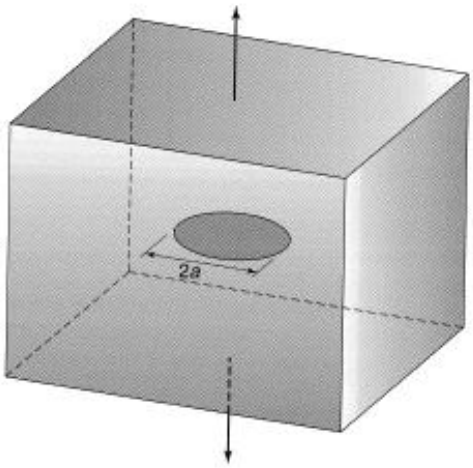

Figure 4.12 A penny-shaped crack in an infinite body [27]

For this problem, equation (4.18) is valid and both theoretical results and results from DCT are converted to non-dimensional values by using eq. (4.30).

$$f = \frac{K_I}{\sigma \cdot \sqrt{\pi \cdot a}} \tag{4.30}$$

Stress intensity factor calculation for embedded crack is made for a material with the properties of *E=210000 MPa*, *v=0.3*. Crack shape has the dimension of 10 mm as "*a*". During finite element modeling, size of the wedge elements' edges lying on the crack are one over twenty-five of the crack length "*a*".

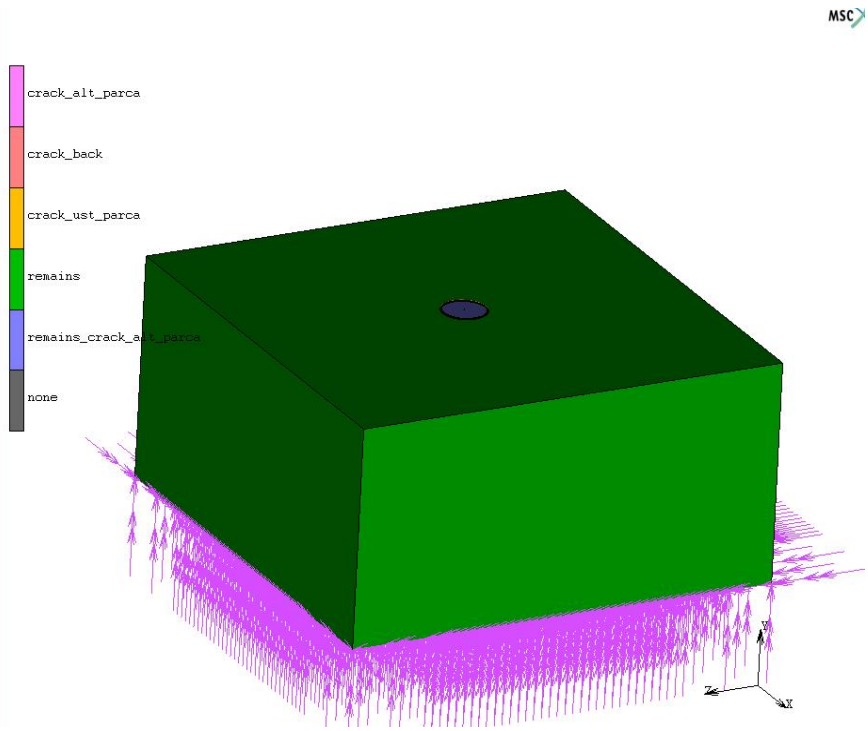

Figure 4.13 General view of the circular crack

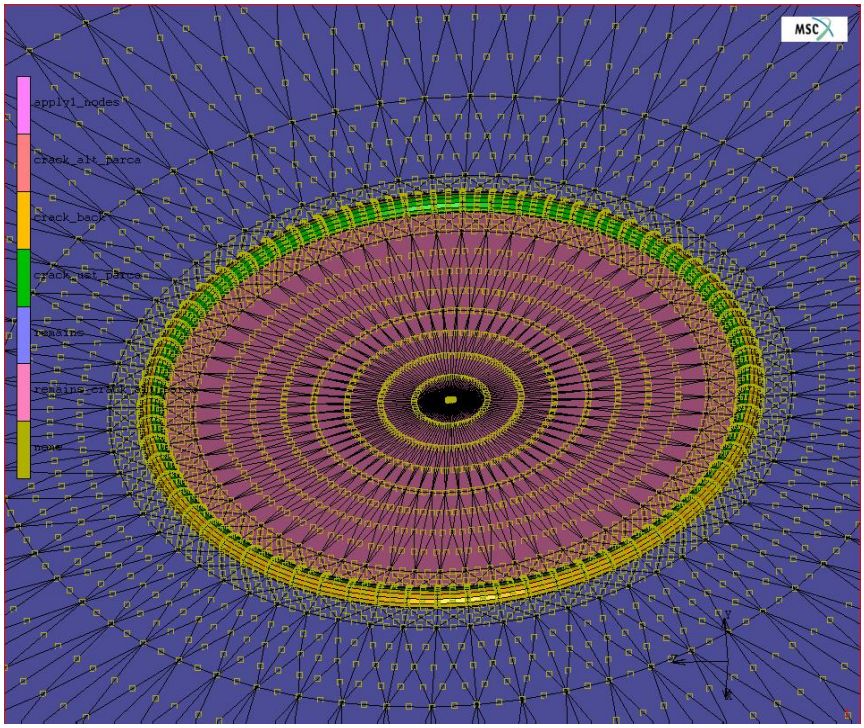

Figure 4.14 Close-up view of the circular crack

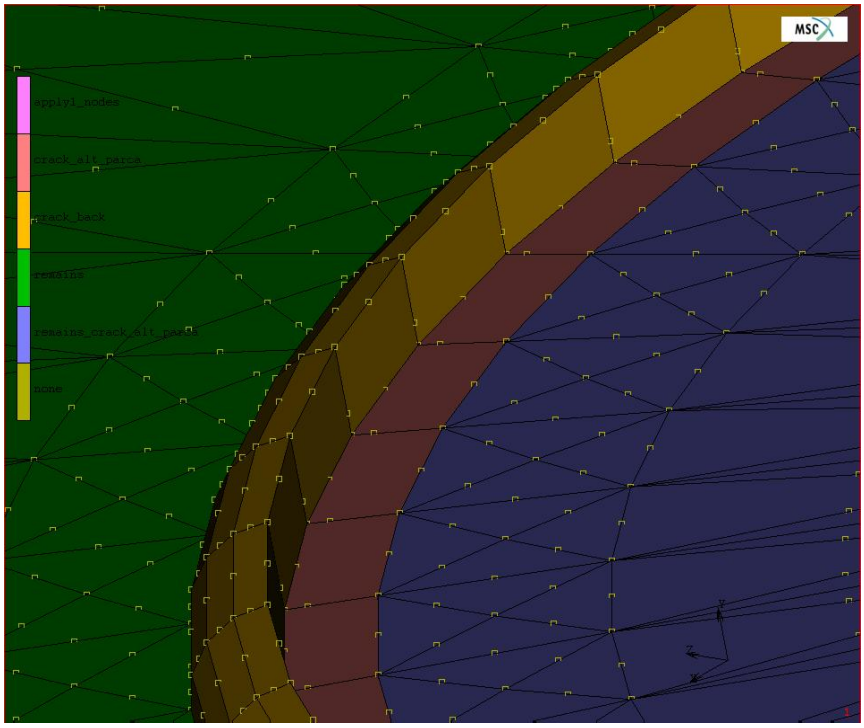

Figure 4.15 Close-up view of circular crack's node structure

Table 4.1 Normalized SIF comparison for penny-shaped crack

E (MPa)	Poisson's ratio	*a* (mm)	Present Study	Sneddon's Solution [27]	Difference (%)
210000	0,298	10	0,6298	0,6366	1,07

Around the crack front, all of the stress intensity factors are the same with the value above.

4.3.2 Verification by using Irwin's Solution

For the problem of an embedded flat elliptical crack in an infinite body loaded in remote tension, Irwin derived an analytical solution for the stress distribution in the neighborhood of the crack and found that a stress singularity occurred all round the perimeter of the crack front characterized by the stress intensity factor, but the magnitude of the stress intensity factor varied around the crack front. Irwin's solution for the variation of *K* is as:

$$K = \frac{\sigma \cdot \sqrt{\pi \cdot a}}{E(\phi)} \cdot \left\{ \sin^2 \phi + \frac{a^2}{c^2} \cdot \cos^2 \phi \right\}^{1/4} \tag{4.31}$$

where *a, c, Φ* are as shown in figure 4.16, and *E (Φ)* is the elliptical integral:

$$E(\phi) = \int_0^{\pi/2} \left\{ 1 - \left[1 - \frac{a^2}{c^2} \right] \cdot \sin^2 \phi \right\}^{1/2} \cdot d\phi \tag{4.32}$$

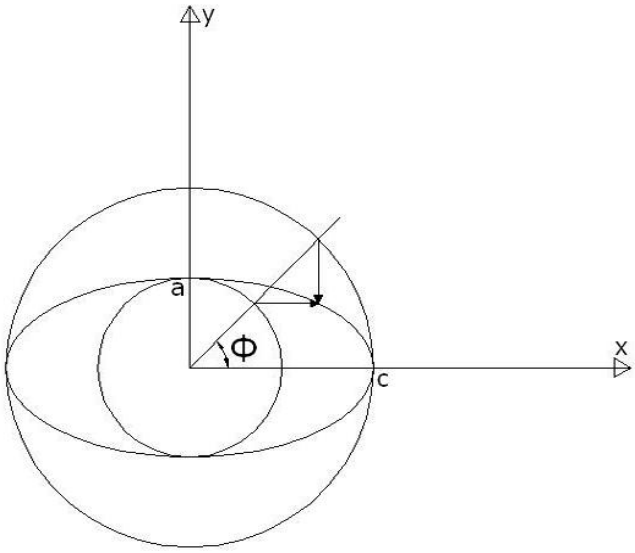

Figure 4.16 Parametric representation of a point on an ellipse

The maximum value of the stress intensity factor appears at the end of the minor axis for Irwin's solution under uniform tension loading. The ratio of the height of the crack (*2a*) to the length of the crack (*2c*) is known as the aspect ratio [38].

Eq. (4.18) is valid for this problem and both theoretical results and results from DCT are converted to non-dimensional values by using eq. (4.30).

In this problem, an infinite body with young's modulus of 210000 MPa and poisson's ratio of 0,298 has been examined. Crack is in the middle of this body and it has the dimensions of 5 mm as the minor axis and 10 mm as the major axis and uniform tension load has applied. By the solution of eq. (4.32) by using MATLAB, for the given "*c*" and "*a*" values, "*E (Φ)*" is equal to 1.21106.

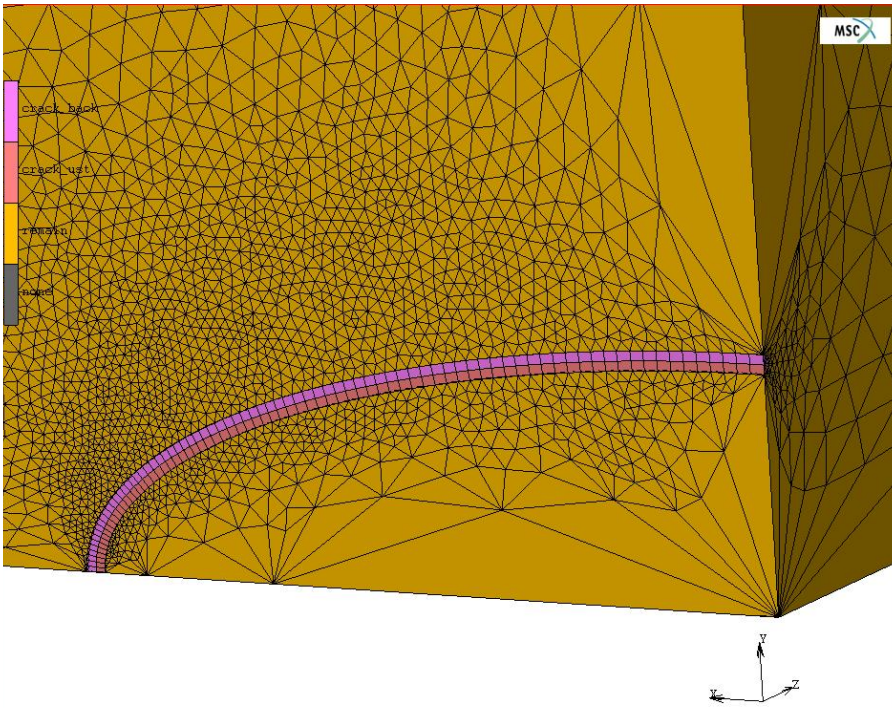

Figure 4.17 Close-up view of elliptic crack

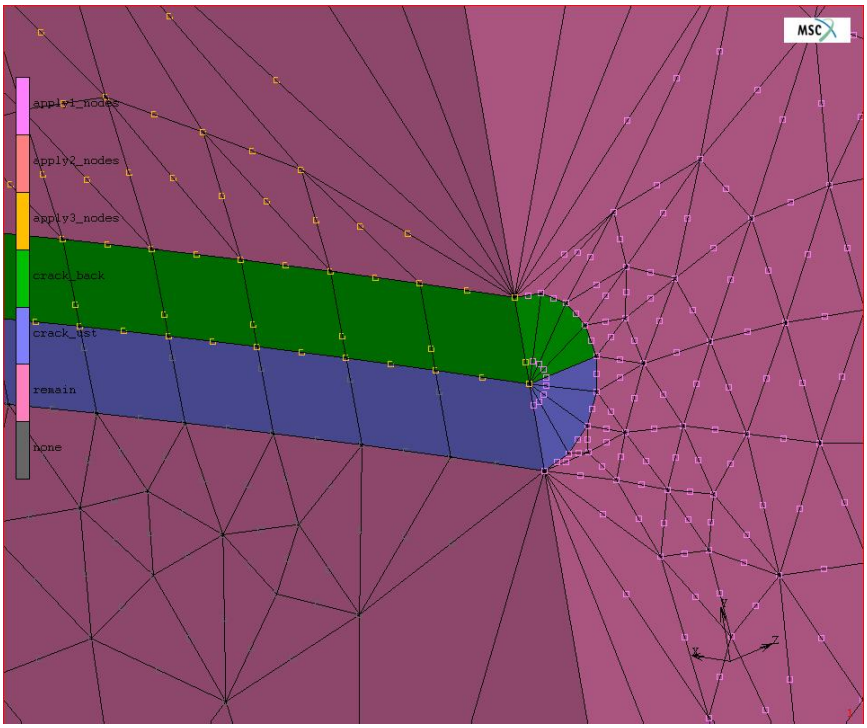

Figure 4.18 Close-up view of elliptic crack's node structure

Table 4.2 Normalized SIF comparison for an elliptical crack

Φ **(degree)**	**Present study**	**Irwin's Solution [27]**	**Difference (%)**
0,00	0,5724	0,5839	1,9650
8,54	0,5822	0,5933	1,8739
16,61	0,6058	0,6168	1,7870
24,02	0,6351	0,6458	1,6666
30,78	0,6646	0,6749	1,5358
36,99	0,6915	0,7017	1,4592
42,78	0,7175	0,7255	1,1083
48,24	0,7392	0,7463	0,9563
53,40	0,7571	0,7641	0,9165
58,36	0,7729	0,7794	0,8342
63,14	0,7859	0,7921	0,7800
67,79	0,7965	0,8026	0,7670
72,33	0,8050	0,8111	0,7485
76,78	0,8140	0,8175	0,4295
81,18	0,8223	0,8221	0,0310
85,54	0,8249	0,8248	0,0102
90,00	0,8254	0,8257	0,0425

4.3.3 Verification of mixed modes stress intensity factors of an inclined semi – elliptical surface crack

In the study of Noda et al. [37], the stress intensity factors along crack front of a 3D inclined semi-elliptical surface crack in a semi-infinite body under tension have been calculated by means of a singular integral equation method.

During the verification, equations (4.18), (4.25) and (4.28) have been used. The modulus of elasticity and the poisson's ratio of the material are 205000 MPa and 0,300. The ratio between major axis and minor axis of the semi-elliptical shape equals to 0.5. The model can be seen in figures 4.19, 4.20, 4.21 and 4.22.

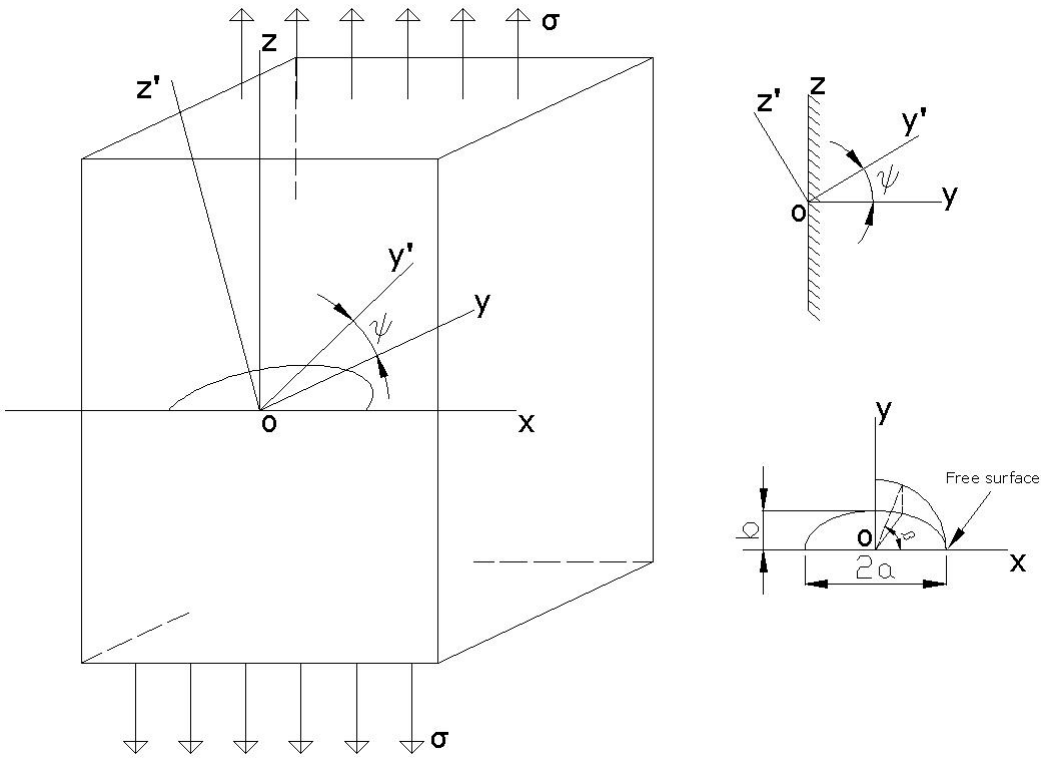

Figure 4.19 An inclined semi-elliptical surface crack in a semi-infinite body

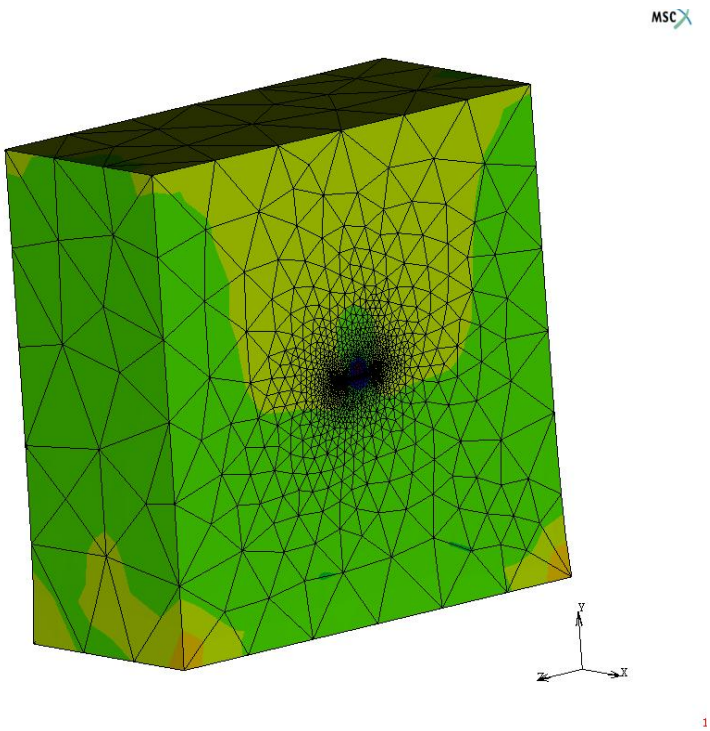

Figure 4.20 General view of the inclined semi-elliptical surface crack

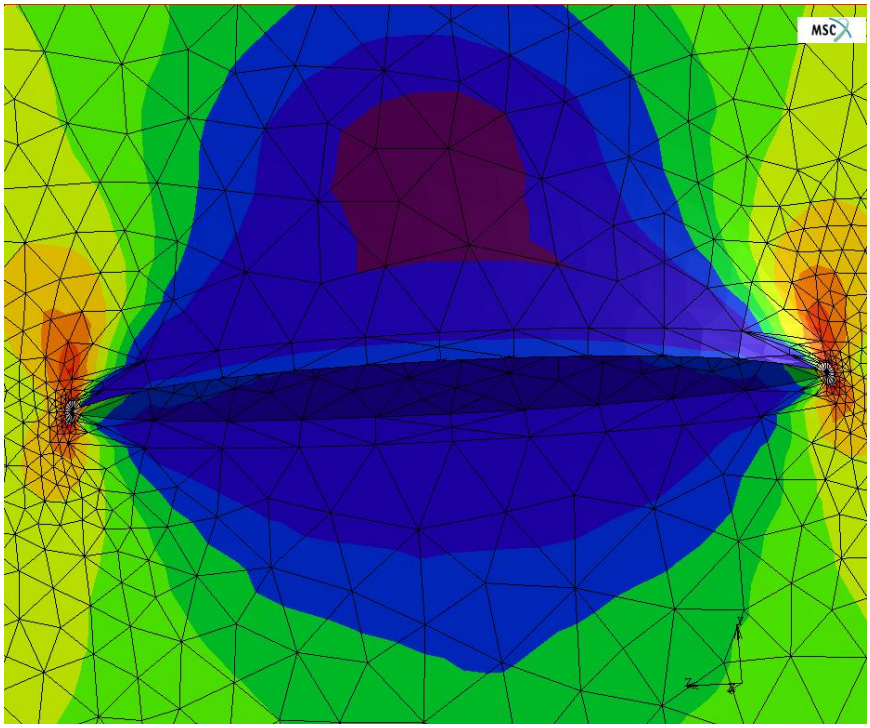

Figure 4.21 Stress concentrations during tensile loading for inclined crack

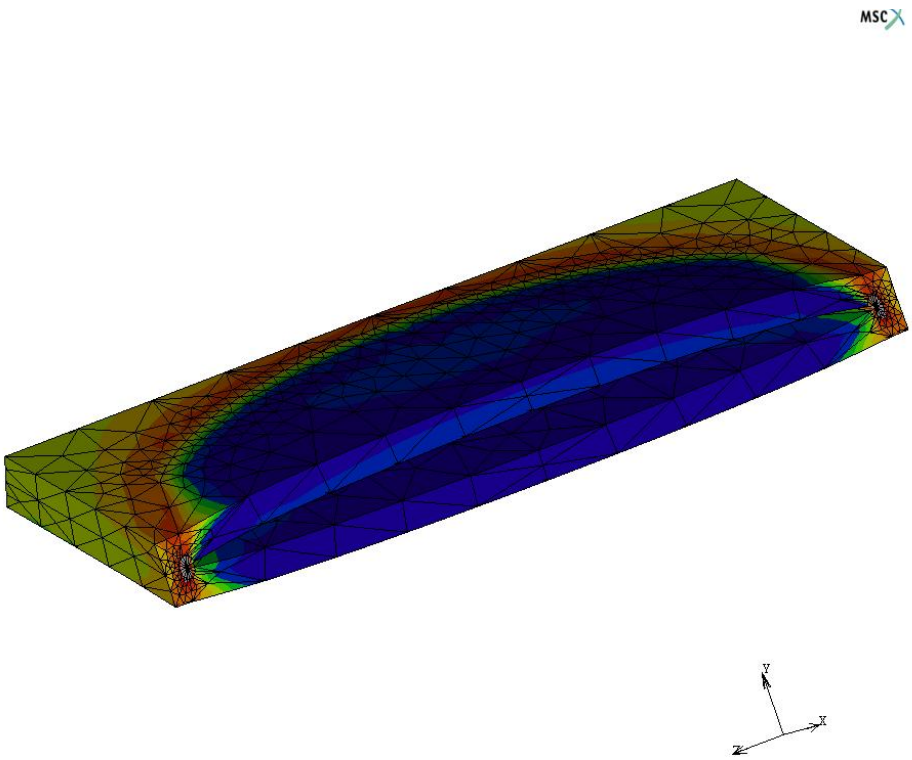

Figure 4.22 Close-up view of the crack opening

Table 4.3 $K_{I\ normalized}$ comparisons for an inclined semi-elliptical surface crack

β **(degree)**	***ψ*** **(degree)**	**Present study**	**Noda's Solution [37]**	**Difference (%)**
90	15	0,8556	0,8444	1,33
90	30	0,7295	0,2797	0,84
90	45	0,5858	0,5816	0,73
90	60	0,4019	0,4204	4,40
79	15	0,8339	0,8407	0,81
79	30	0,7323	0,7320	0,04
79	45	0,5810	0,5725	1,48
79	60	0,3971	0,4093	2,99

Table 4.4 $K_{II\ normalized}$ comparisons for an inclined semi-elliptical surface crack

β **(degree)**	***ψ*** **(degree)**	**Present study**	**Noda's Solution [37]**	**Difference (%)**
90	15	0,1580	0,1577	0,19
90	30	0,2740	0,2797	2,00
90	45	0,3373	0,3399	0,77
90	60	0,3129	0,3303	5,28
79	15	0,1485	0,1521	2,35
79	30	0,2694	0,2707	0,50
79	45	0,3269	0,3273	0,11
79	60	0,3136	0,3128	0,26

Table 4.5 $K_{III\ normalized}$ comparisons for an inclined semi-elliptical surface crack

β **(degree)**	***ψ*** **(degree)**	**Present study**	**Noda's Solution [37]**	**Difference (%)**
90	15	0,0023	0	N/A
90	30	0,0025	0	N/A
90	45	0,0008	0	N/A
90	60	0,0016	0	N/A
79	15	0,0250	0,0251	0,58
79	30	0,0443	0,0471	5,86
79	45	0,0562	0,0649	13,44
79	60	0,0515	0,0921	44,09

4.3.4 Conclusion

As can be seen from the comparison tables 4.1, 4.2, 4.3, 4.4 and 4.5, computed stress intensity factors are approximately the same with referred values except near the free surface for large inclination angle. From these results, it is easily said that displacement correlation technique is suitable in order to find out the stress intensity factors along crack front of a 3D model and equations (4.18), (4.25) and (4.28) can be used for these types of problems.

CHAPTER 5

NUMERICAL RESULTS AND DISCUSSION

5.1 Introduction

In this chapter, implementation of the displacement correlation technique is carried out and the numerical results obtained are presented. For this purpose, the mixed modes stress intensity factors; K_I, K_{II} and K_{III}, and energy release rate, G, are studied for a range of crack angles, ψ, at various crack locations in the test specimen. K_I, K_{II}, K_{III} and G are found along the crack front at 0, $\pi/6$, $\pi/3$, $\pi/2$ angles (β). The specimen is examined by considering axial and bending types of loading. The effects of the crack geometry, crack place and weld geometry on the mixed modes stress intensity factors and energy release rate are examined in figures 5.1 – 5.96 for a crack subjected to uniform stress and bending load. As mentioned in chapter 4, crack depth is depicted by a; crack length by c; base material thickness by $t1$. In the figures, the normalization constants for the mixed modes stress intensity factors and energy release rate are $K_o = \sigma_o (\pi c)^{1/2}$ and $G_o = \sigma_o^2 (\pi c) / E_o$ for uniform tension, $K_o = \sigma_b (\pi c)^{1/2}$ and $G_o = \sigma_b^2 (\pi c) / E_o$ for bending load.

5.2 Mechanical Loading on the T-shaped Specimen

In this section, two different mechanical loading types, namely uniform tension and bending, are considered to be applied to the T-shaped

specimen. The normalized K_I, K_{II}, K_{III} and G are computed for various parameters of the specimen. Finite element analyses are carried out by the material with 200000 MPa of modulus of elasticity and 0.29 of poisson's ratio.

5.2.1 Uniform Tension

In this section, T-shaped specimen is assumed to be subjected to uniform tension σ at the ends of the specimen as shown in figure 5.1. The stress equals to 100 MPa.

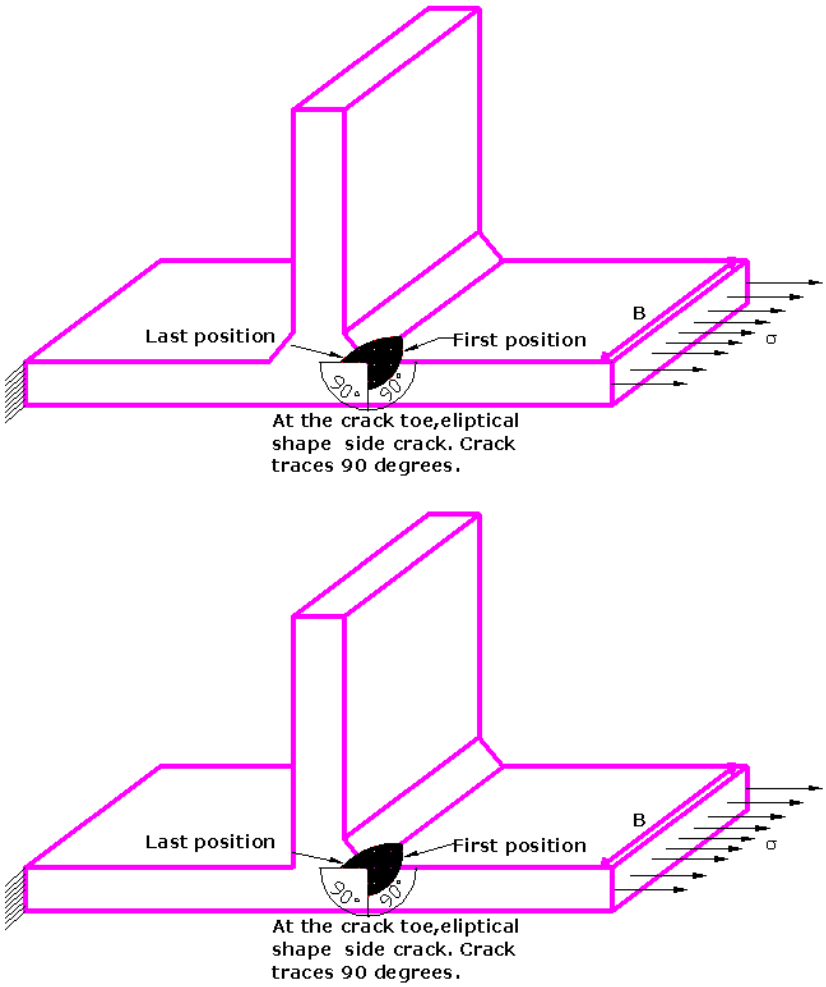

Figure 5.1 Uniform tension σ at the ends of the T-shaped specimen

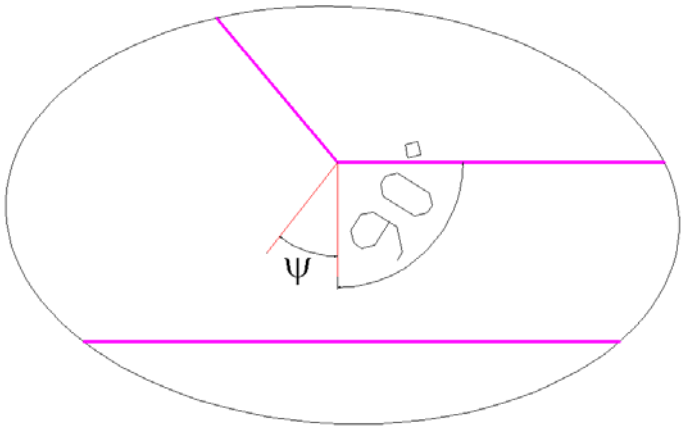

Figure 5.2 Trace angle (ψ)

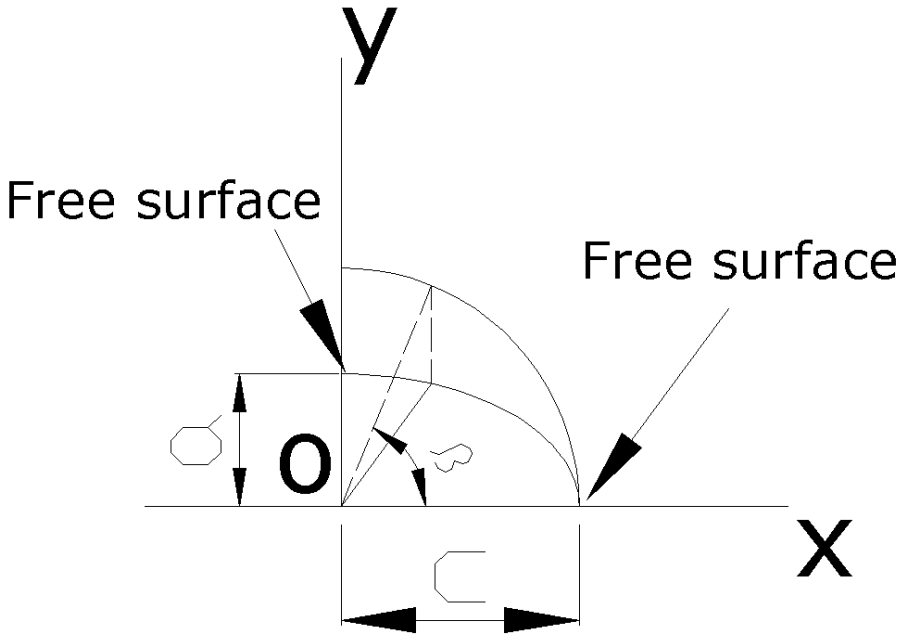

Figure 5.3 Parametric view of the crack front

5.2.1.1 Loading of a Crack at the Side of the Weld Toe

In this section, a specimen that is constructed with a crack at the side part of the weld toe is subjected to tensile loading. Crack dimensions are identified as parameters of the base sheet metal. The normalized K_I, K_{II}, K_{III} and G for four β (Figure 5.3) are presented in the following figures 5.4 – 5.19.

In Figures 5.1-5.16, the variations of the normalized stress intensity factors and normalized energy release rate are plotted with respect to normalized crack angle, $2\psi/\pi$. In all these plots, it can be seen that the normalized mixed modes stress intensity factors and normalized energy release rate have nearly the same behavior whether the specimen has the double-sided fillet weld or one-sided fillet weld for this type of loading. The maximum and the minimum normalized stress intensity factor are obtained at free surfaces $\beta=\pi/2$ and $\beta=0$. The normalized mode I stress intensity factor and the normalized energy release rate have a tendency to decrease with the rise of the crack angle. On the other hand, the normalized mode II, mode III stress intensity factors rise up when the crack angle increases. The main difference occurs at $\beta=\pi/2$ and $\psi=0$ for the normalized mode I SIF.

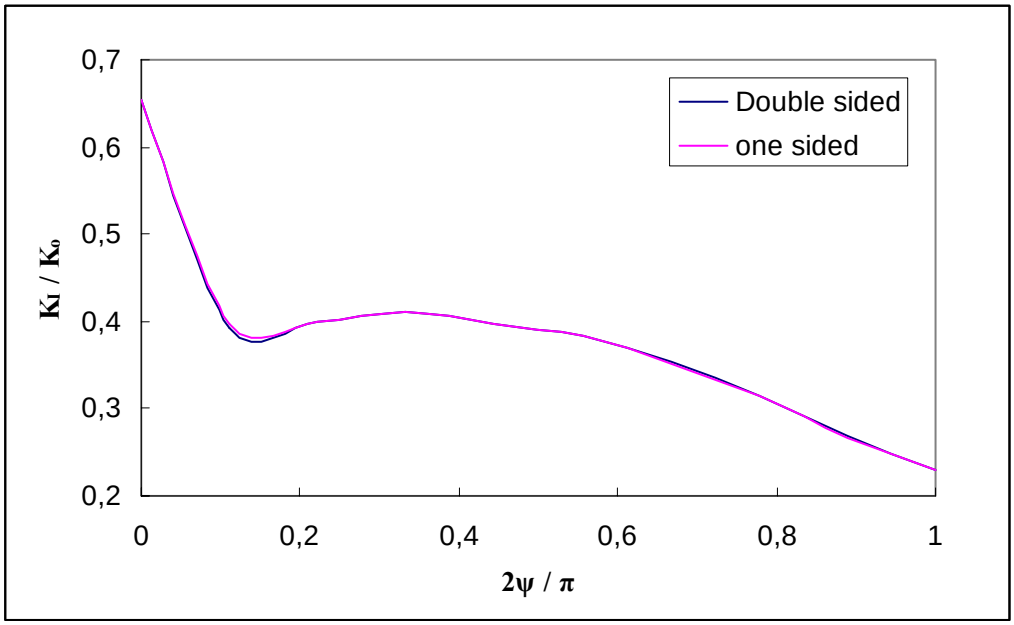

Figure 5.4 Normalized mode I SIF versus crack angle parameter ψ and the weld option parameter for a surface crack, β=0, $a / t1$=0.1, $c / t1$=0.3.

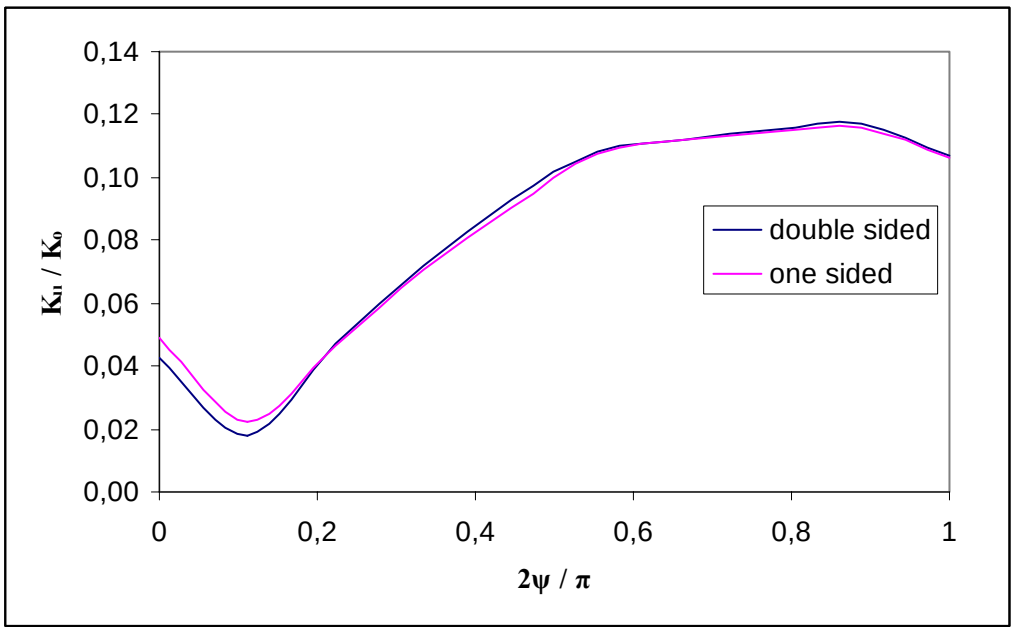

Figure 5.5 Normalized mode II SIF versus crack angle parameter ψ and the weld option parameter for a surface crack, β=0, $a / t1$=0.1, $c / t1$=0.3.

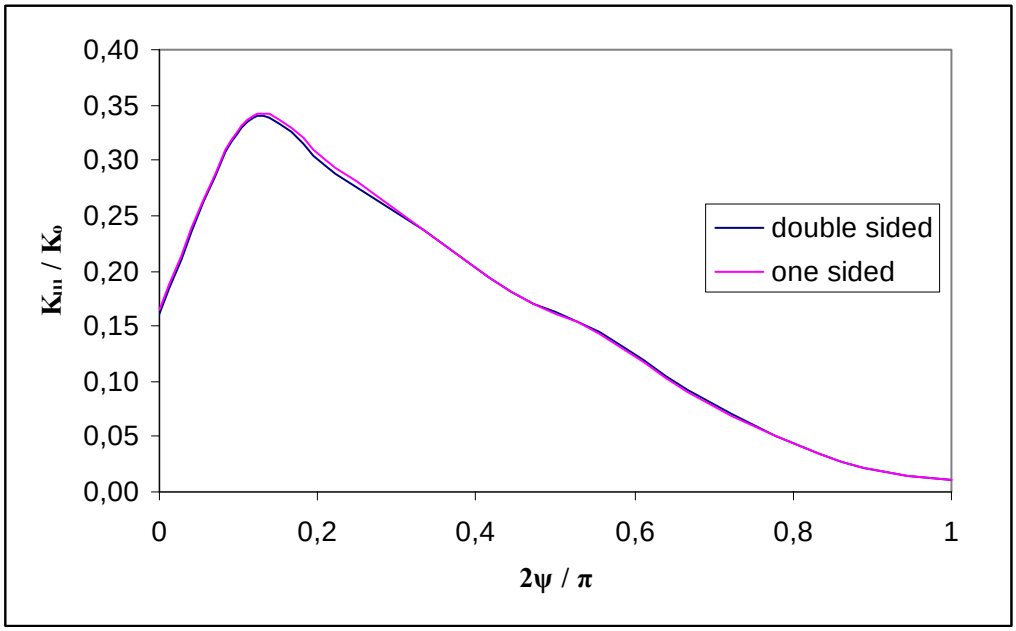

Figure 5.6 Normalized mode III SIF versus crack angle parameter ψ and the weld option parameter for a surface crack, β=0, *a / t1*=0.1, *c / t1*=0.3.

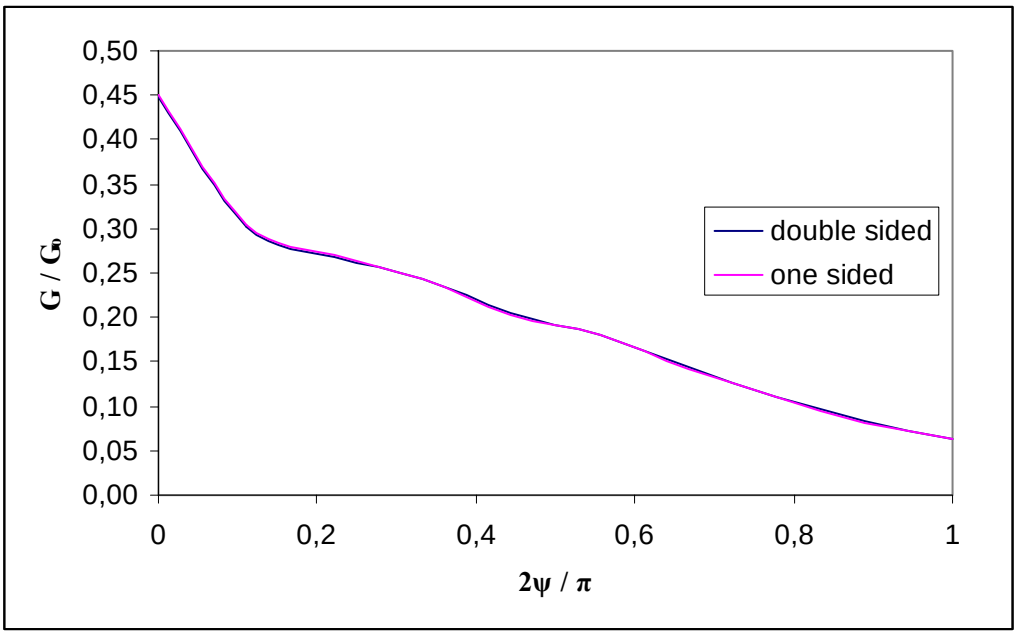

Figure 5.7 Normalized energy release rate versus crack angle parameter ψ and the weld option parameter for a surface crack, β=0, *a / t1*=0.1, *c / t1*=0.3.

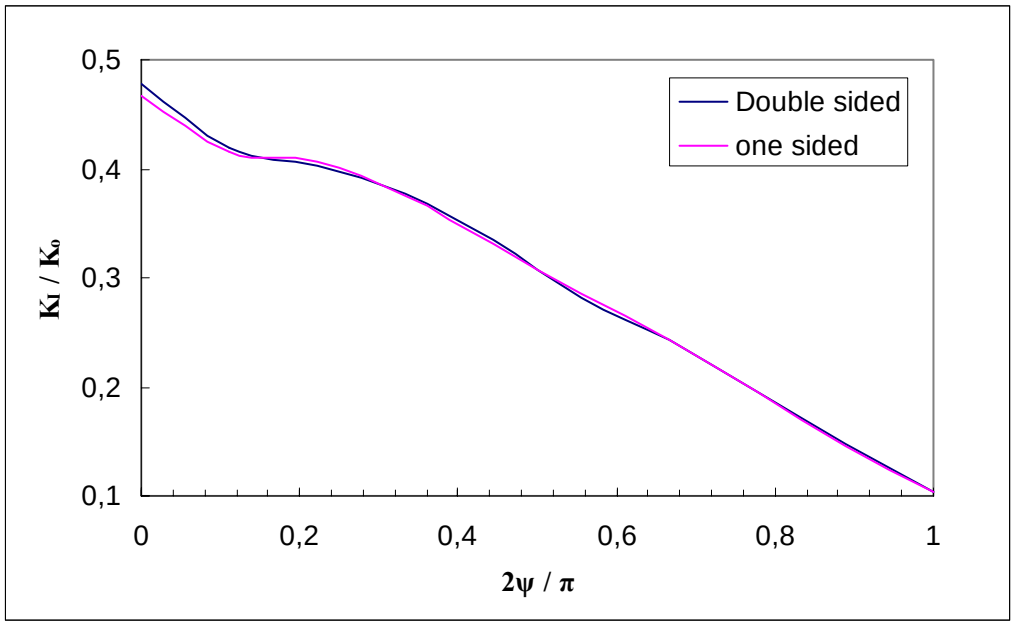

Figure 5.8 Normalized mode I SIF versus crack angle parameter ψ and the weld option parameter for a surface crack, $\beta=\pi/6$, $a / t1=0.1$, $c / t1=0.3$.

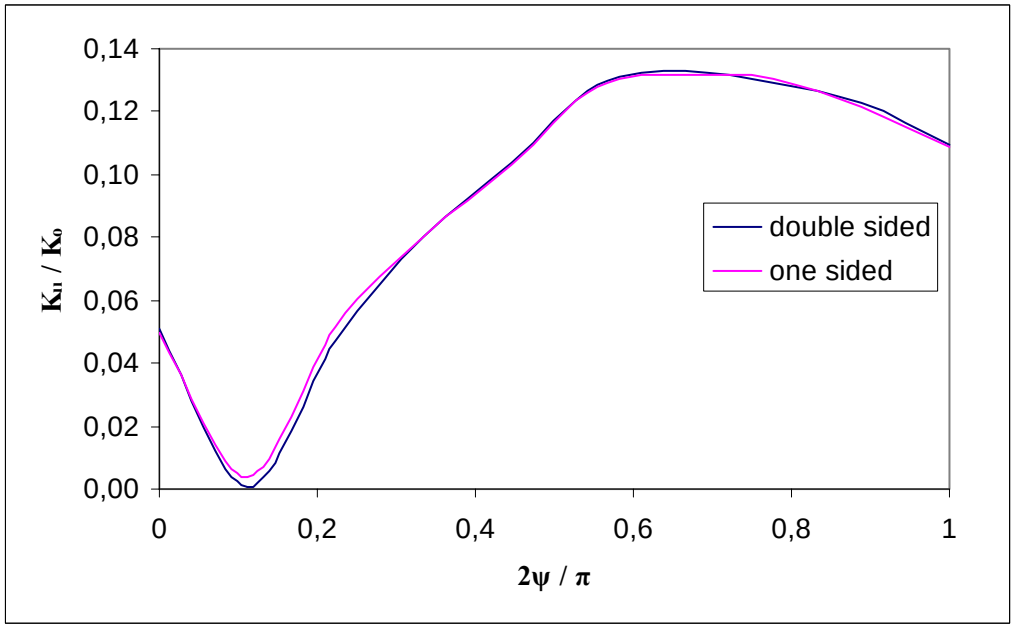

Figure 5.9 Normalized mode II SIF versus crack angle parameter ψ and the weld option parameter for a surface crack, $\beta= \pi/6$, $a / t1=0.1$, $c / t1=0.3$.

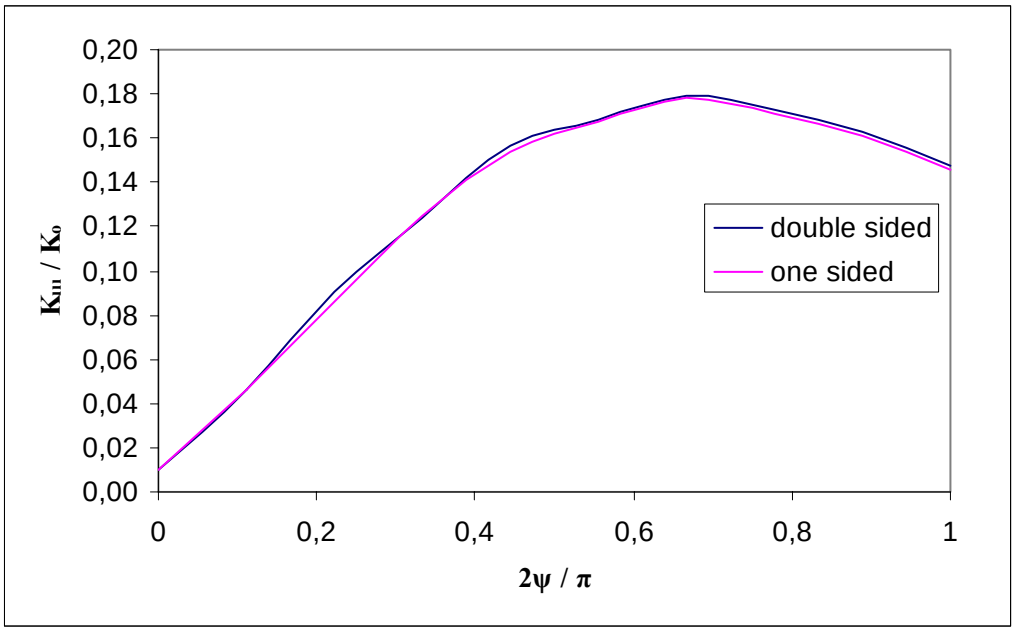

Figure 5.10 Normalized mode III SIF versus crack angle parameter ψ and the weld option parameter for a surface crack, $\beta = \pi/6$, $a / t1$=0.1, $c / t1$=0.3.

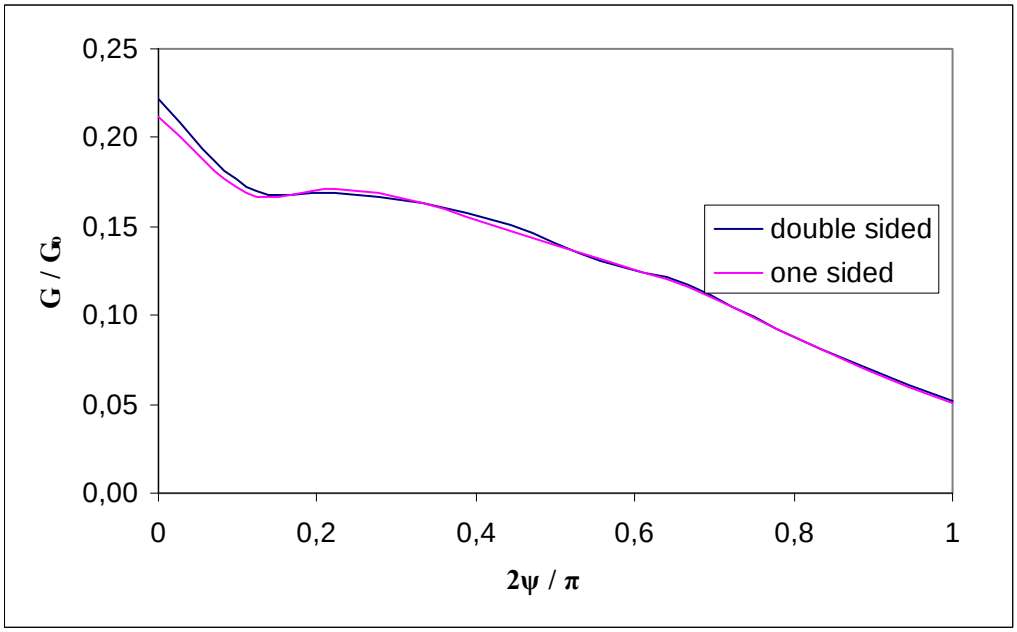

Figure 5.11 Normalized energy release rate versus crack angle parameter ψ and the weld option parameter for a surface crack, $\beta = \pi/6$, $a/t1$=0.1, $c/t1$=0.3.

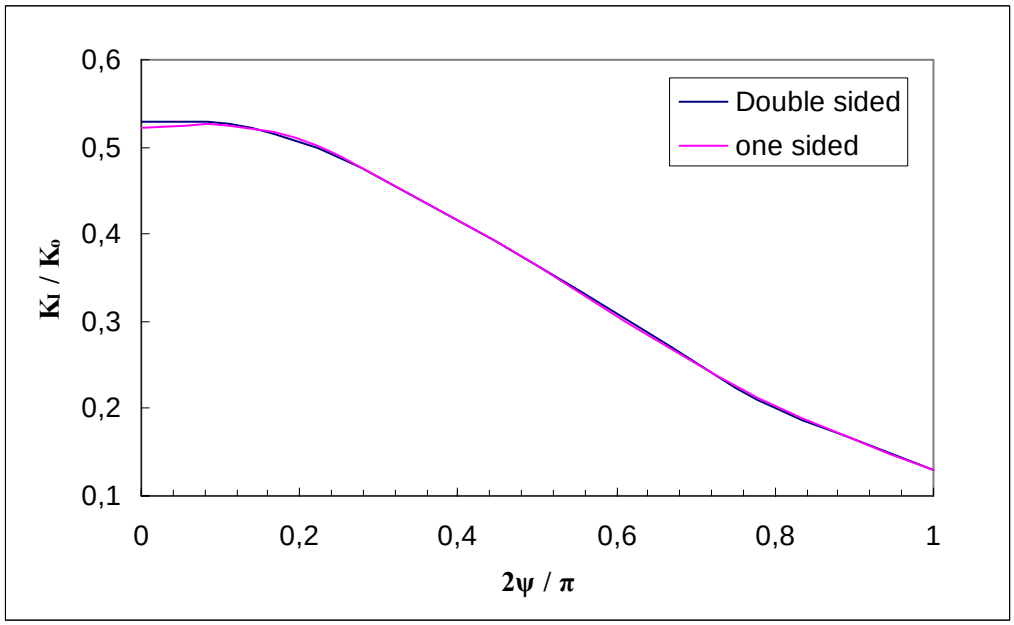

Figure 5.12 Normalized mode I SIF versus crack angle parameter ψ and the weld option parameter for a surface crack, $\beta=\pi/3$, $a / t1=0.1$, $c / t1=0.3$.

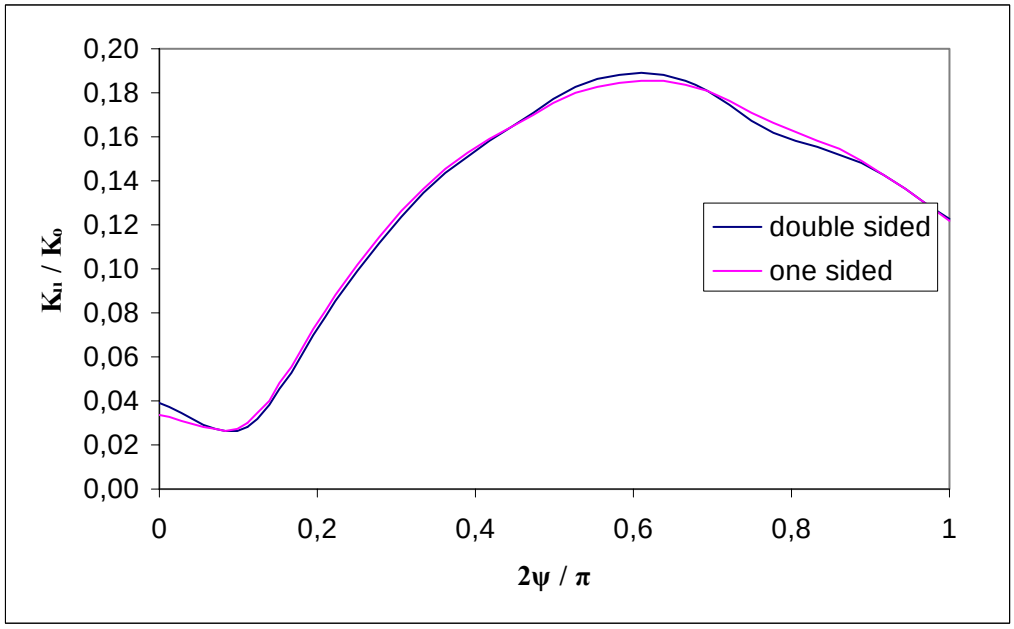

Figure 5.13 Normalized mode II SIF versus crack angle parameter ψ and the weld option parameter for a surface crack, $\beta= \pi/3$, $a / t1=0.1$, $c / t1=0.3$.

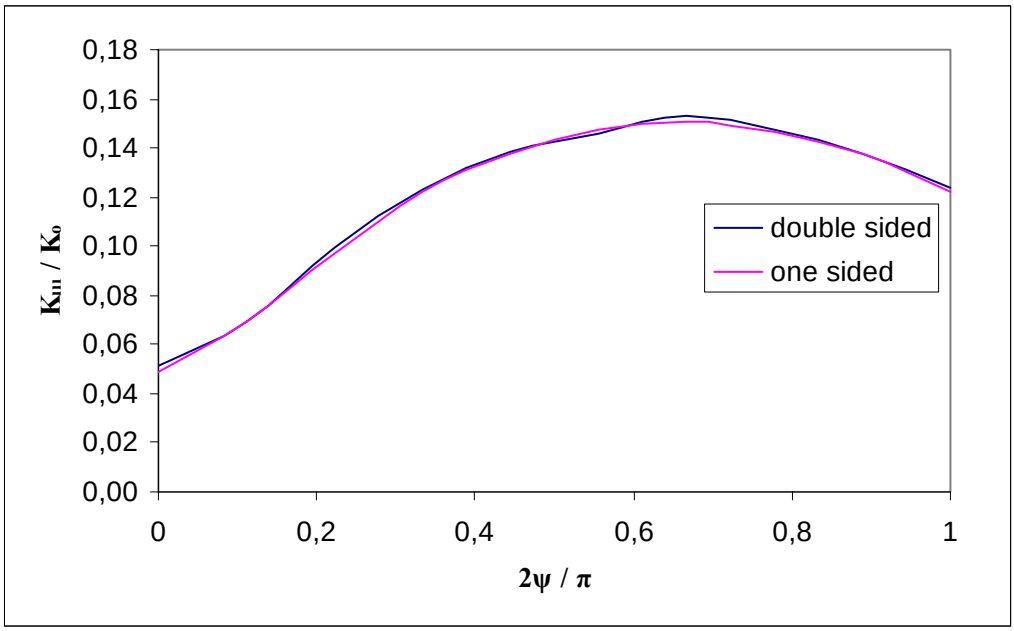

Figure 5.14 Normalized mode III SIF versus crack angle parameter ψ and the weld option parameter for a surface crack, $\beta = \pi/3$, $a / t1$=0.1, $c / t1$=0.3.

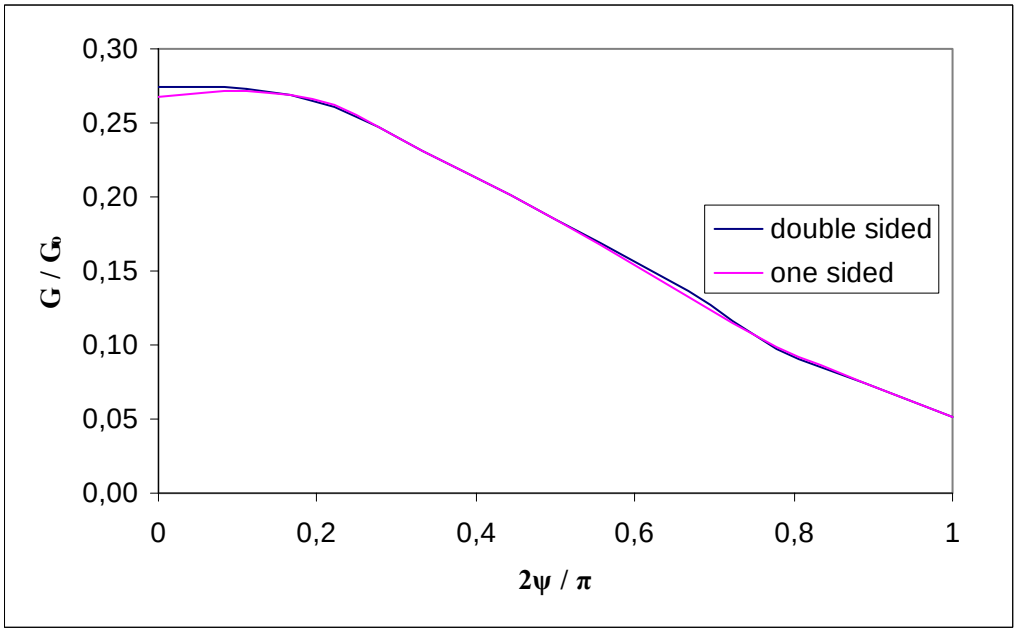

Figure 5.15 Normalized energy release rate versus crack angle parameter ψ and the weld option parameter for a surface crack, $\beta = \pi/3$, $a/t1$=0.1, $c/t1$=0.3.

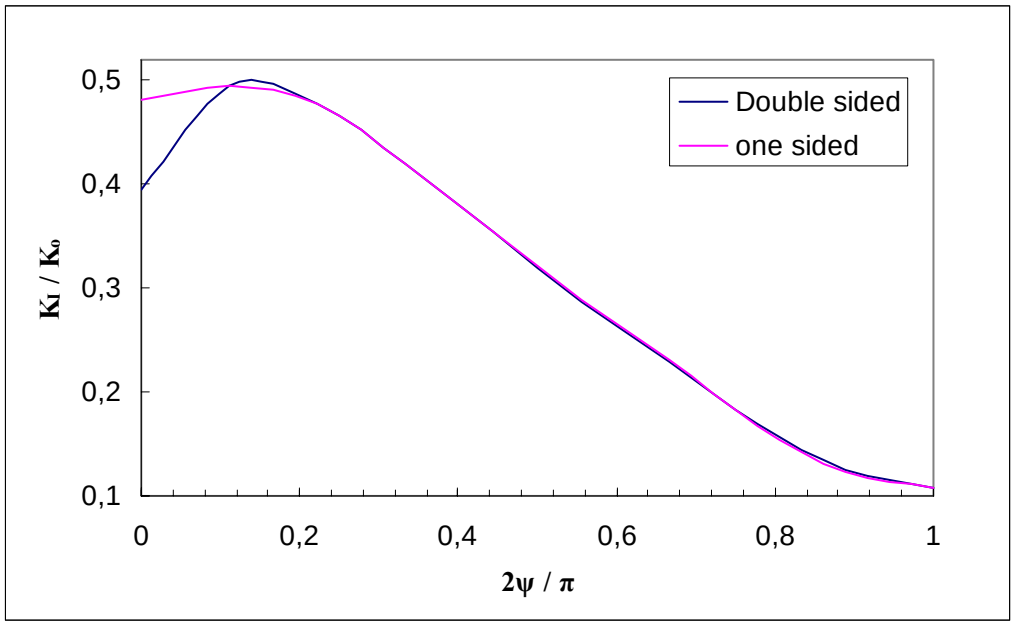

Figure 5.16 Normalized mode I SIF versus crack angle parameter ψ and the weld option parameter for a surface crack, $\beta=\pi/2$, $a / t1=0.1$, $c / t1=0.3$.

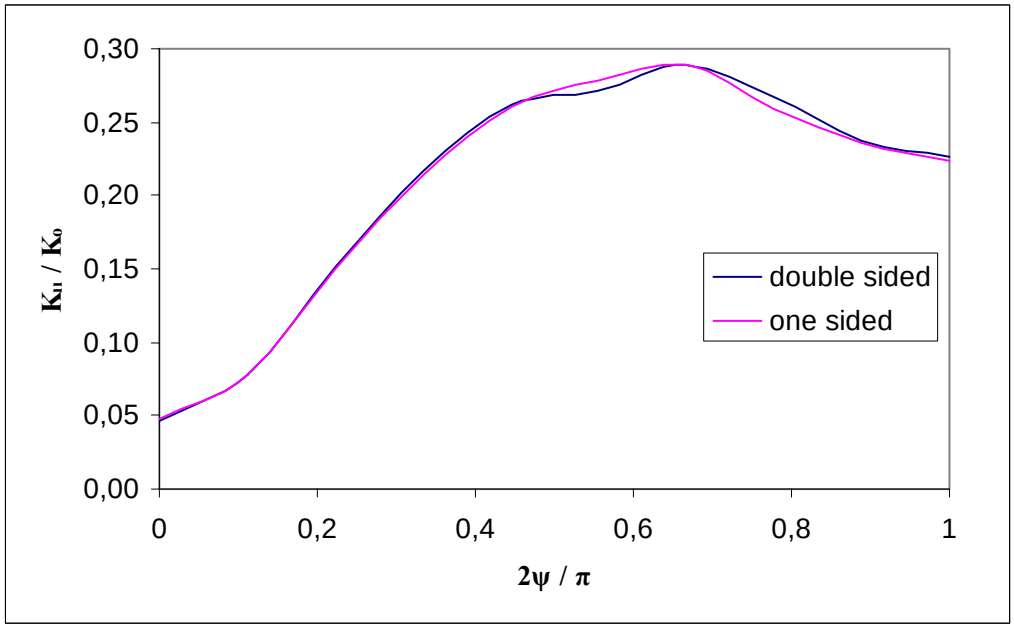

Figure 5.17 Normalized mode II SIF versus crack angle parameter ψ and the weld option parameter for a surface crack, $\beta= \pi/2$, $a / t1=0.1$, $c / t1=0.3$.

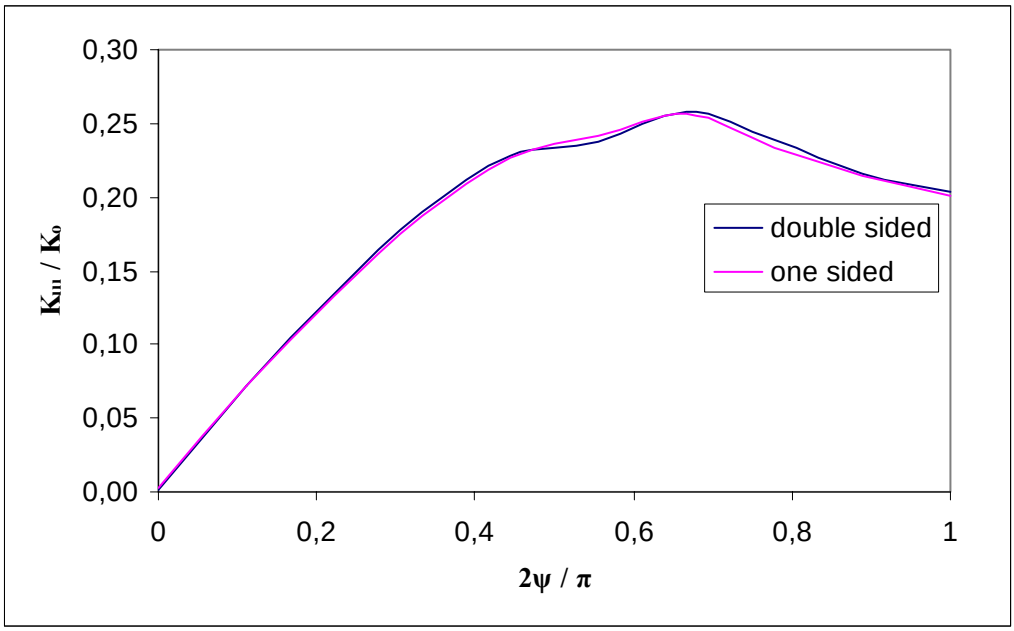

Figure 5.18 Normalized mode III SIF versus crack angle parameter ψ and the weld option parameter for a surface crack, $\beta = \pi/2$, $a / t1$=0.1, $c / t1$=0.3.

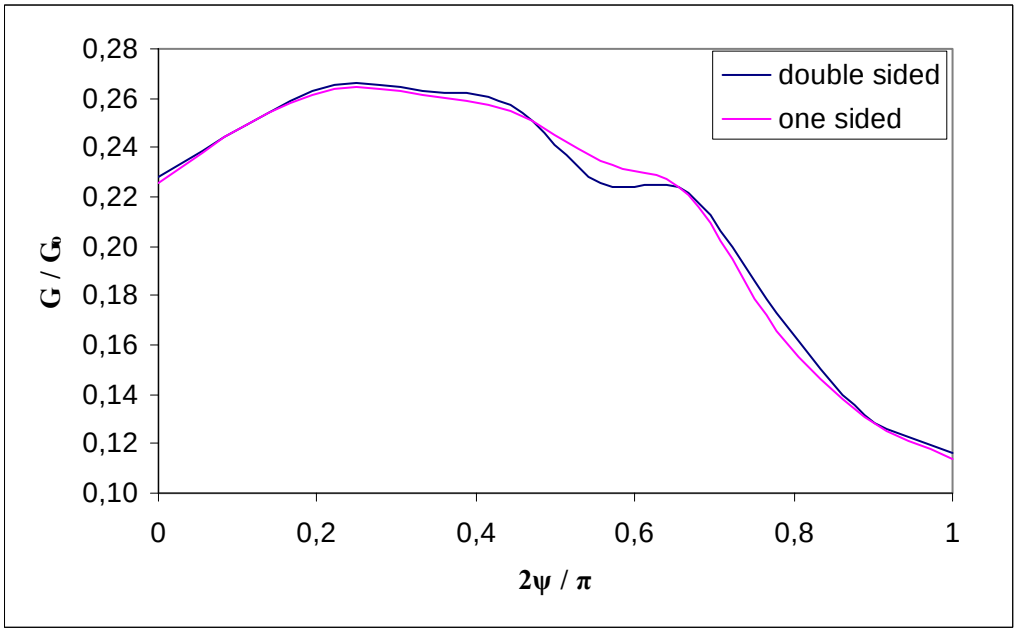

Figure 5.19 Normalized energy release rate versus crack angle parameter ψ and the weld option parameter for a surface crack, $\beta = \pi/2$, $a/t1$=0.1, $c/t1$=0.3.

5.2.1.2 Loading of a Crack at the Side of the Weld Toe for Various Weld Shape

In this section, a specimen with various weld geometry that is constructed with a crack at the side part of the weld toe is subjected to tensile loading. Crack dimensions are identified as parameters of the base sheet metal and the weld geometry is defined as K_v=12 mm and K_h=10, 11, 12, 13, 14 mm (Figure 5.20). The normalized K_I, K_{II}, K_{III} and G for four β (Figure 5.3) are presented in the following figures 5.21 – 5.36.

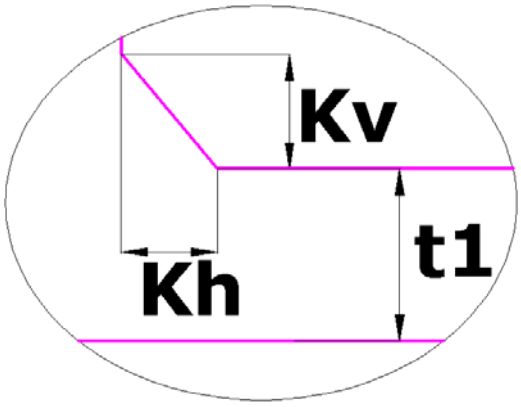

Figure 5.20 Dimensions of the weld

In Figures 5.21-5.36, the variations of the normalized stress intensity factors and normalized energy release rate are plotted with respect to normalized crack angle, $2\psi/\pi$ for different weld geometry with respect to horizontal leg of the fillet weld (K_h). In all these plots, it can be seen that the normalized mode I stress intensity factor has nearly the same behavior for various weld geometry. However, as normalized ψ approaches to unit value, the higher K_h

values reduce the normalized mode II, mode III stress intensity factors and the normalized energy release rate compared to lower ones. The normalized mode II and mode III stress intensity factors reach the maximum point at nearly half of the crack angle. The main difference occurs at $\beta = \pi/2$ and $\psi = 0$ for the normalized mode I SIF and the maximum values of the normalized K_I, K_{II}, K_{III} and G are seen at $\beta = 0$ and $\psi = 0$, free end of the specimen. No crack closure is observed during the calculations.

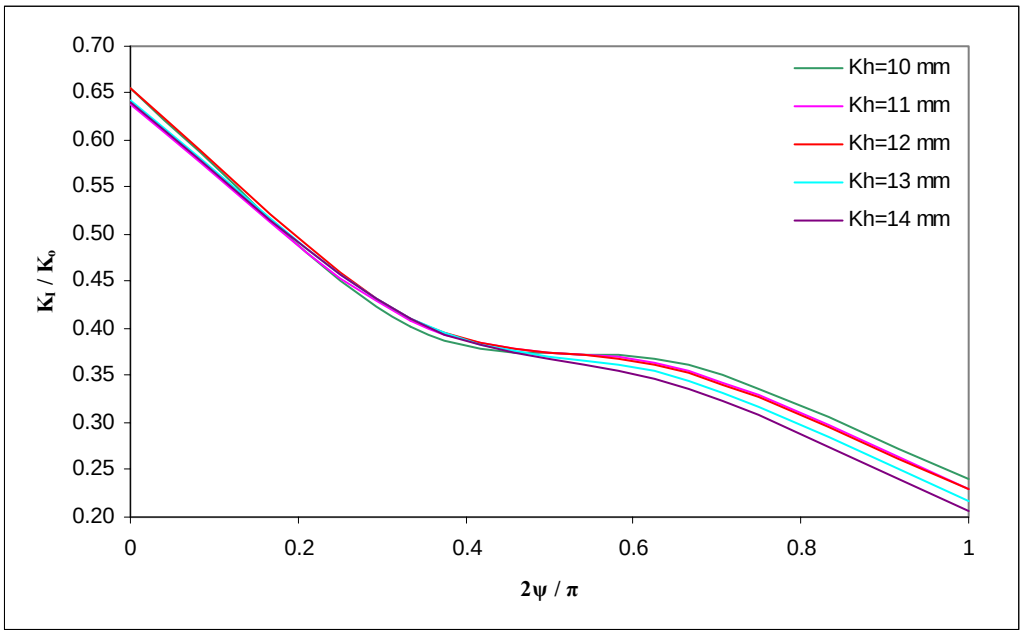

Figure 5.21 Normalized mode I SIF versus crack angle parameter ψ for a surface crack, β=0, $a / t1$=0.1, $c / t1$=0.3, K_V=12 mm.

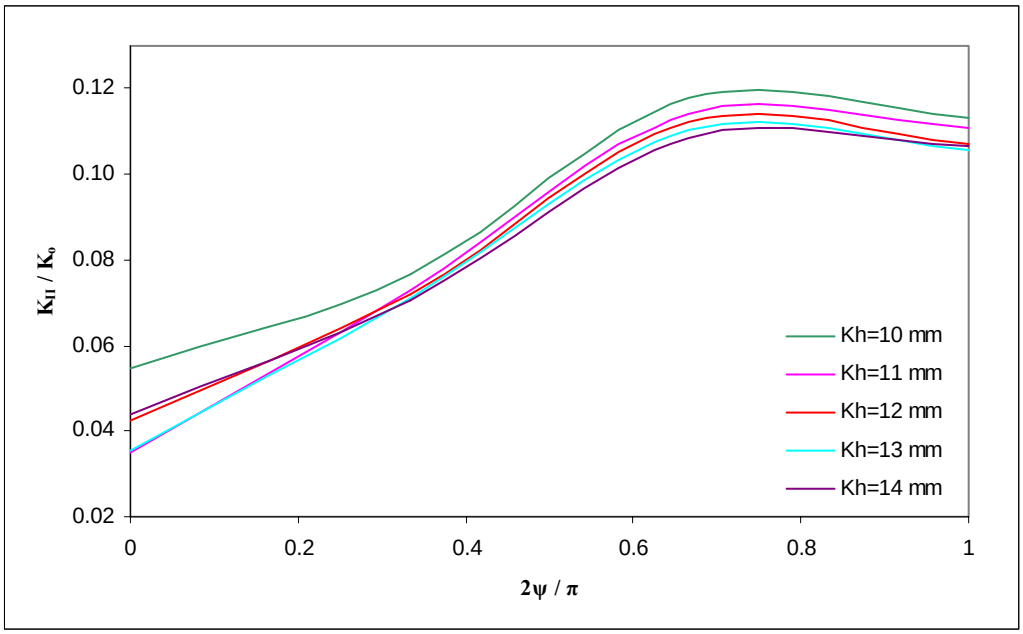

Figure 5.22 Normalized mode II SIF versus crack angle parameter ψ for a surface crack, β=0, $a / t1$=0.1, $c / t1$=0.3, K_V=12 mm.

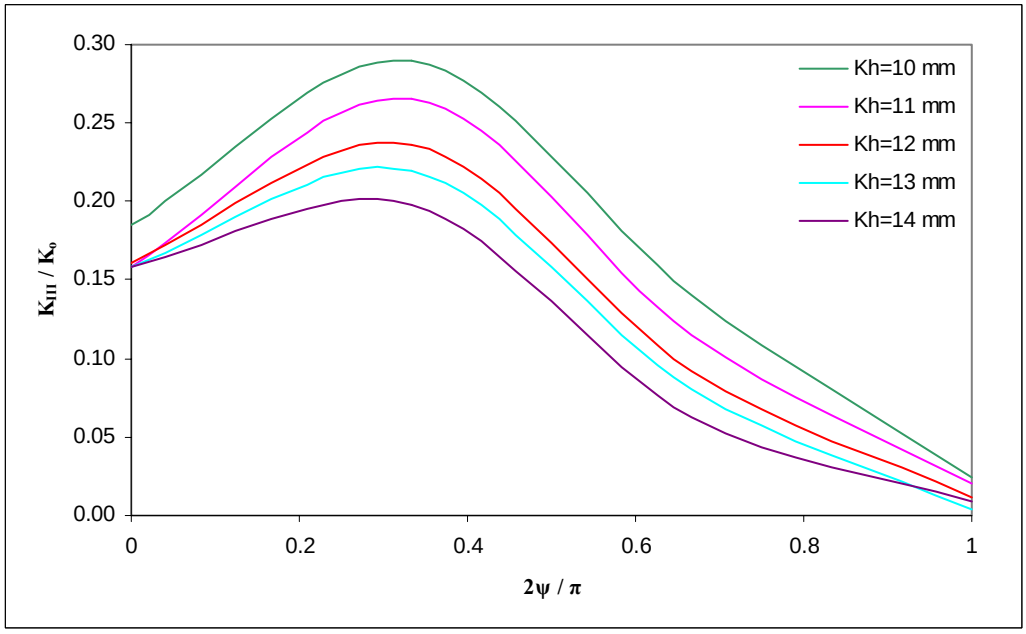

Figure 5.23 Normalized mode III SIF versus crack angle parameter ψ for a surface crack, β=0, $a / t1$=0.1, $c / t1$=0.3, K_V=12 mm.

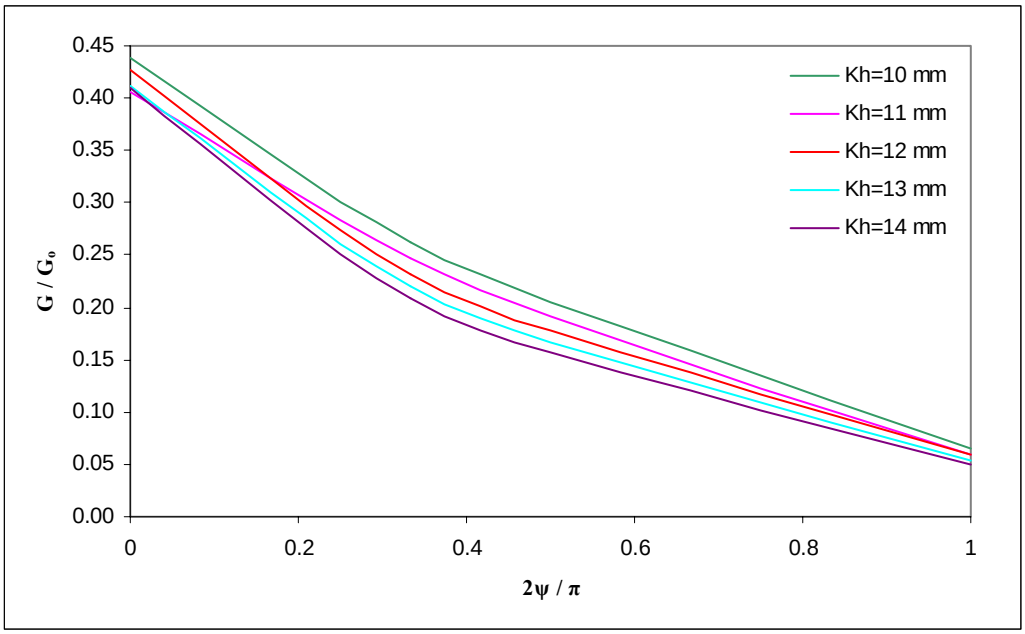

Figure 5.24 Normalized energy release rate versus crack angle parameter ψ for a surface crack, β=0, a / $t1$=0.1, c / $t1$=0.3, K_V=12 mm.

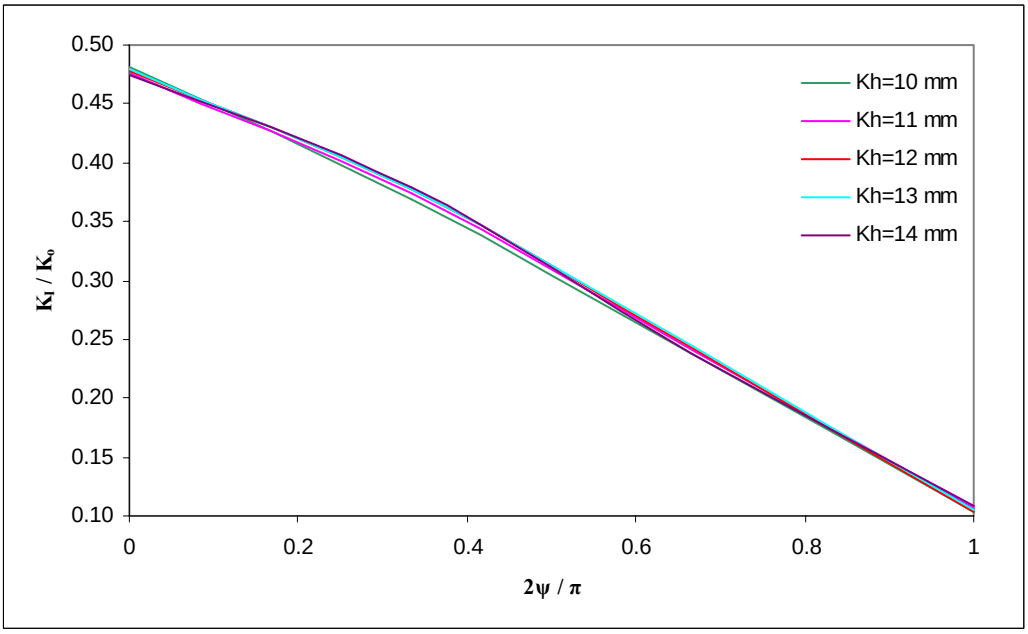

Figure 5.25 Normalized mode I SIF versus crack angle parameter ψ for a surface crack, β=π/6, a / $t1$=0.1, c / $t1$=0.3, K_V=12 mm.

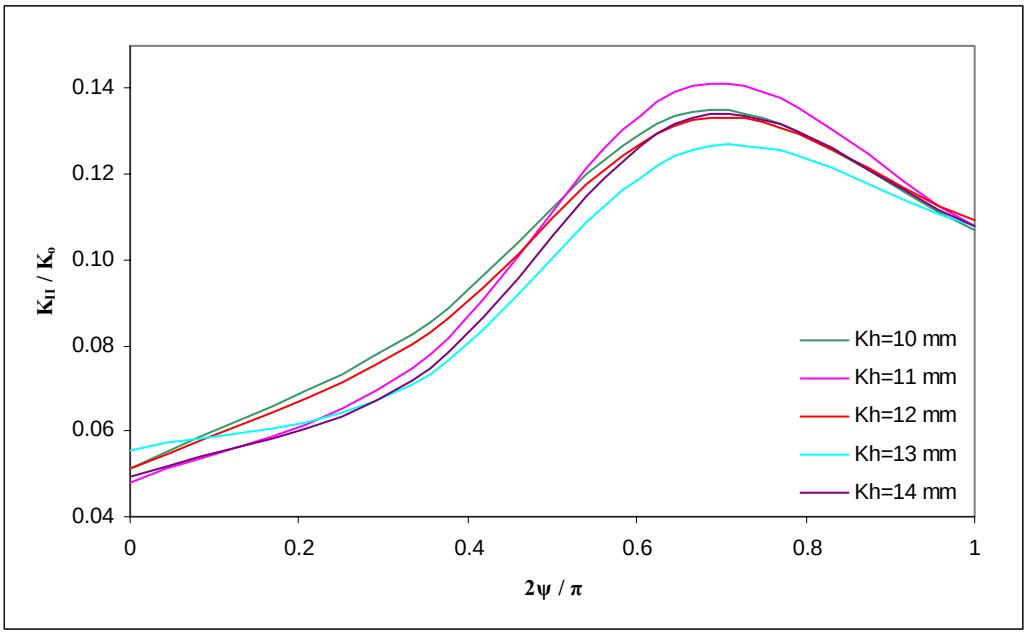

Figure 5.26 Normalized mode II SIF versus crack angle parameter ψ for a surface crack, β=π/6, a / $t1$=0.1, c / $t1$=0.3, K_v=12 mm.

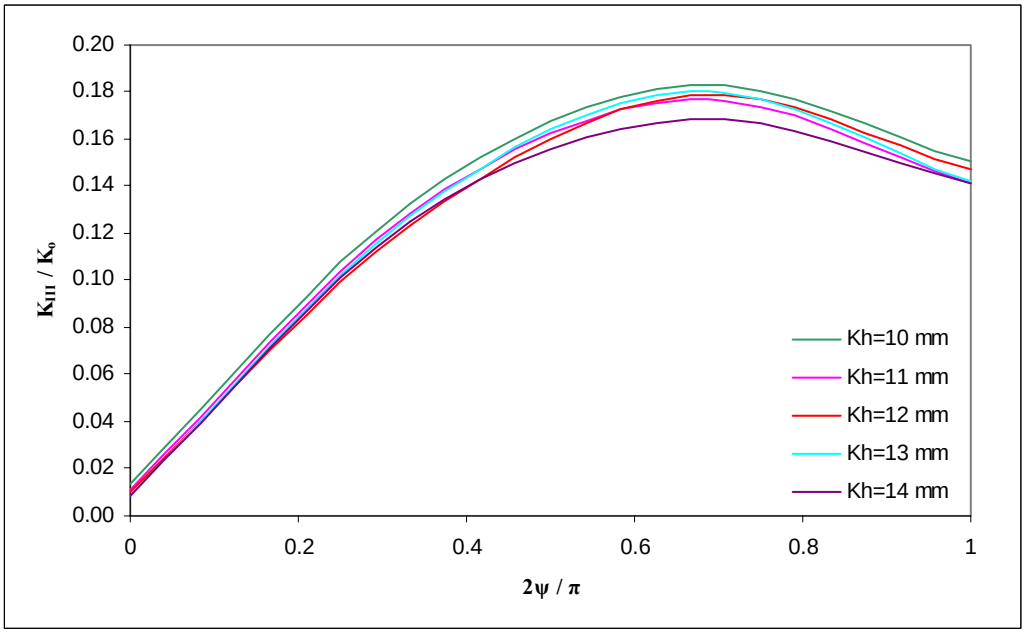

Figure 5.27 Normalized mode III SIF versus crack angle parameter ψ for a surface crack, β=π/6, a / $t1$=0.1, c / $t1$=0.3, K_v=12 mm.

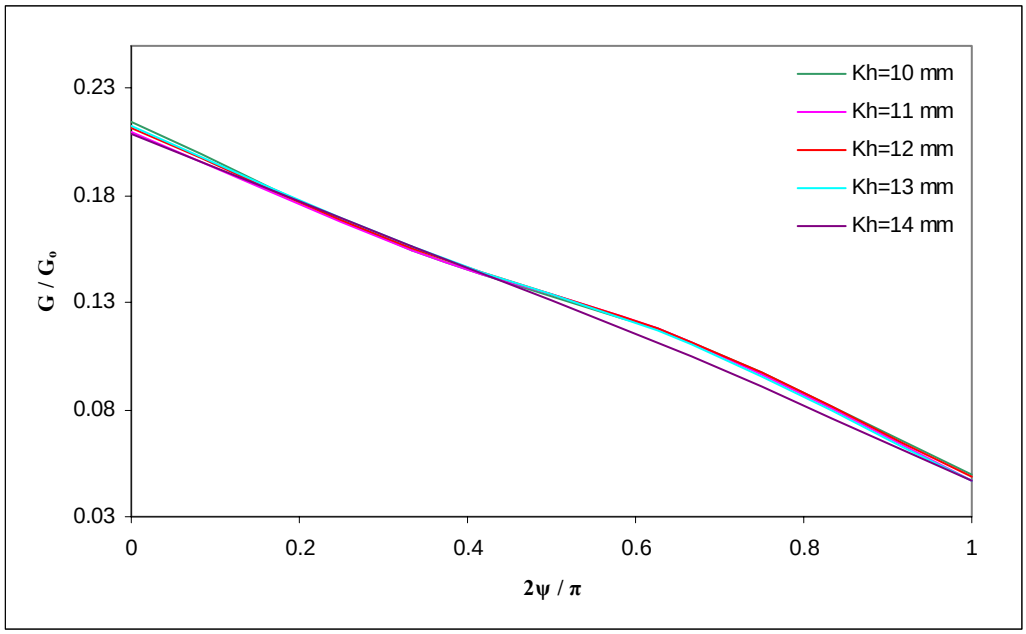

Figure 5.28 Normalized energy release rate versus crack angle parameter ψ for a surface crack, $\beta=\pi/6$, $a / t1=0.1$, $c / t1=0.3$, $K_v=12$ mm.

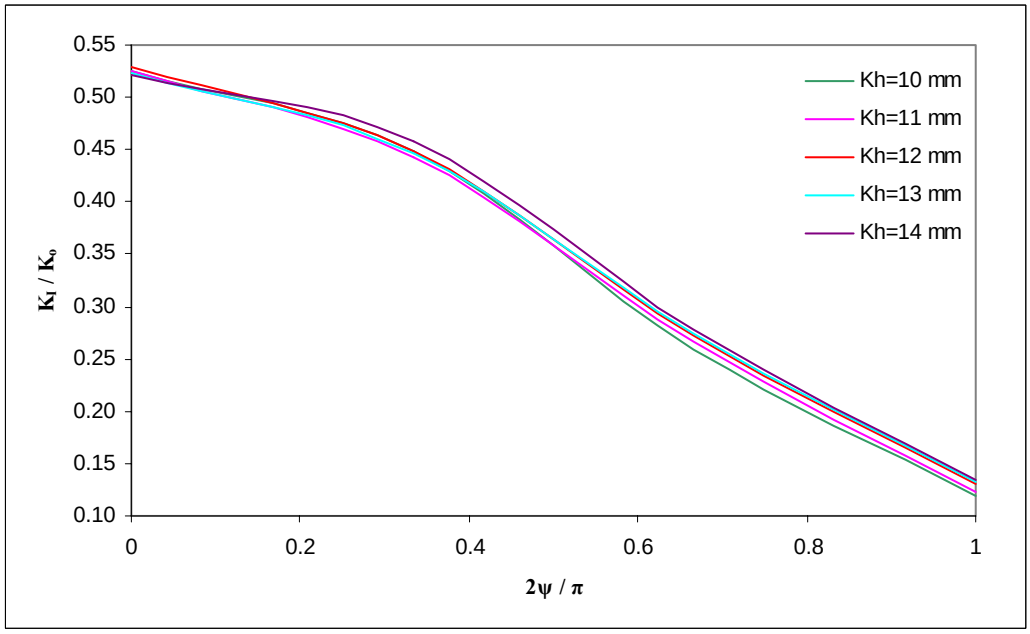

Figure 5.29 Normalized mode I SIF versus crack angle parameter ψ for a surface crack, $\beta=\pi/3$, $a / t1=0.1$, $c / t1=0.3$, $K_v=12$ mm.

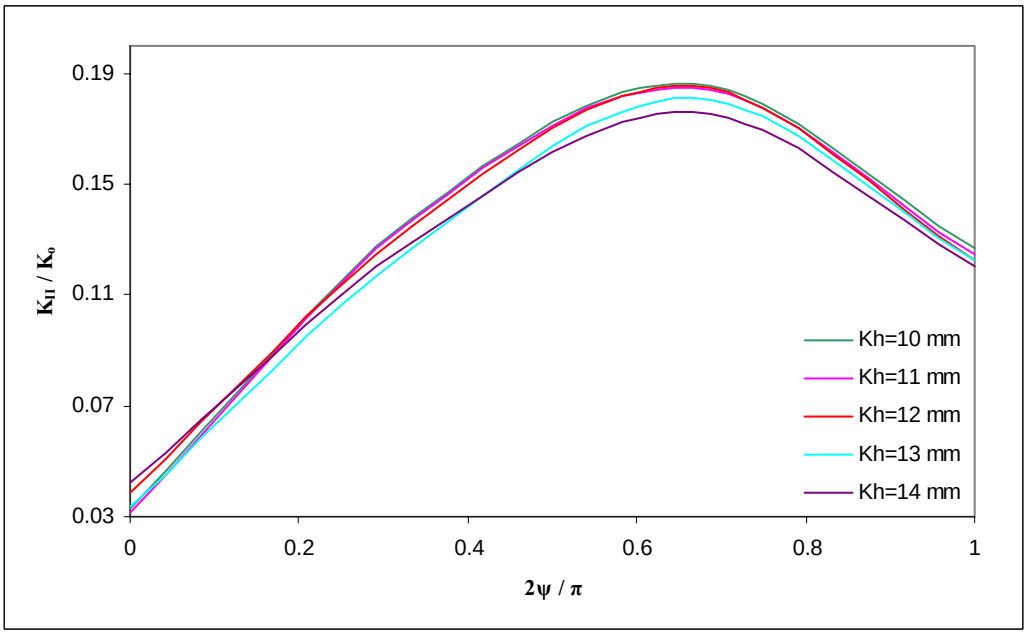

Figure 5.30 Normalized mode II SIF versus crack angle parameter ψ for a surface crack, β=π/3, a / $t1$=0.1, c / $t1$=0.3, K_V=12 mm.

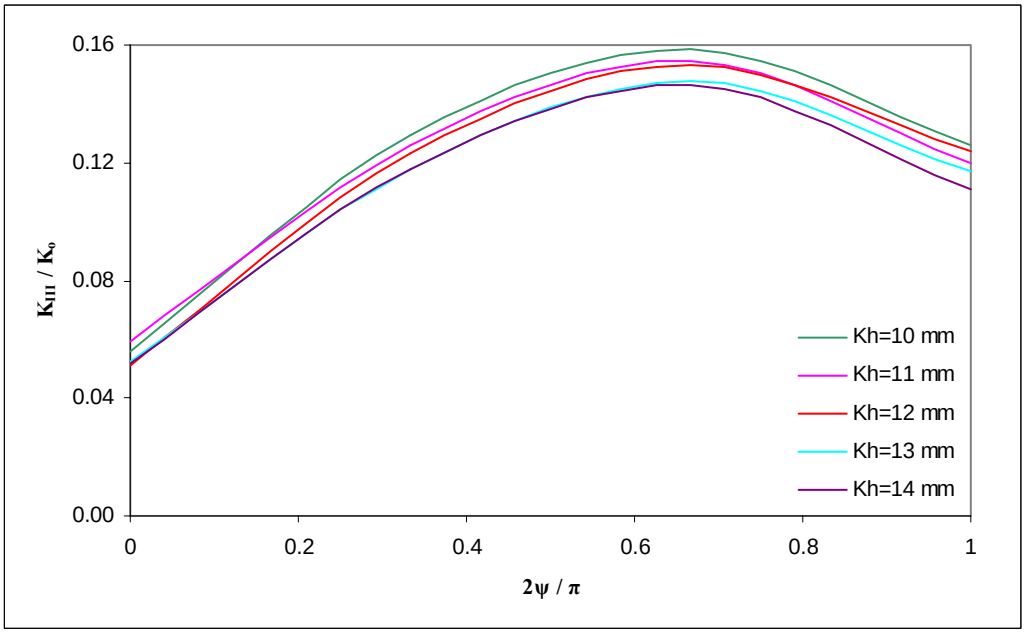

Figure 5.31 Normalized mode III SIF versus crack angle parameter ψ for a surface crack, β=π/3, a / $t1$=0.1, c / $t1$=0.3, K_V=12 mm.

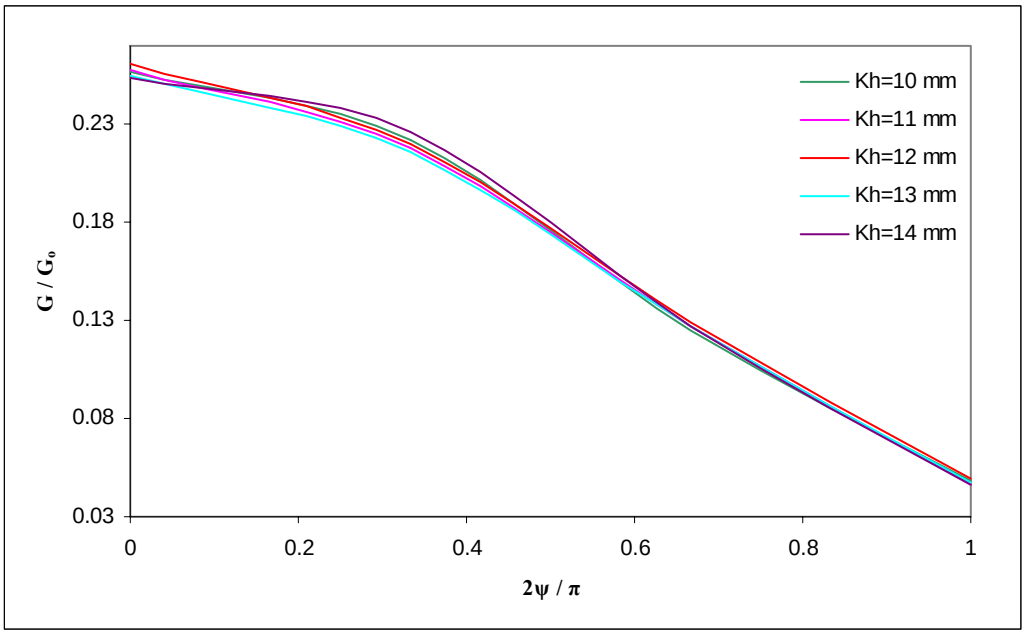

Figure 5.32 Normalized energy release rate versus crack angle parameter ψ for a surface crack, $\beta=\pi/3$, $a / t1=0.1$, $c / t1=0.3$, $K_v=12$ mm.

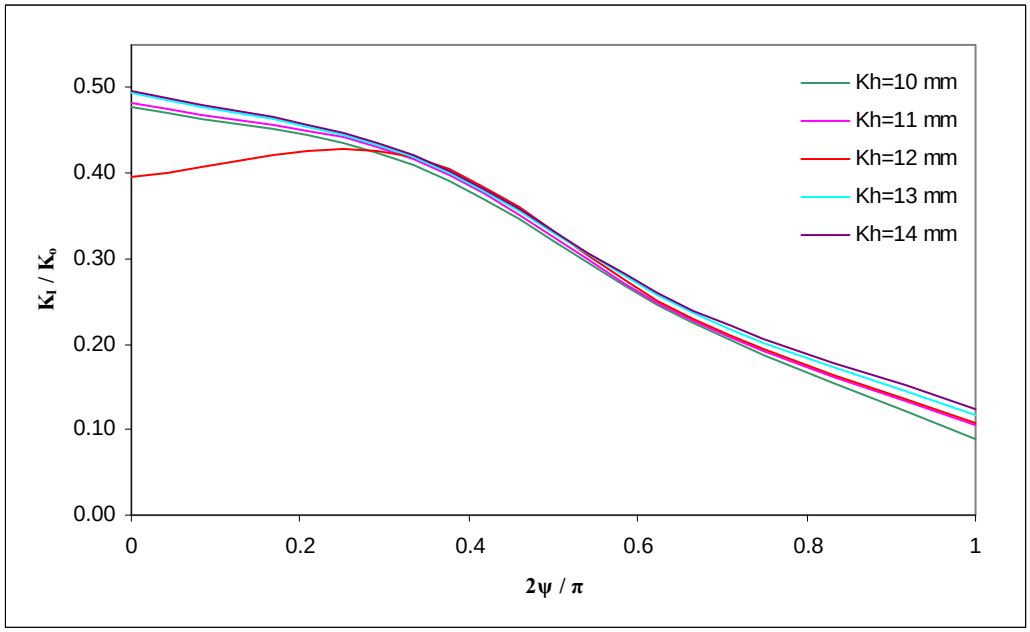

Figure 5.33 Normalized mode I SIF versus crack angle parameter ψ for a surface crack, $\beta=\pi/2$, $a / t1=0.1$, $c / t1=0.3$, $K_v=12$ mm.

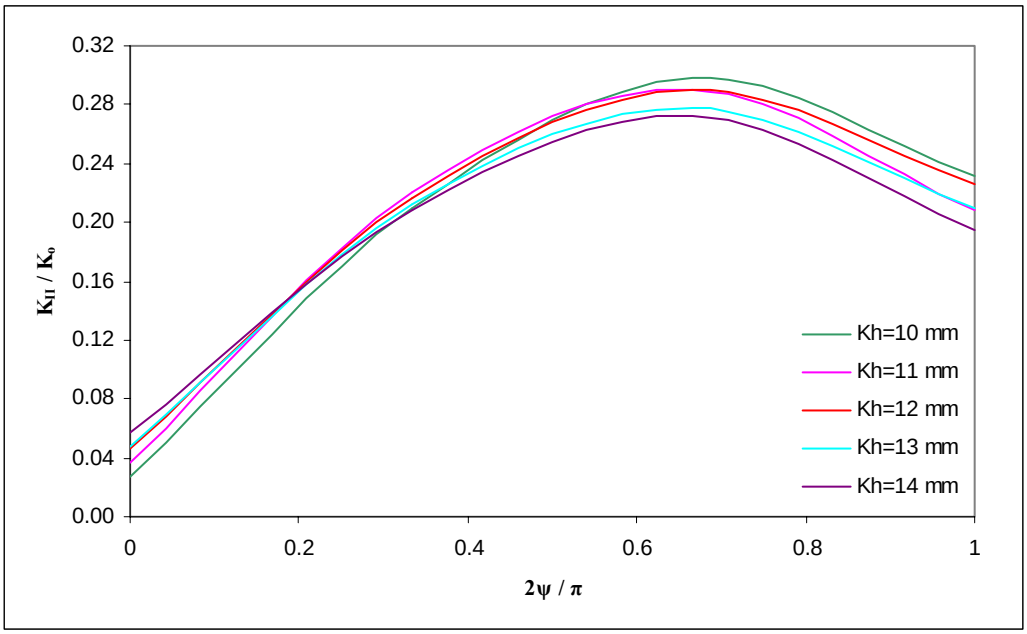

Figure 5.34 Normalized mode II SIF versus crack angle parameter ψ for a surface crack, $\beta=\pi/2$, $a / t1=0.1$, $c / t1=0.3$, $K_v=12$ mm.

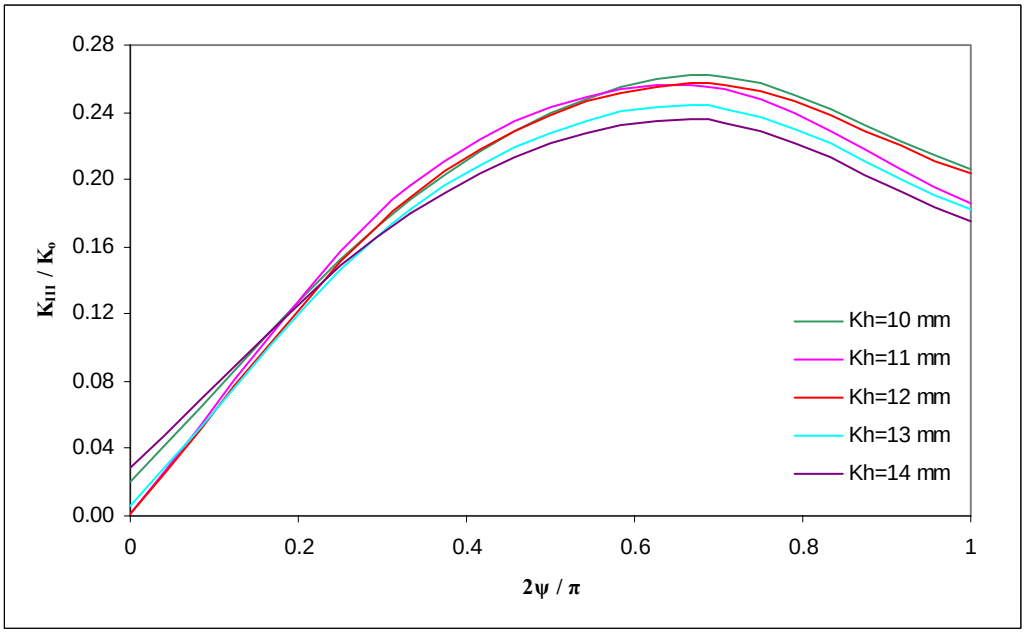

Figure 5.35 Normalized mode III SIF versus crack angle parameter ψ for a surface crack, $\beta=\pi/2$, $a / t1=0.1$, $c / t1=0.3$, $K_v=12$ mm.

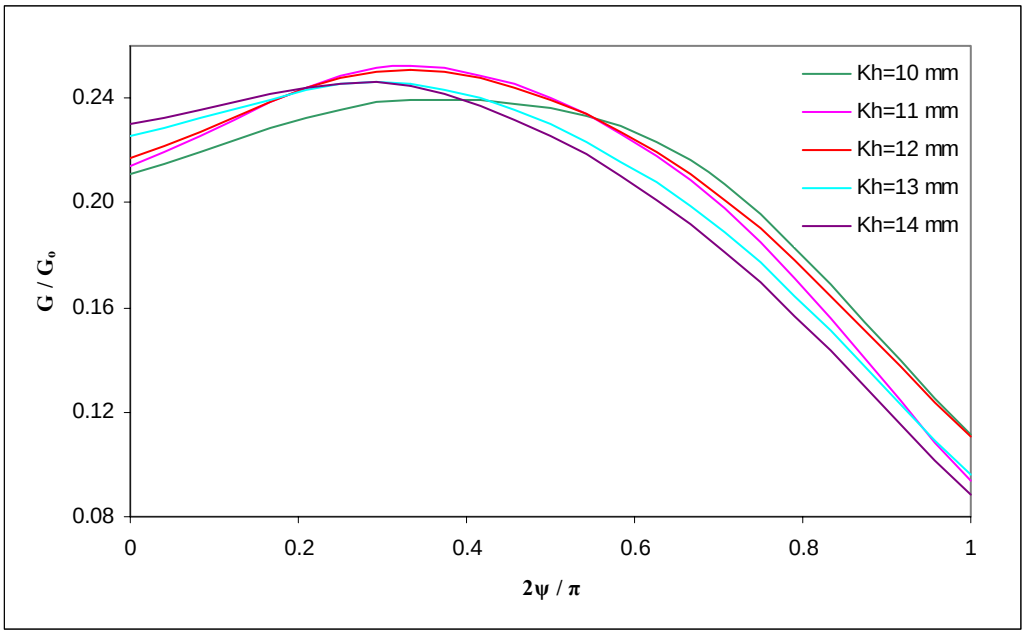

Figure 5.36 Normalized energy release rate versus crack angle parameter ψ for a surface crack, $\beta=\pi/2$, $a / t1=0.1$, $c / t1=0.3$, $K_v=12$ mm.

5.2.1.3 Loading of a Crack at the Side of the Weld Root for Various Crack Depth

In this section, a specimen with various crack geometry that is constructed with a crack at the side part of the weld root is subjected to tensile loading (Figure 5.37). Crack dimensions are identified as parameters of the base sheet metal and the weld geometry is defined as K_v=12 mm and K_h=12 mm. The normalized K_I, K_{II}, K_{III} and G for four β are presented in the following figures 5.39 – 5.54.

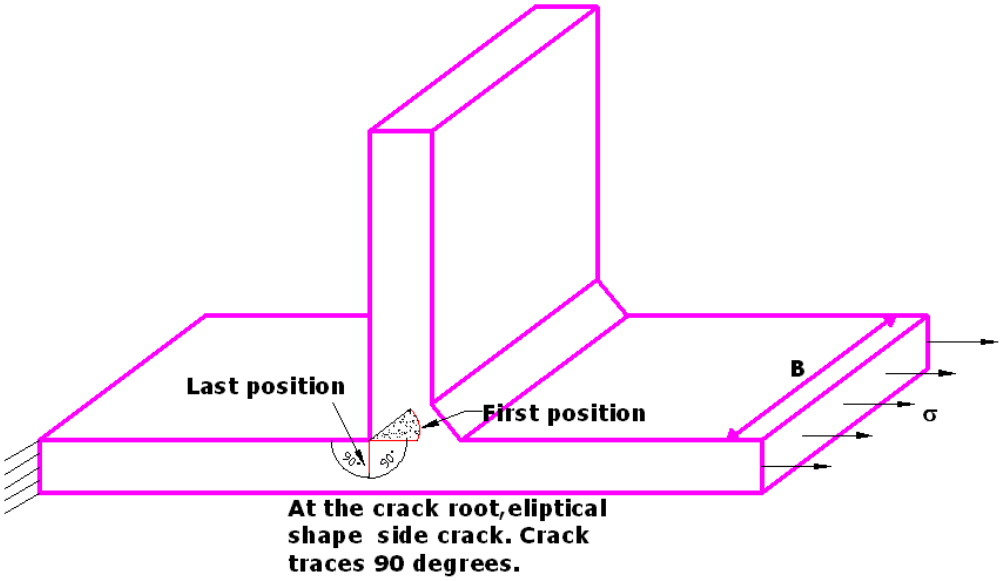

Figure 5.37 Crack at the root of the weld

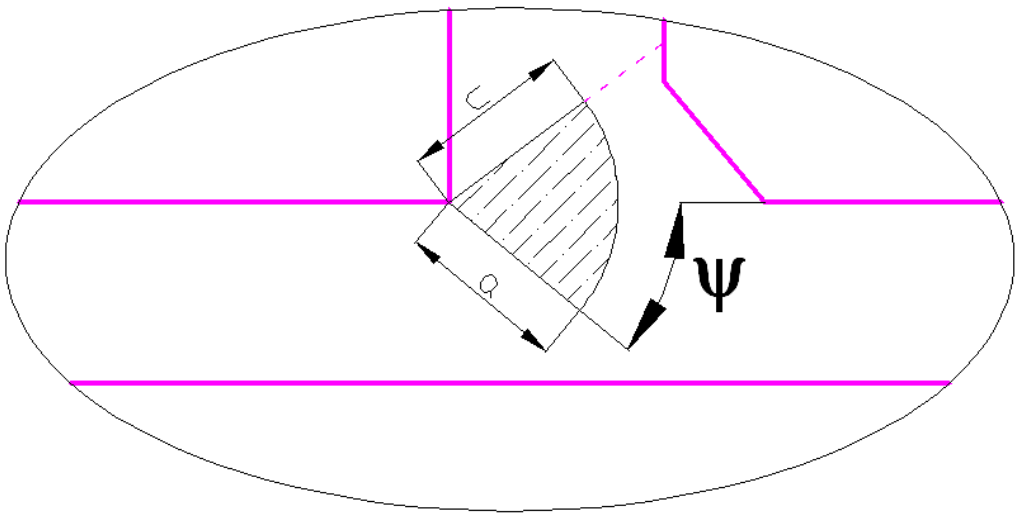

Figure 5.38 Close-up view of the root crack

In Figures 5.39-5.54, the variations of the normalized stress intensity factors and normalized energy release rate are plotted with respect to normalized crack angle, $2\psi/\pi$ for different crack geometry with respect to crack depth (*a*). In all these plots, it can be seen that the normalized energy release rate becomes higher for all β as the crack deepens. For higher crack depth values, the changes in the normalized K_I, K_{II}, K_{III} and G are much more remarkable. The normalized mode II and mode III stress intensity factors reach the maximum point at nearly half of the crack angle. The maximum values of the normalized K_I, K_{II}, K_{III} and G are seen at various β and ψ, not in the free ends of the specimen. Crack closure is observed for specimen with *a/t1*=0.4 and *a/t1*=0.5 for β=π/6 (see figure 5.37). For these parameters, the normalized mode I stress intensity factor is smaller than zero.

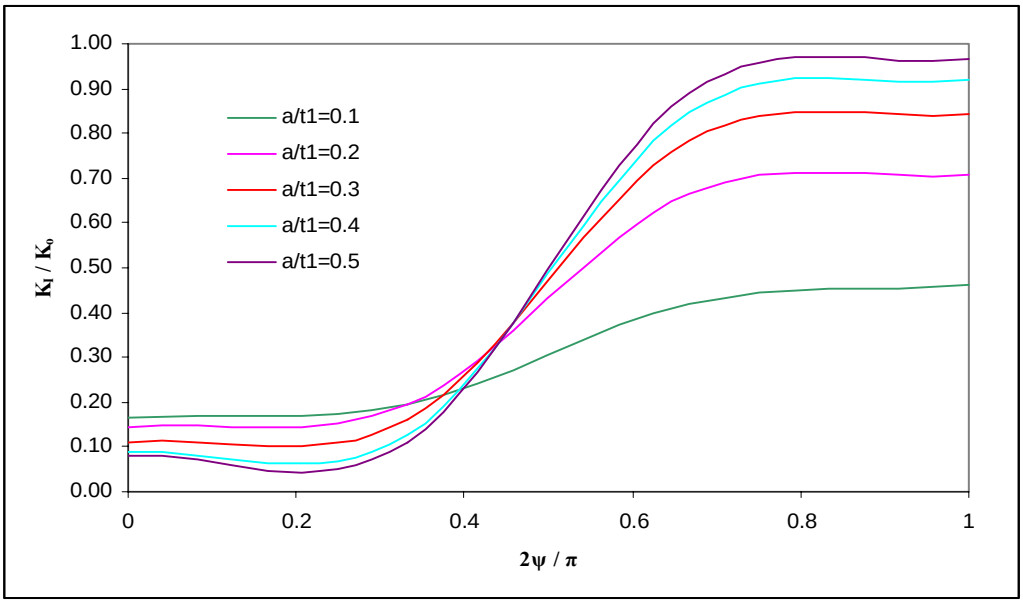

Figure 5.39 Normalized mode I SIF versus crack angle parameter ψ for a surface crack, β=0, $c/t1$=0.3, K_v=12 mm, K_h=12 mm.

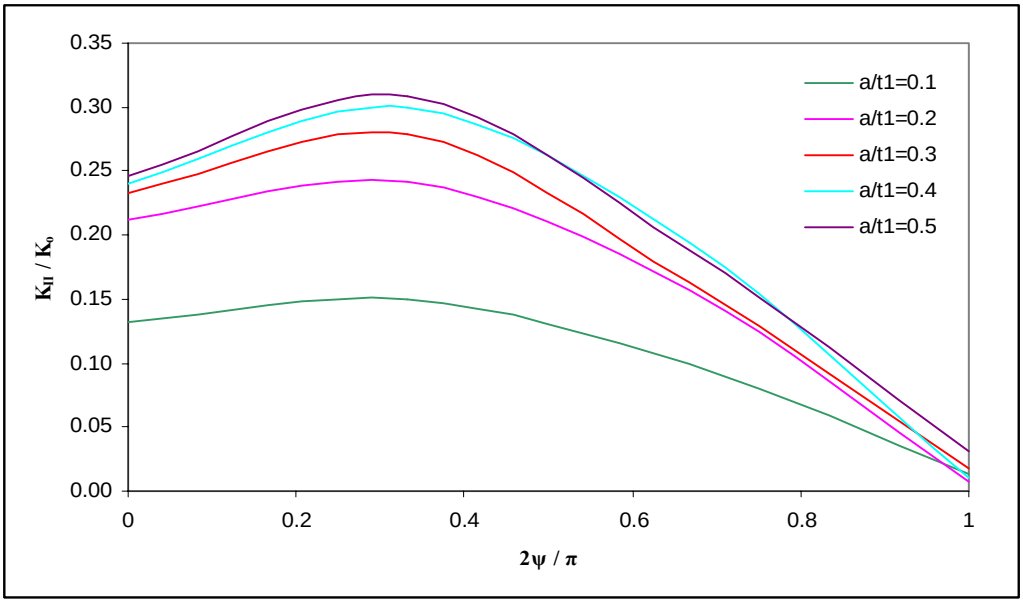

Figure 5.40 Normalized mode II SIF versus crack angle parameter ψ for a surface crack, β=0, $c / t1$=0.3, K_v=12 mm, K_h=12 mm.

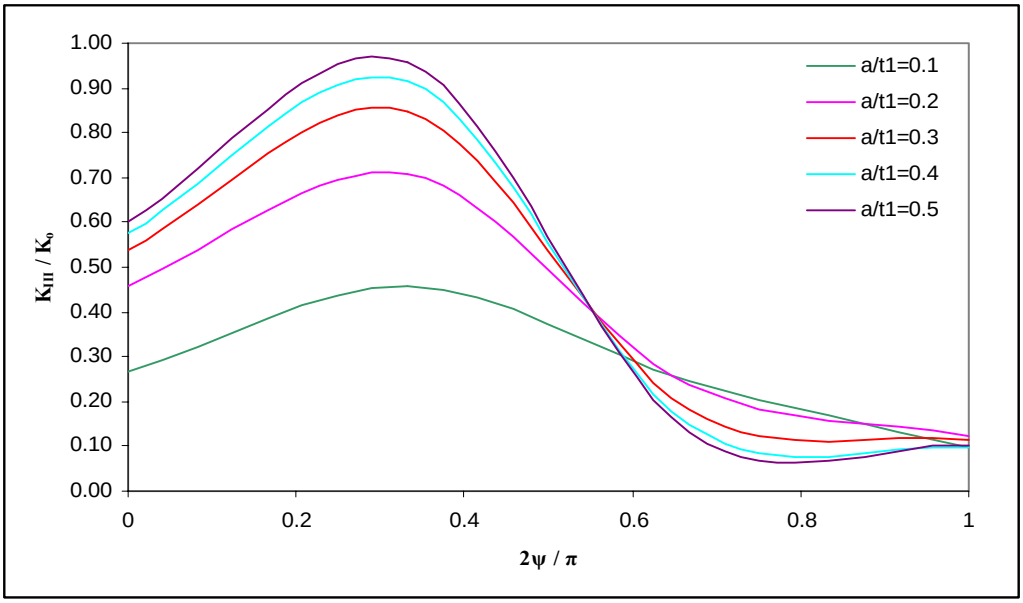

Figure 5.41 Normalized mode III SIF versus crack angle parameter ψ for a surface crack, β=0, $c / t1$=0.3, K_v=12 mm, K_h=12 mm.

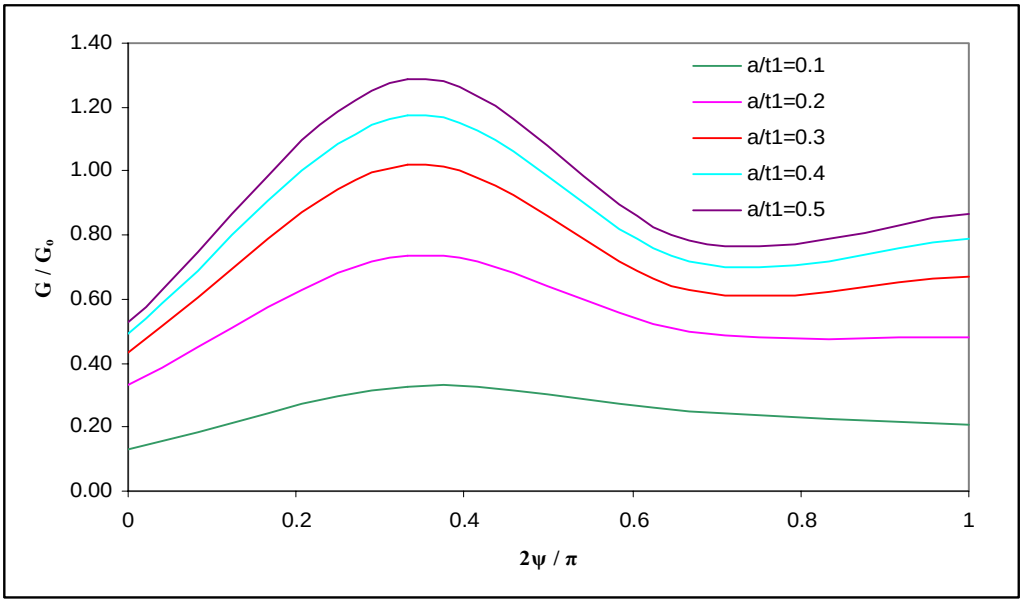

Figure 5.42 Normalized energy release rate versus crack angle parameter ψ for a surface crack, β=0, c / $t1$=0.3, K_v=12 mm, K_h=12 mm.

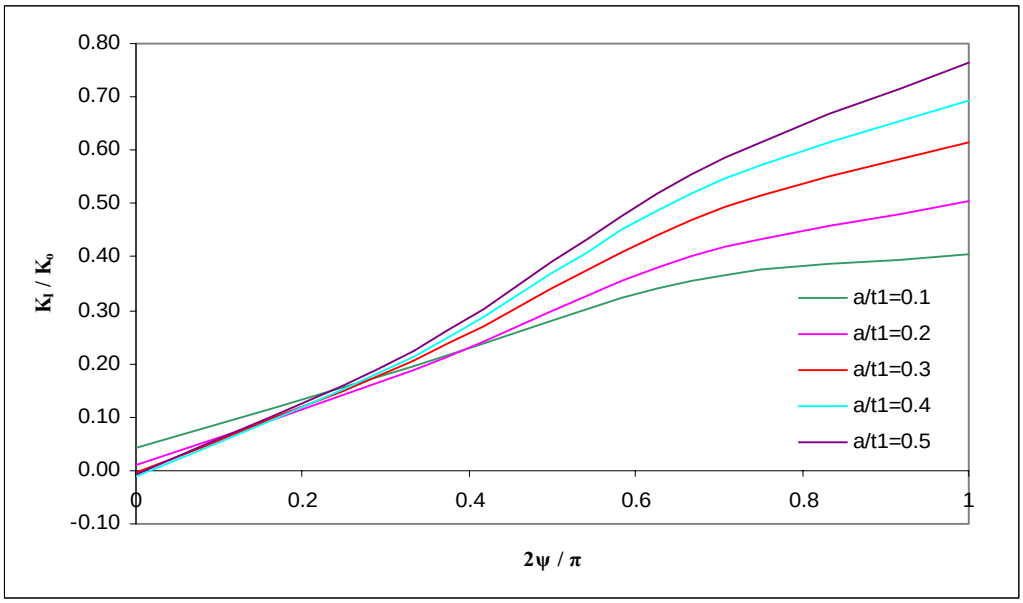

Figure 5.43 Normalized mode I SIF versus crack angle parameter ψ for a surface crack, β=π/6, c / $t1$=0.3, K_v=12 mm, K_h=12 mm.

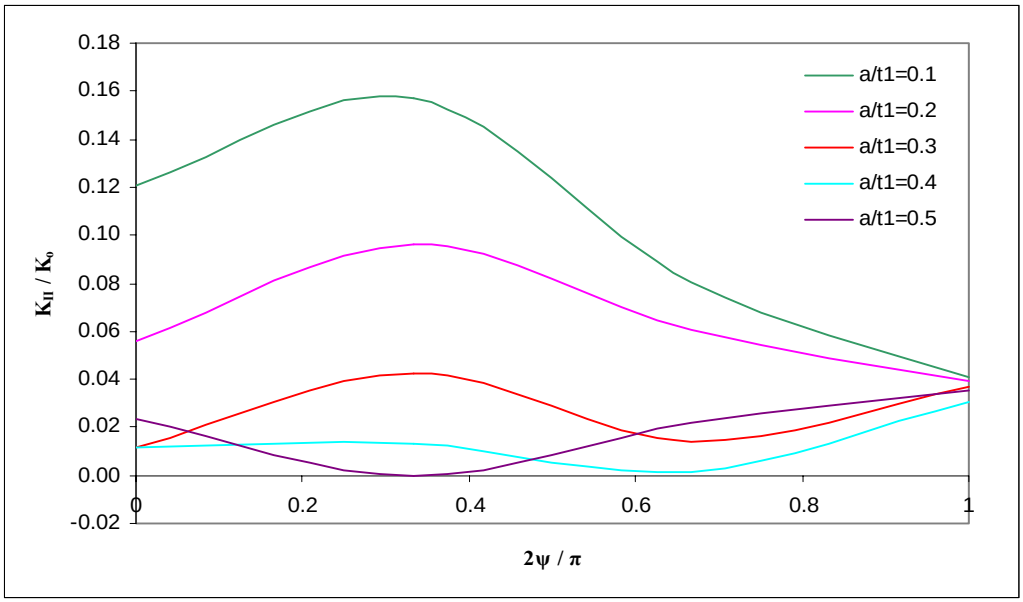

Figure 5.44 Normalized mode II SIF versus crack angle parameter ψ for a surface crack, $\beta=\pi/6$, $c / t1=0.3$, $K_v=12$ mm, $K_h=12$ mm.

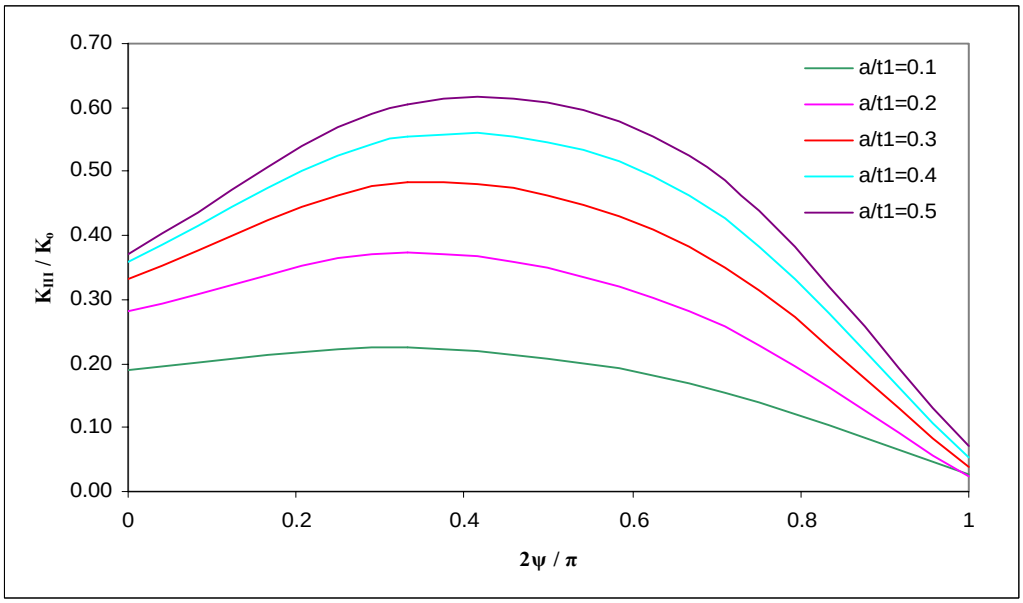

Figure 5.45 Normalized mode III SIF versus crack angle parameter ψ for a surface crack, $\beta=\pi/6$, $c / t1=0.3$, $K_v=12$ mm, $K_h=12$ mm.

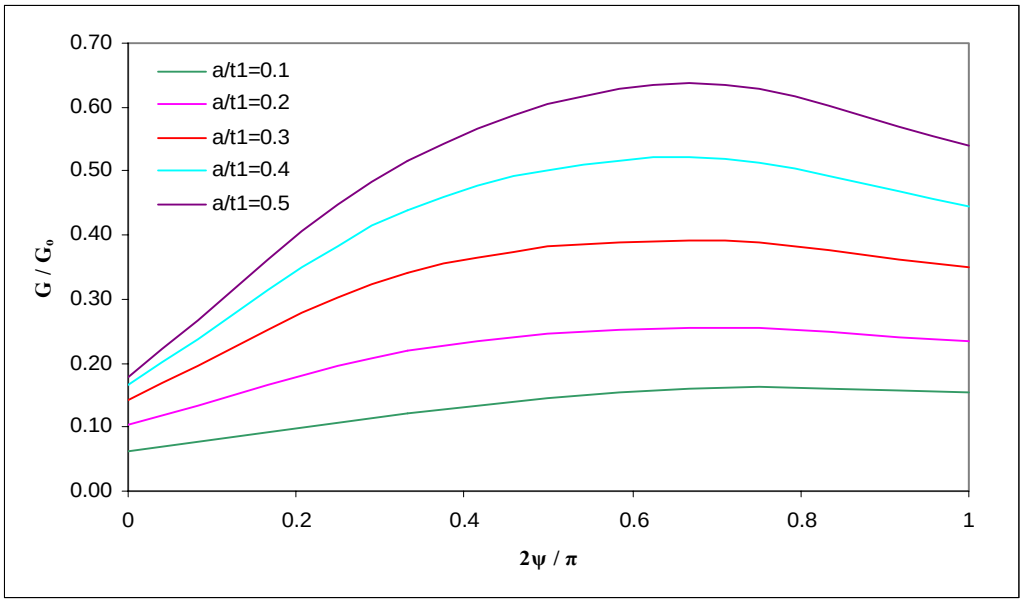

Figure 5.46 Normalized energy release rate versus crack angle parameter ψ for a surface crack, $\beta=\pi/6$, $c / t1=0.3$, $K_v=12$ mm, $K_h=12$ mm.

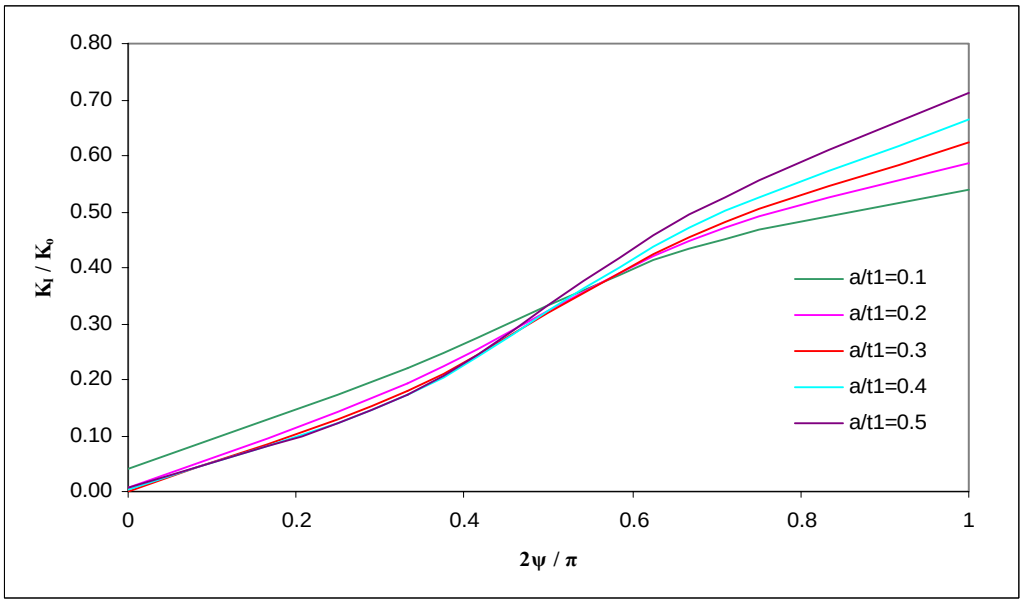

Figure 5.47 Normalized mode I SIF versus crack angle parameter ψ for a surface crack, $\beta=\pi/3$, $c / t1=0.3$, $K_v=12$ mm, $K_h=12$ mm.

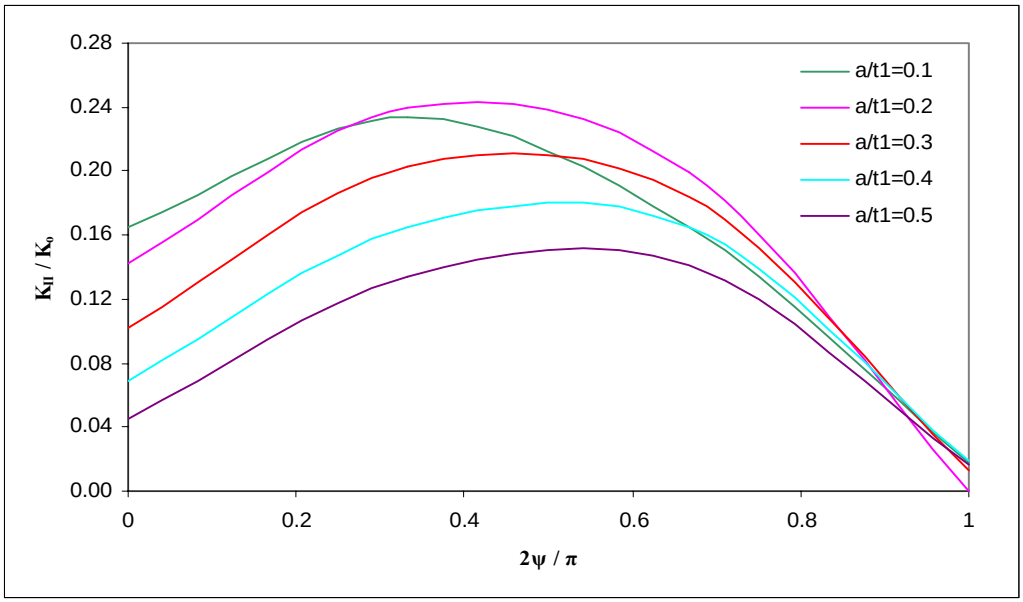

Figure 5.48 Normalized mode II SIF versus crack angle parameter ψ for a surface crack, $\beta=\pi/3$, $c / t1=0.3$, $K_v=12$ mm, $K_h=12$ mm.

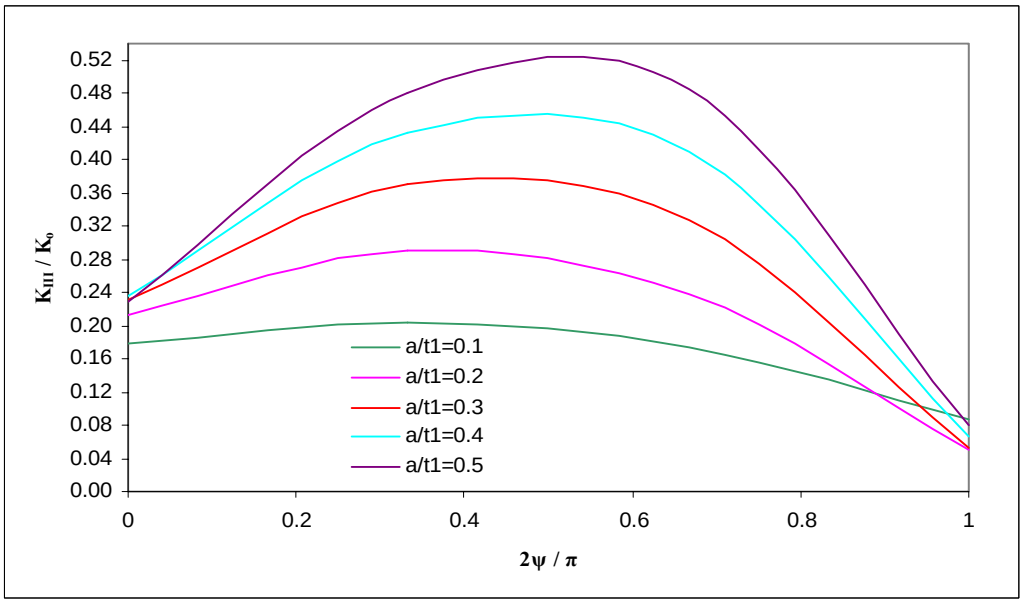

Figure 5.49 Normalized mode III SIF versus crack angle parameter ψ for a surface crack, $\beta=\pi/3$, $c / t1=0.3$, $K_v=12$ mm, $K_h=12$ mm.

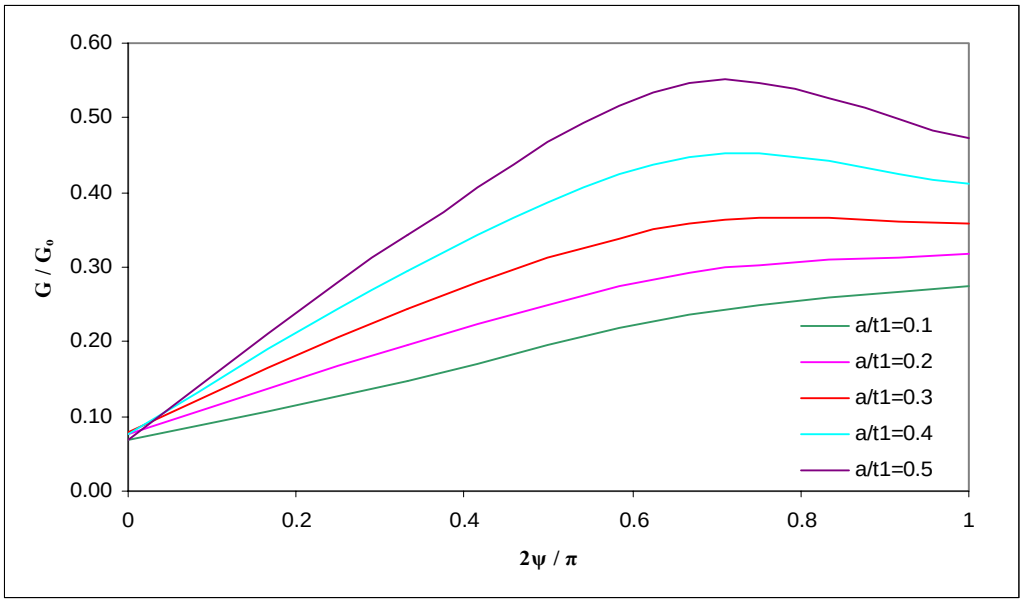

Figure 5.50 Normalized energy release rate versus crack angle parameter ψ for a surface crack, $\beta=\pi/3$, $c / t1=0.3$, $K_v=12$ mm, $K_h=12$ mm.

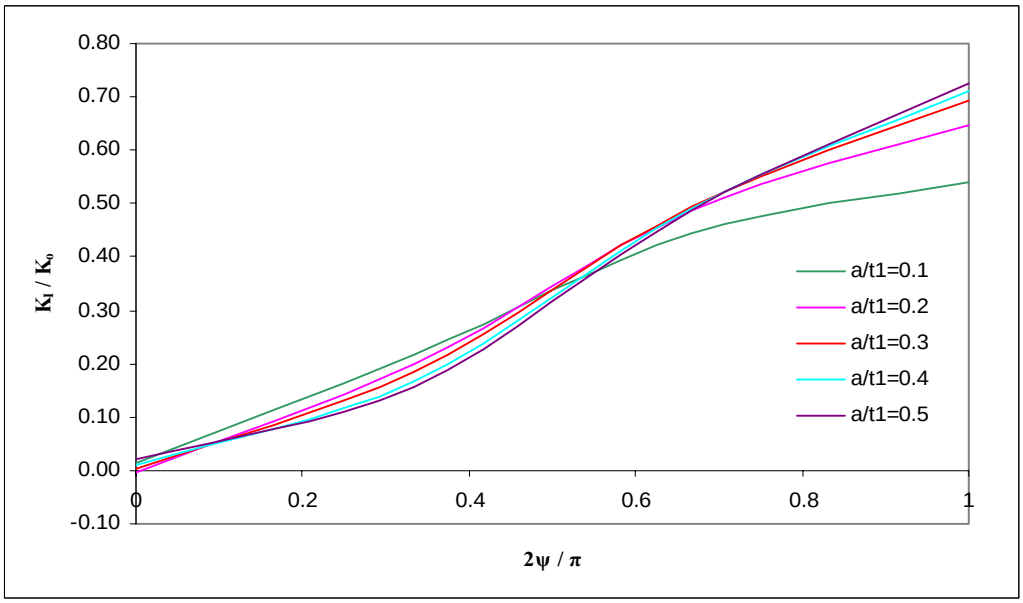

Figure 5.51 Normalized mode I SIF versus crack angle parameter ψ for a surface crack, $\beta=\pi/2$, $c / t1=0.3$, $K_v=12$ mm, $K_h=12$ mm.

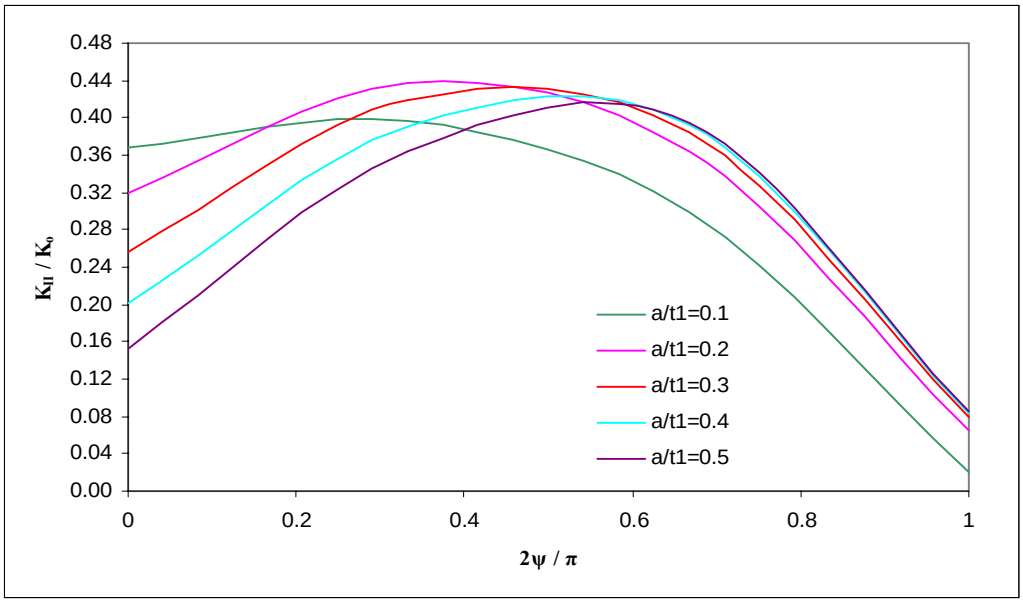

Figure 5.52 Normalized mode II SIF versus crack angle parameter ψ for a surface crack, $\beta=\pi/2$, $c / t1=0.3$, $K_v=12$ mm, $K_h=12$ mm.

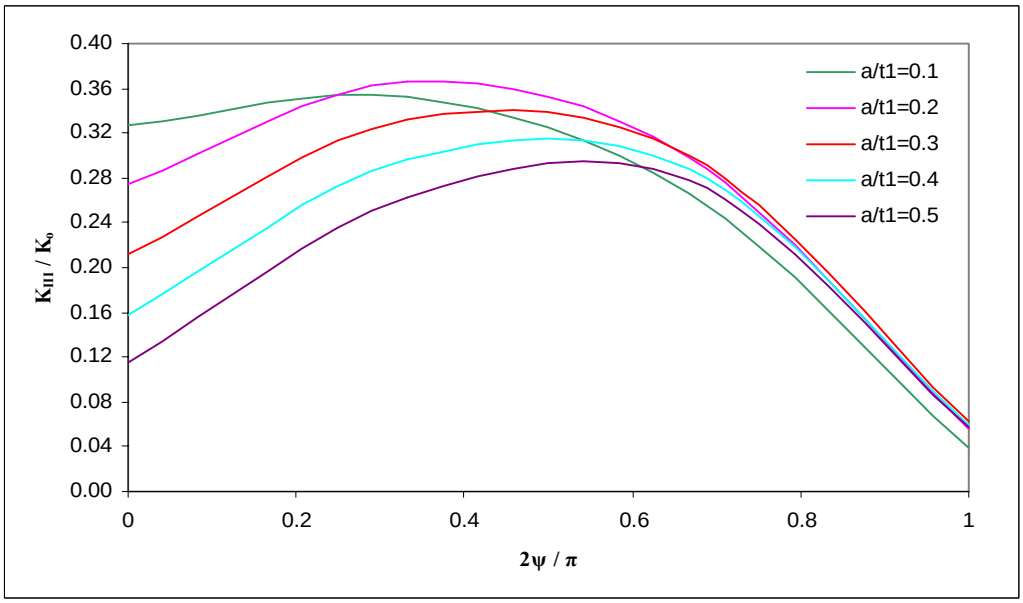

Figure 5.53 Normalized mode III SIF versus crack angle parameter ψ for a surface crack, $\beta=\pi/2$, $c / t1=0.3$, $K_v=12$ mm, $K_h=12$ mm.

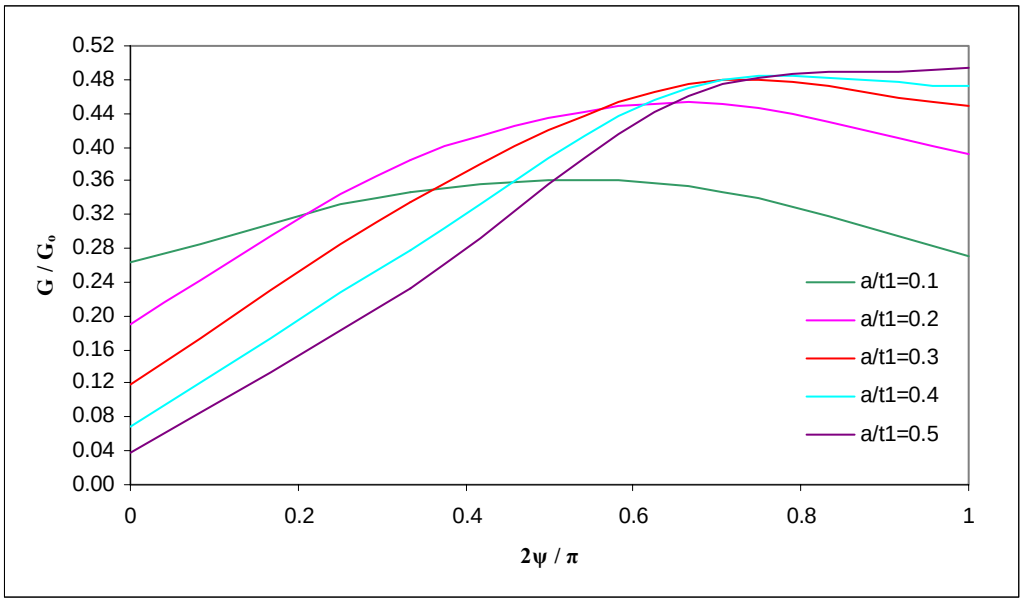

Figure 5.54 Normalized energy release rate versus crack angle parameter ψ for a surface crack, $\beta=\pi/2$, $c / t1=0.3$, $K_v=12$ mm, $K_h=12$ mm.

5.2.2 Bending

In this section, T-shaped specimen is assumed to be subjected to bending load *F* at the ends of the specimen as shown in figure 5.55. The bending load equals to 715 N.

5.2.2.1 Loading of a Crack at the Side of the Weld Toe

In this section, a specimen that is constructed with a crack at the side part of the weld toe is subjected to bending load. Crack dimensions are identified as parameters of the base sheet metal and crack place can be seen in figure 5.1. The normalized K_I, K_{II}, K_{III} and G for four β are presented in the following figures 5.56– 5.71.

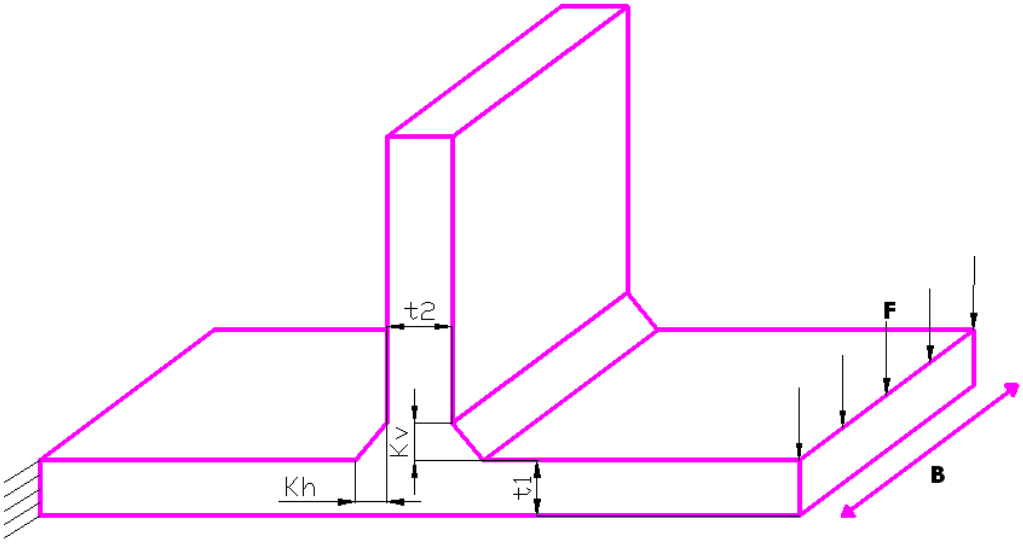

Figure 5.55 Bending load at the end of the T-shaped specimen

In Figures 5.56-5.71, the variations of the normalized stress intensity factors and normalized energy release rate are plotted with respect to normalized crack angle, $2\psi/\pi$. In all these plots, it can be easily depicted that the normalized mixed modes stress intensity factors and normalized energy release rate have nearly the same behavior, except when $2\psi/\pi$ is smaller than 0.2, whether the specimen has the double-sided fillet weld or one-sided fillet weld for this type of loading. The minimum and the maximum normalized mode I stress intensity factors are obtained at free surfaces $\beta=\pi/2$ and $\beta=0$. The normalized mode II stress intensity factor is nearly the same for all β values. The normalized mode I stress intensity factor and the normalized energy release rate have a tendency to decrease with the rise of the crack angle. On the other hand, the normalized mode II, mode III stress intensity factors rise up when the crack angle increases for $\beta=\pi/6$, $\pi/3$, $\pi/2$. The main difference occurs at $\beta=\pi/2$ and $\psi=0$ for the normalized mode I SIF.

,

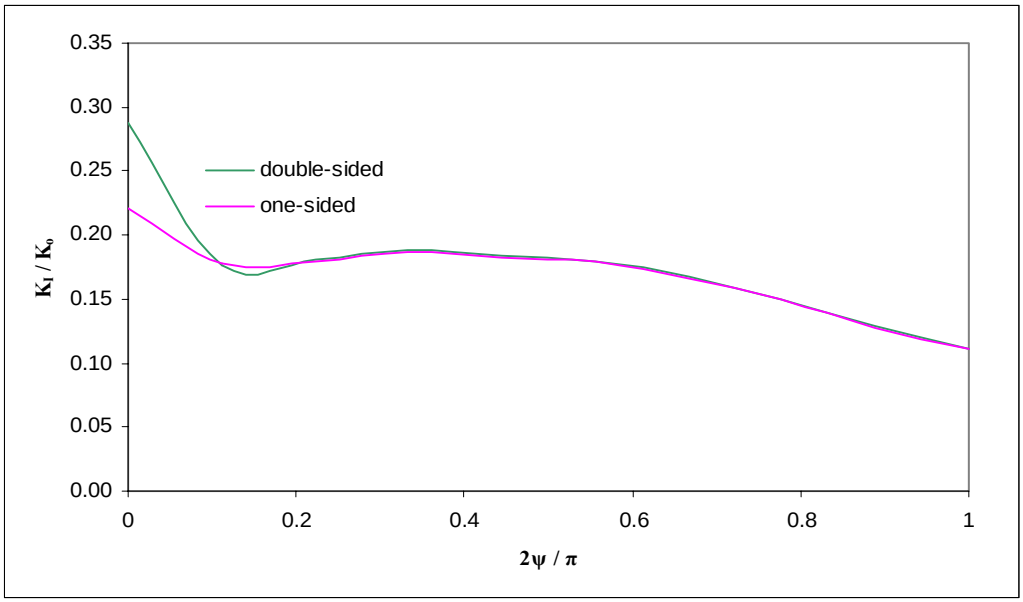

Figure 5.56 Normalized mode I SIF versus crack angle parameter ψ and the weld option parameter for a surface crack, β=0, *a / t1*=0.1, *c / t1*=0.3.

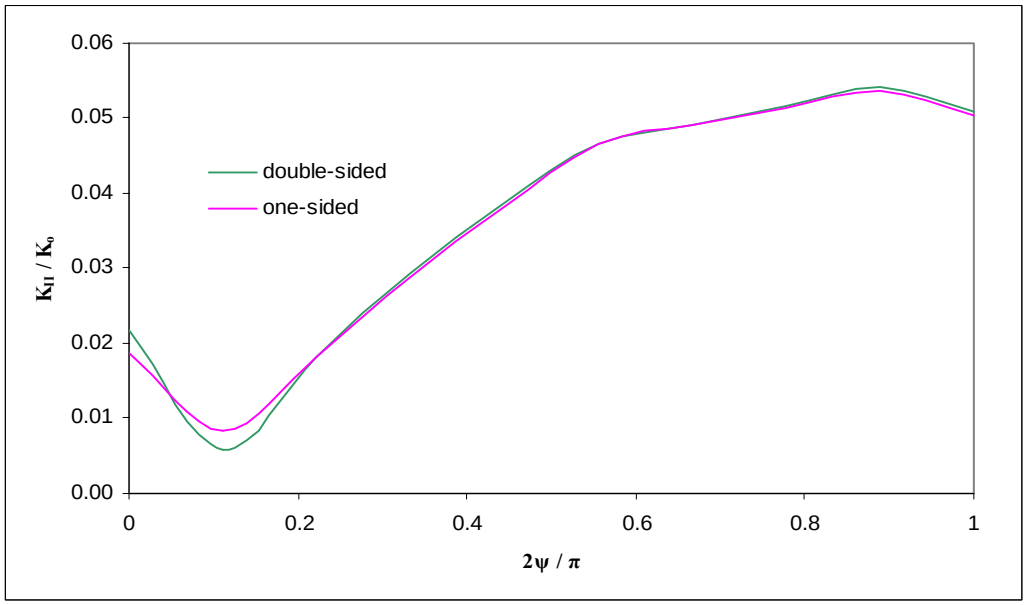

Figure 5.57 Normalized mode II SIF versus crack angle parameter ψ and the weld option parameter for a surface crack, β=0, *a / t1*=0.1, *c / t1*=0.3.

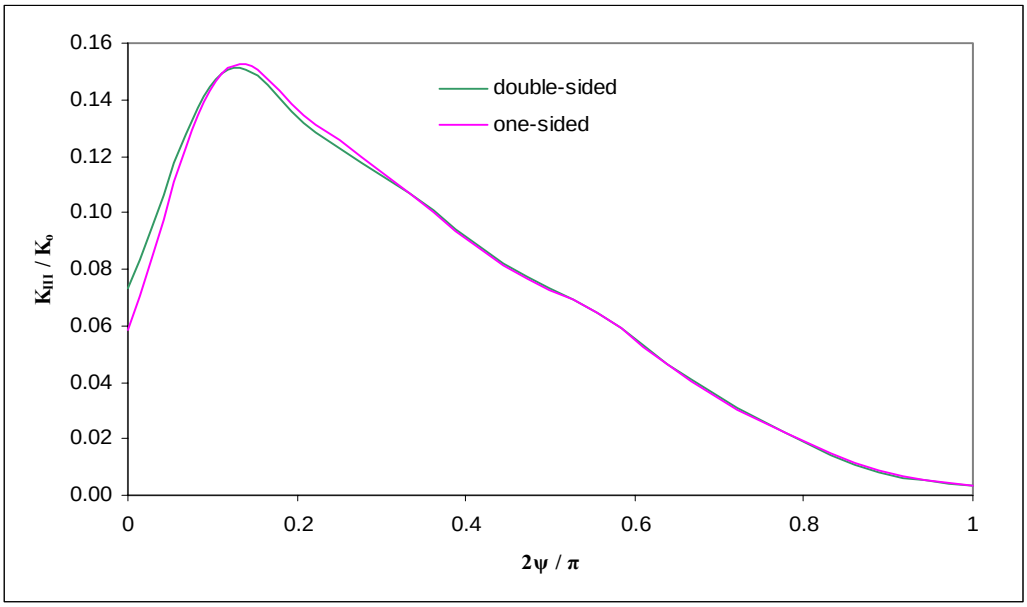

Figure 5.58 Normalized mode III SIF versus crack angle parameter ψ and the weld option parameter for a surface crack, β=0, *a / t1*=0.1, *c / t1*=0.3.

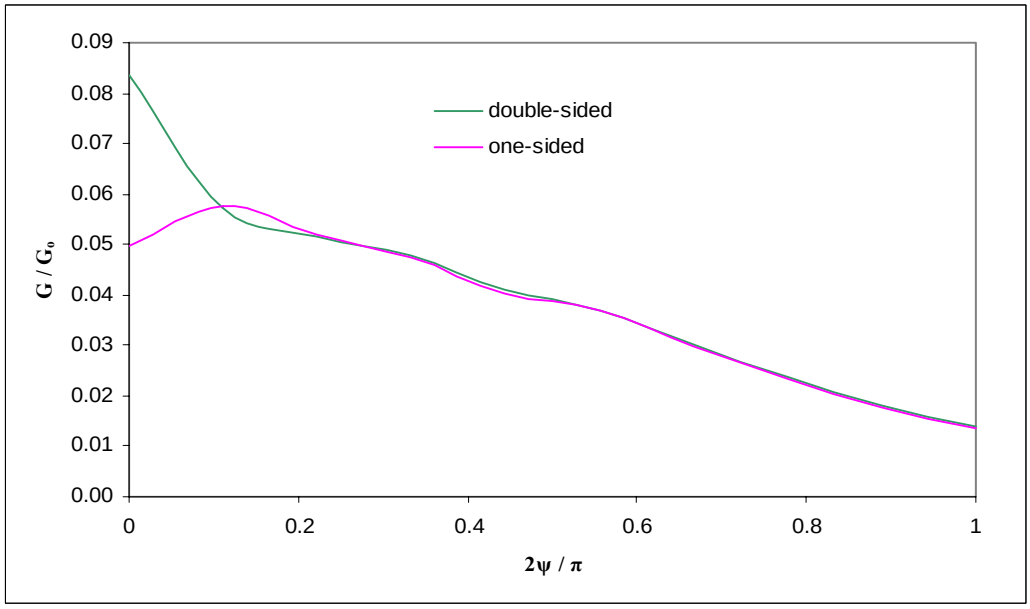

Figure 5.59 Normalized energy release rate versus crack angle parameter ψ and the weld option parameter for a surface crack, β=0, *a / t1*=0.1, *c / t1*=0.3.

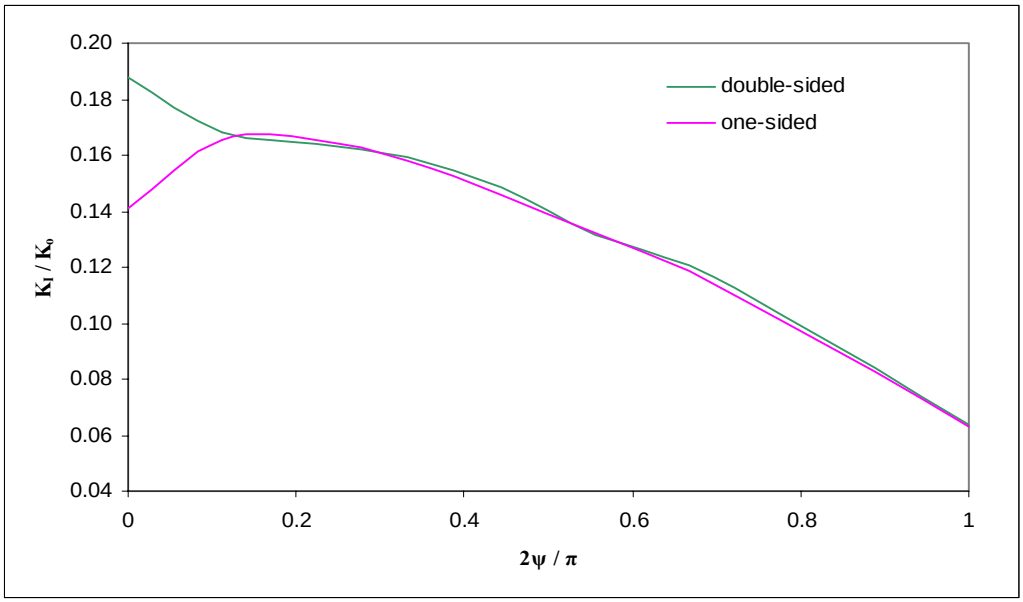

Figure 5.60 Normalized mode I SIF versus crack angle parameter ψ and the weld option parameter for a surface crack, $\beta=\pi/6$, $a / t1=0.1$, $c / t1=0.3$.

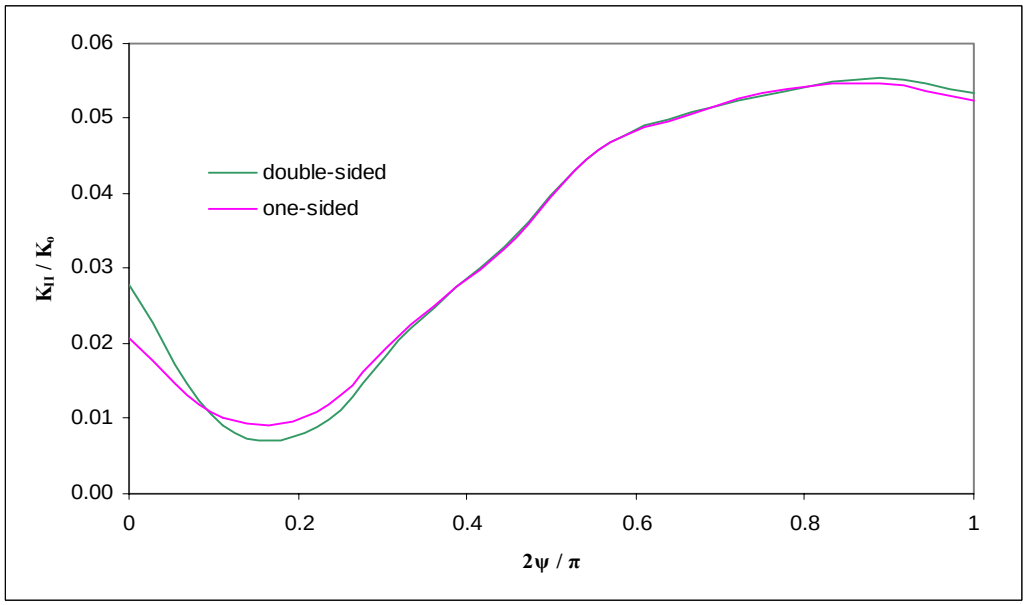

Figure 5.61 Normalized mode II SIF versus crack angle parameter ψ and the weld option parameter for a surface crack, $\beta= \pi/6$, $a / t1=0.1$, $c / t1=0.3$.

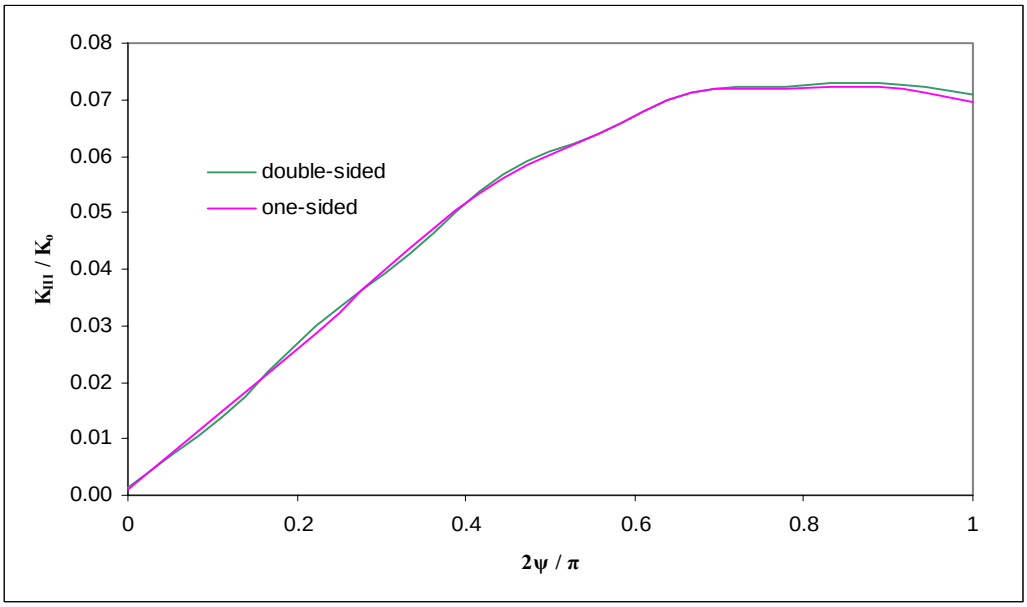

Figure 5.62 Normalized mode III SIF versus crack angle parameter ψ and the weld option parameter for a surface crack, $\beta = \pi/6$, $a / t1$=0.1, $c / t1$=0.3.

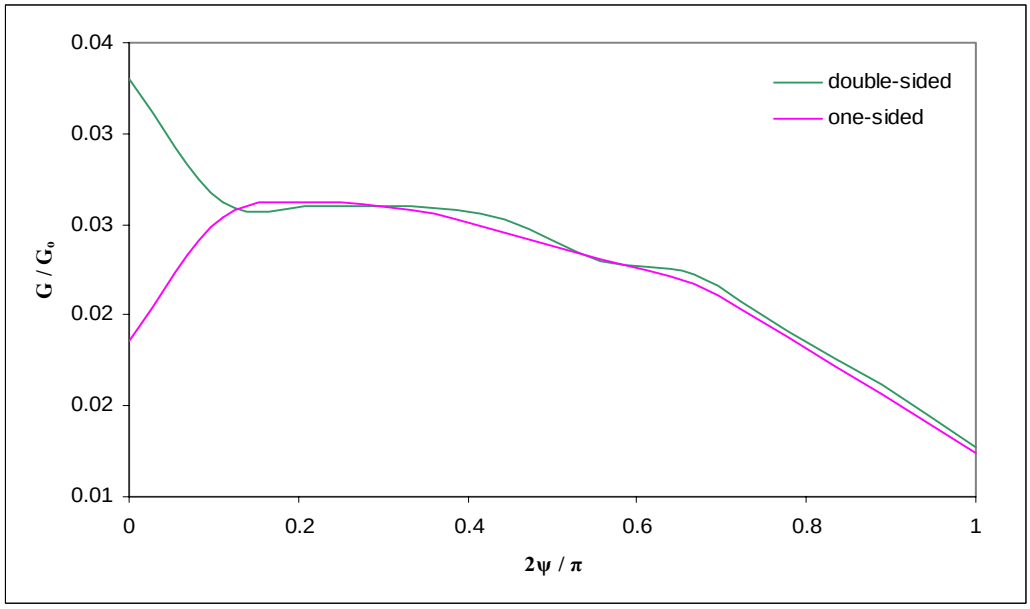

Figure 5.63 Normalized energy release rate versus crack angle parameter ψ and the weld option parameter for a surface crack, $\beta = \pi/6$, $a/t1$=0.1, $c/t1$=0.3.

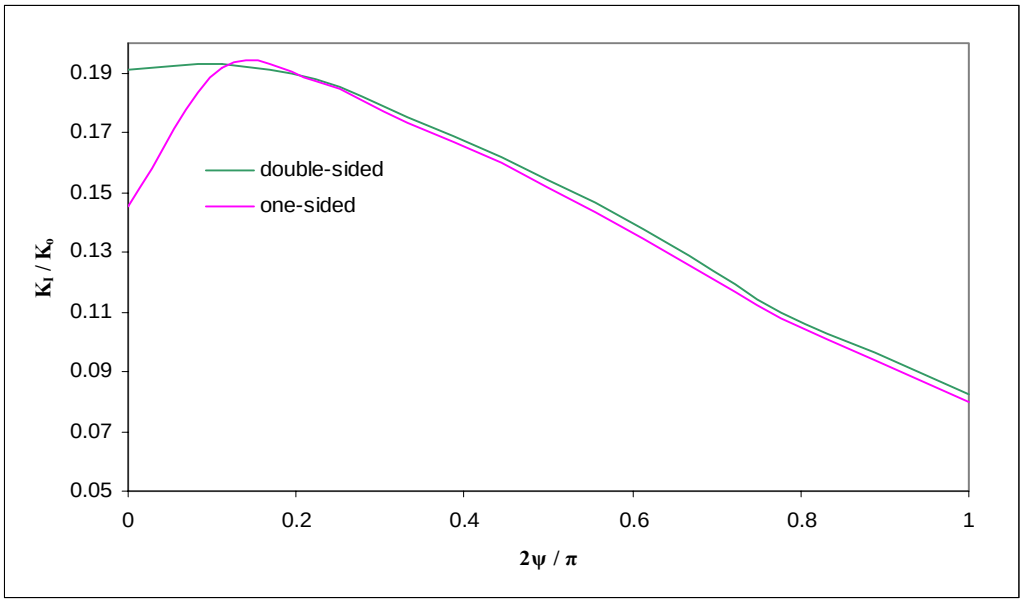

Figure 5.64 Normalized mode I SIF versus crack angle parameter ψ and the weld option parameter for a surface crack, $\beta=\pi/3$, $a / t1=0.1$, $c / t1=0.3$.

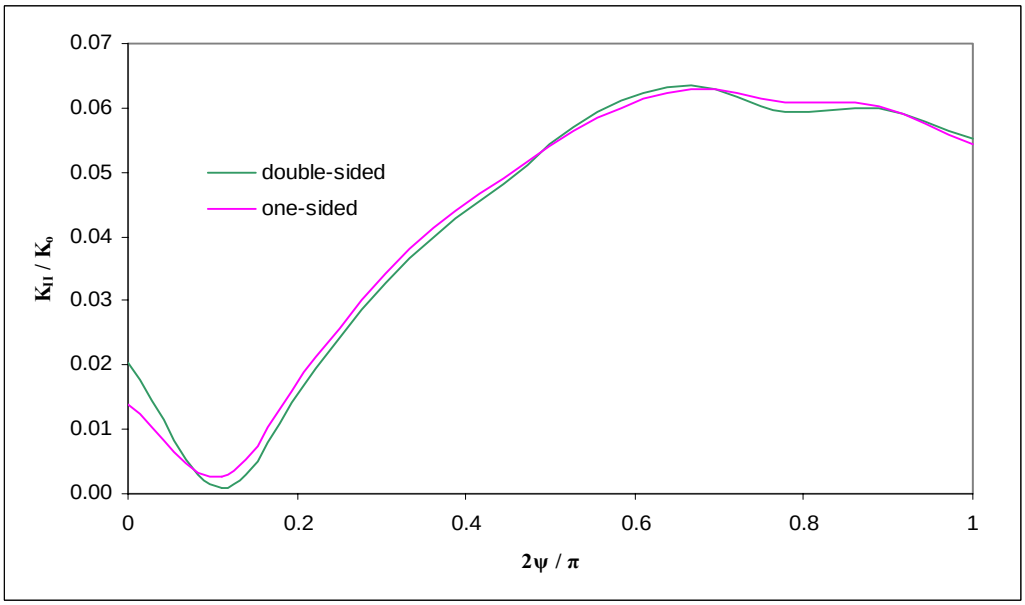

Figure 5.65 Normalized mode II SIF versus crack angle parameter ψ and the weld option parameter for a surface crack, $\beta= \pi/3$, $a / t1=0.1$, $c / t1=0.3$.

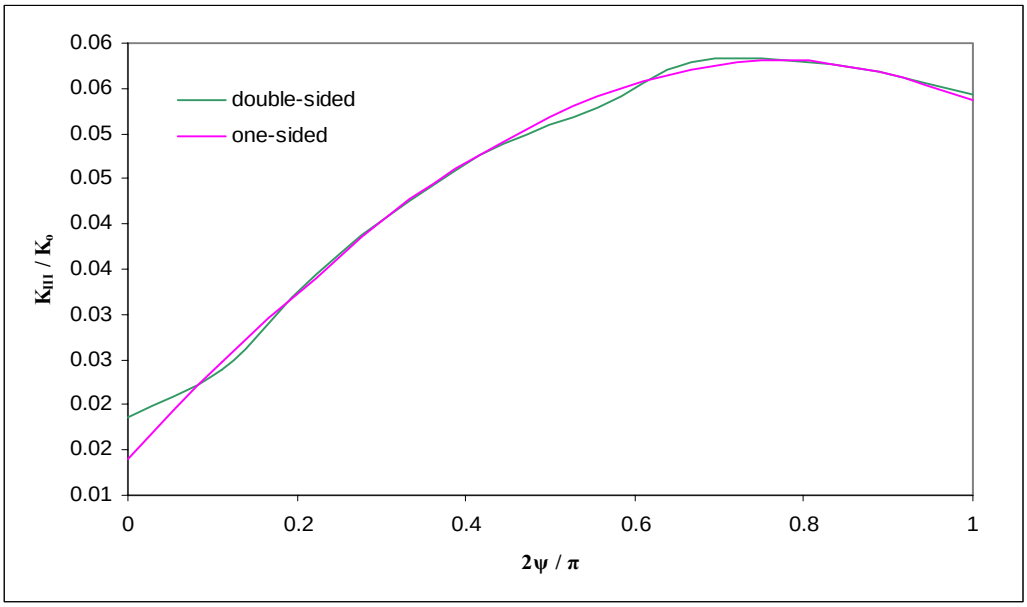

Figure 5.66 Normalized mode III SIF versus crack angle parameter ψ and the weld option parameter for a surface crack, $\beta = \pi/3$, $a / t1$=0.1, $c / t1$=0.3.

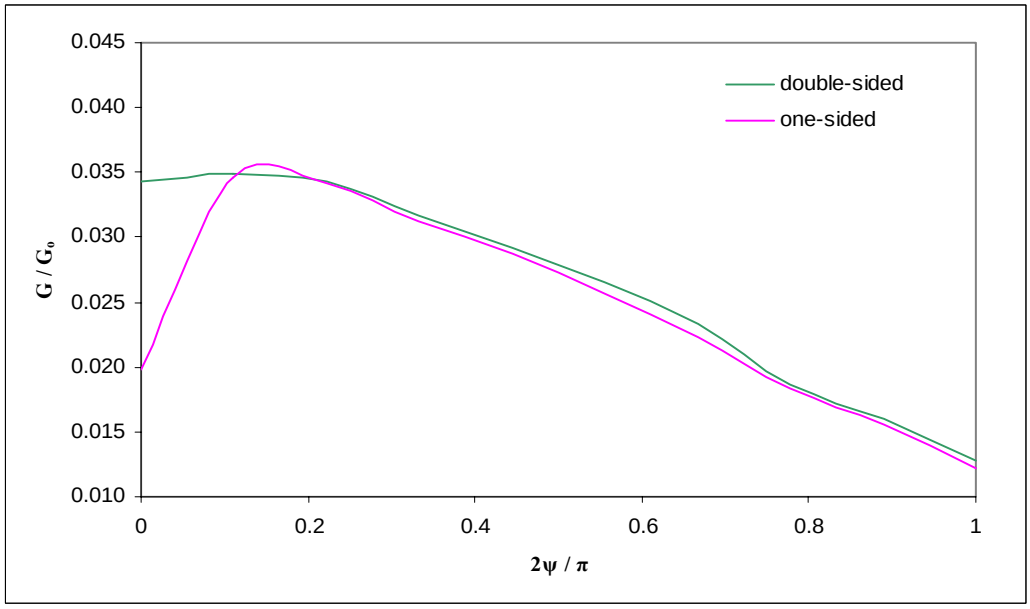

Figure 5.67 Normalized energy release rate versus crack angle parameter ψ and the weld option parameter for a surface crack, $\beta = \pi/3$, $a/t1$=0.1, $c/t1$=0.3.

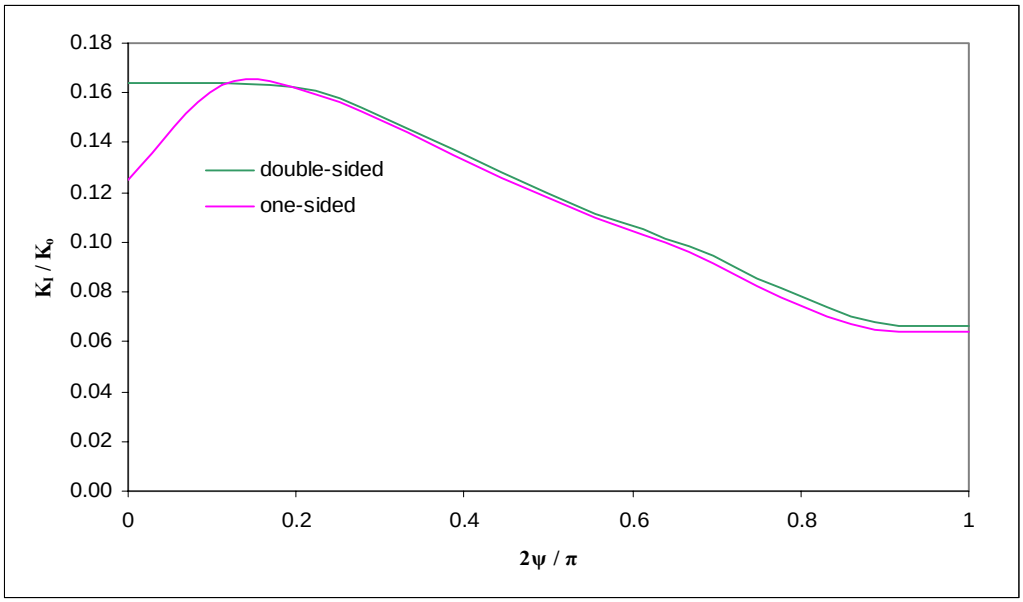

Figure 5.68 Normalized mode I SIF versus crack angle parameter ψ and the weld option parameter for a surface crack, $\beta=\pi/2$, $a / t1=0.1$, $c / t1=0.3$.

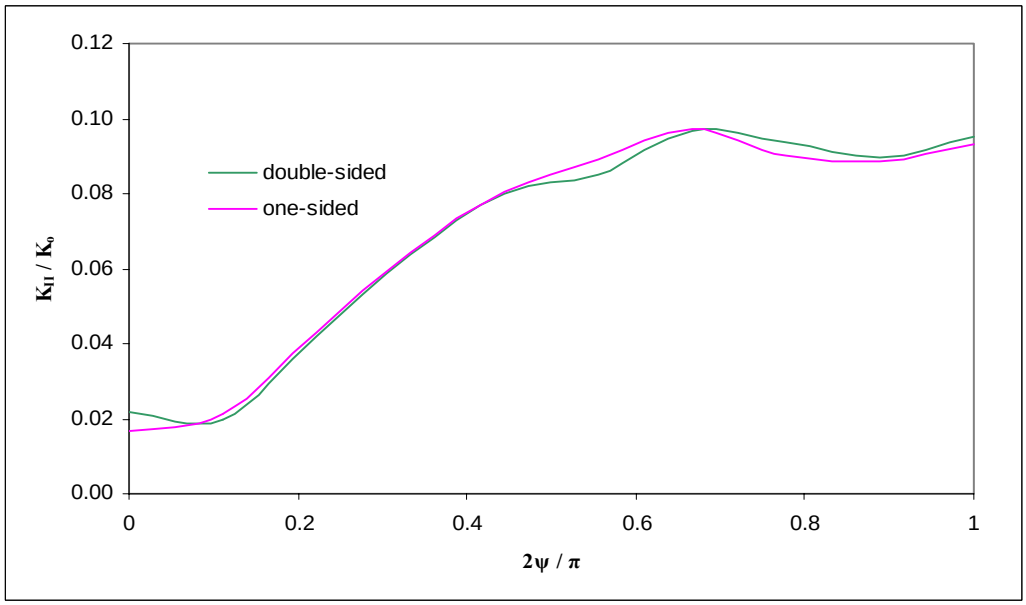

Figure 5.69 Normalized mode II SIF versus crack angle parameter ψ and the weld option parameter for a surface crack, $\beta= \pi/2$, $a / t1=0.1$, $c / t1=0.3$.

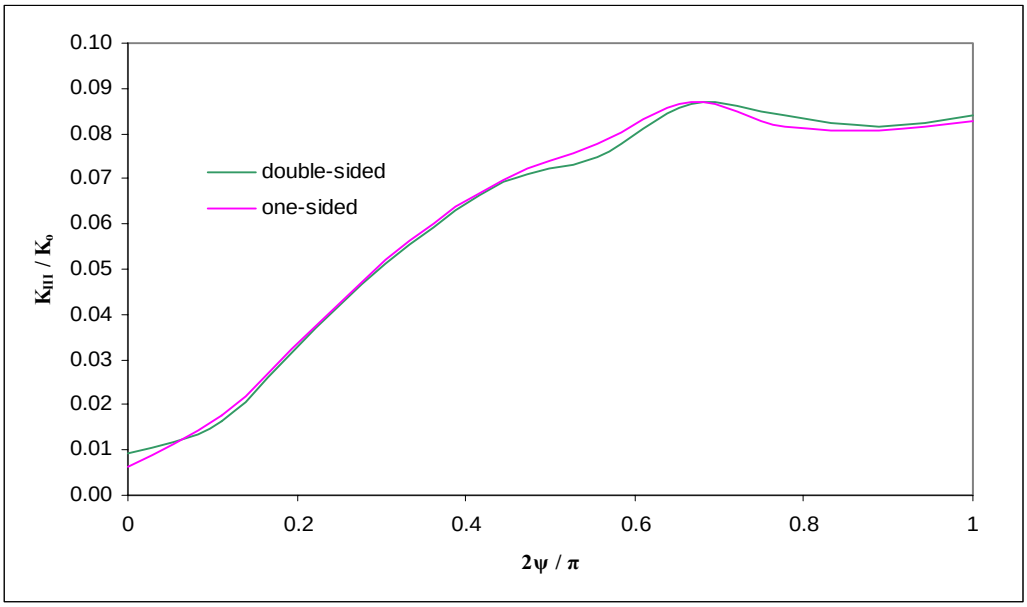

Figure 5.70 Normalized mode III SIF versus crack angle parameter ψ and the weld option parameter for a surface crack, $\beta = \pi/2$, $a / t1$=0.1, $c / t1$=0.3.

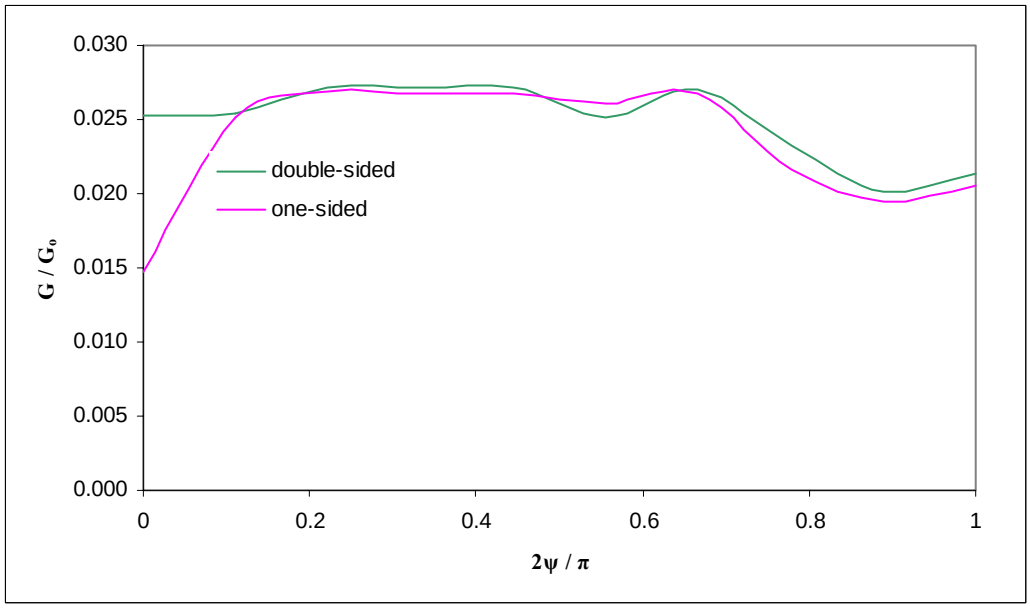

Figure 5.71 Normalized energy release rate versus crack angle parameter ψ and the weld option parameter for a surface crack, $\beta = \pi/2$, $a/t1$=0.1, $c/t1$=0.3.

5.2.2.2 Loading of a Crack at the Side of the Weld Toe for Various Weld Shape

In this section, a bending load is applied to five specimens with various weld geometry (Figure 5.20) that is constructed with a crack at the side part of the weld toe. Crack dimensions are identified as parameters of the base sheet metal and the weld geometry is defined as K_v=12 mm and K_h=10, 11, 12, 13, 14 mm. The normalized K_I, K_{II}, K_{III} and G for four β are presented in the following figures 5.72 – 5.87.

In Figures 5.72-5.87, the variations of the normalized stress intensity factors and normalized energy release rate are plotted with respect to normalized crack angle, $2\psi/\pi$ for different weld geometry with respect to horizontal leg of the fillet weld (K_h). As $2\psi/\pi$ approaches to unit value, the higher K_h values make the normalized K_I, K_{II}, K_{III} and G decay compared to lower ones. The normalized mode II and mode III stress intensity factors come up to the maximum point at nearly half of the crack angle. Unlikely, K_I, K_{II}, K_{III} and G have their maximum values at $2\psi/\pi=0$ and minimum values at $2\psi/\pi$ =1. The main difference occurs at $\beta=\pi/2$ and $2\psi/\pi=0$ for the normalized mode I SIF and the maximum values of the normalized K_I, K_{II}, K_{III} and G are seen at $\beta=0$ and $2\psi/\pi=0$, free end of the specimen. No crack closure is observed during the calculations.

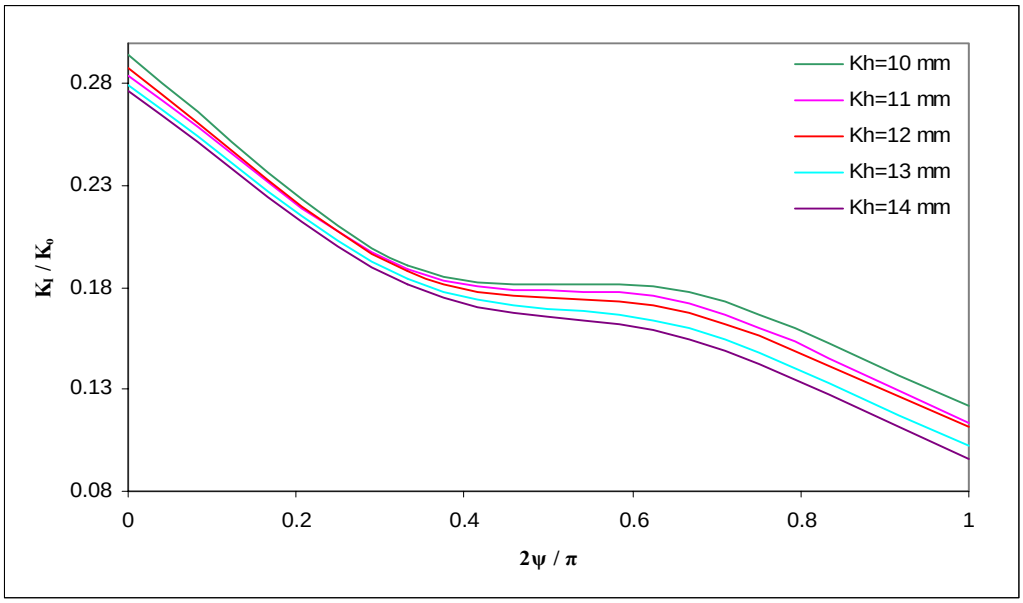

Figure 5.72 Normalized mode I SIF versus crack angle parameter ψ for a surface crack, β=0, $a / t1$=0.1, $c / t1$=0.3, K_V=12 mm.

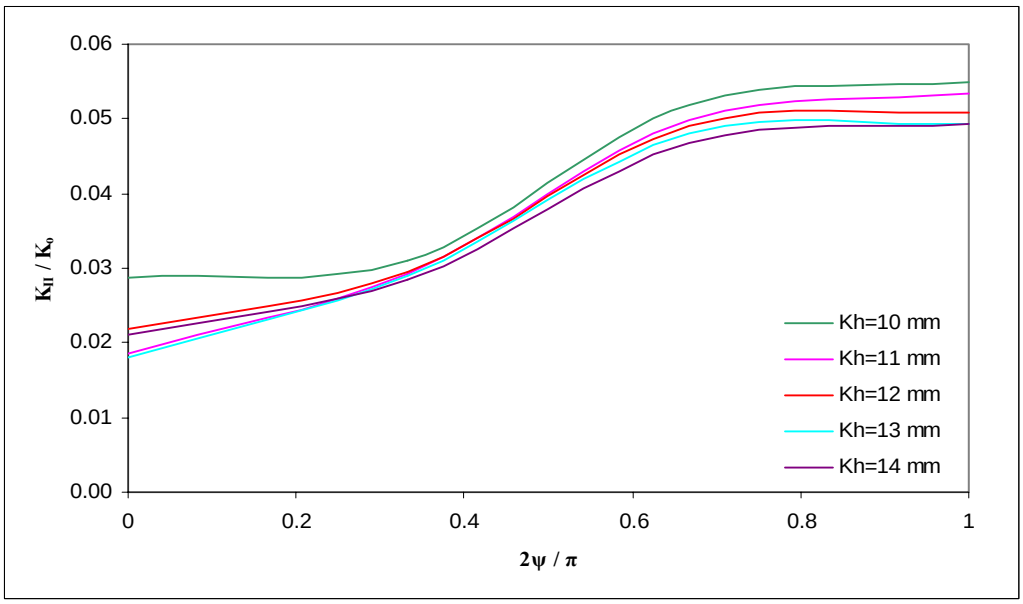

Figure 5.73 Normalized mode II SIF versus crack angle parameter ψ for a surface crack, β=0, $a / t1$=0.1, $c / t1$=0.3, K_V=12 mm.

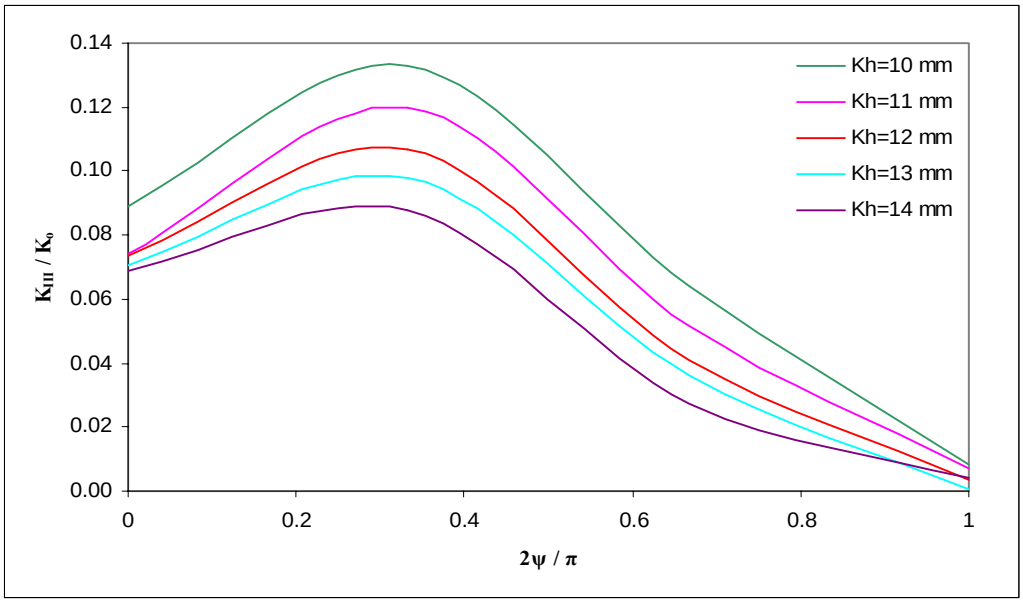

Figure 5.74 Normalized mode III SIF versus crack angle parameter ψ for a surface crack, β=0, $a / t1$=0.1, $c / t1$=0.3, K_V=12 mm.

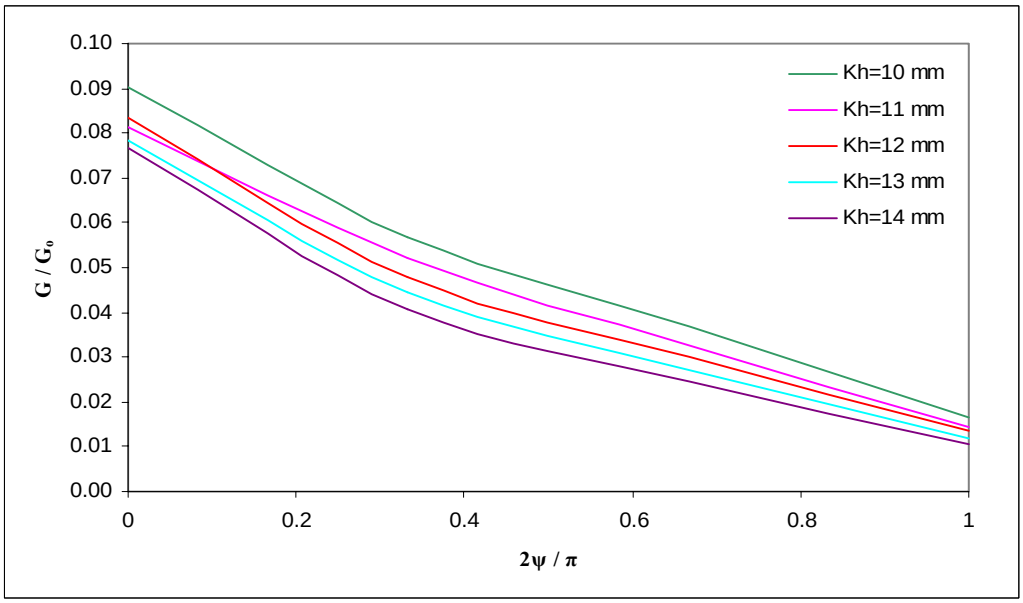

Figure 5.75 Normalized energy release rate versus crack angle parameter ψ for a surface crack, β=0, $a / t1$=0.1, $c / t1$=0.3, K_V=12 mm.

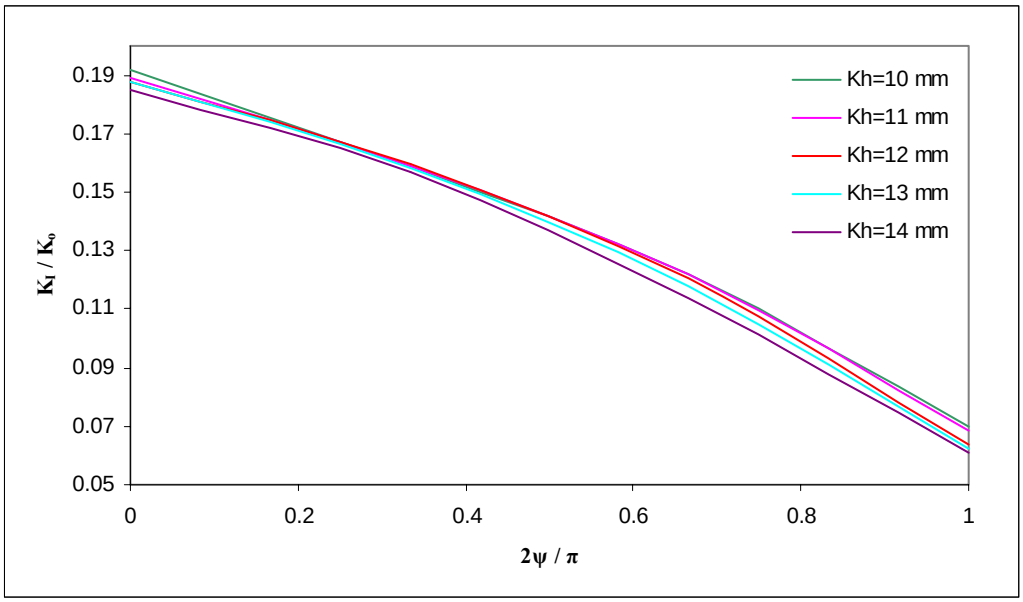

Figure 5.76 Normalized mode I SIF versus crack angle parameter ψ for a surface crack, $\beta=\pi/6$, $a / t1=0.1$, $c / t1=0.3$, $K_v=12$ mm.

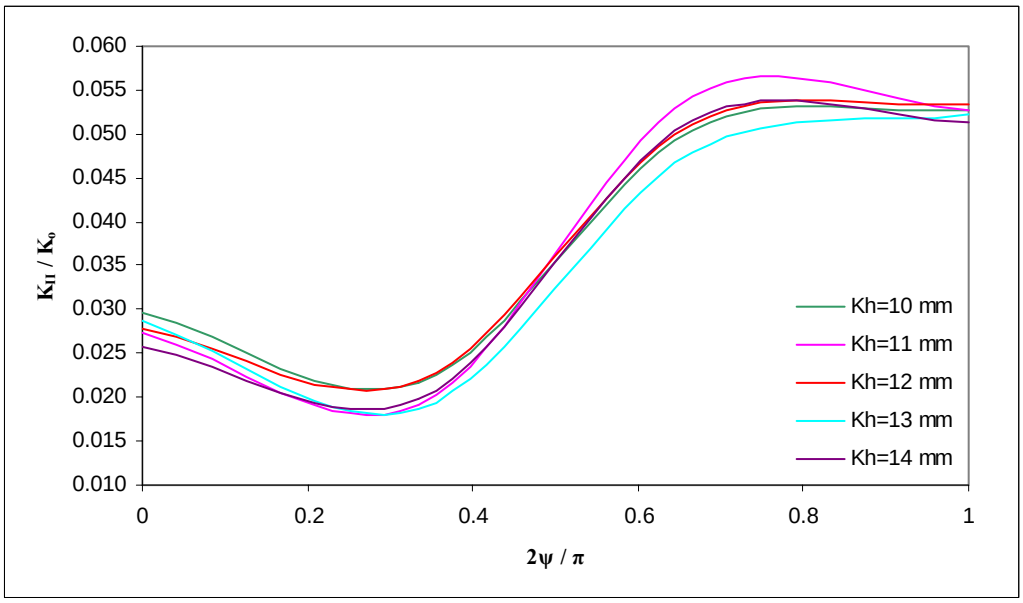

Figure 5.77 Normalized mode II SIF versus crack angle parameter ψ for a surface crack, $\beta=\pi/6$, $a / t1=0.1$, $c / t1=0.3$, $K_v=12$ mm.

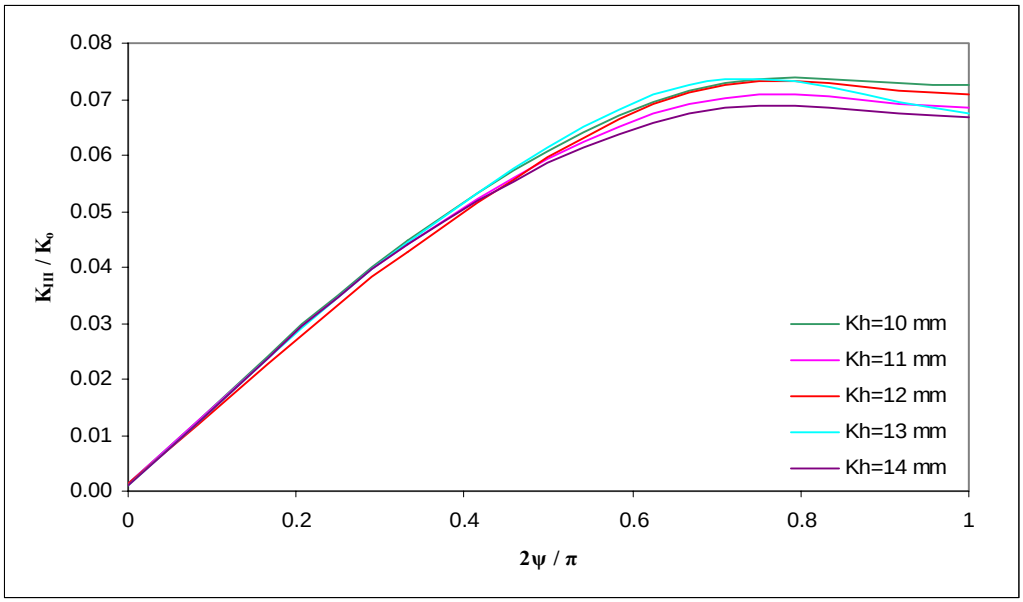

Figure 5.78 Normalized mode III SIF versus crack angle parameter ψ for a surface crack, $\beta=\pi/6$, $a / t1=0.1$, $c / t1=0.3$, $K_v=12$ mm.

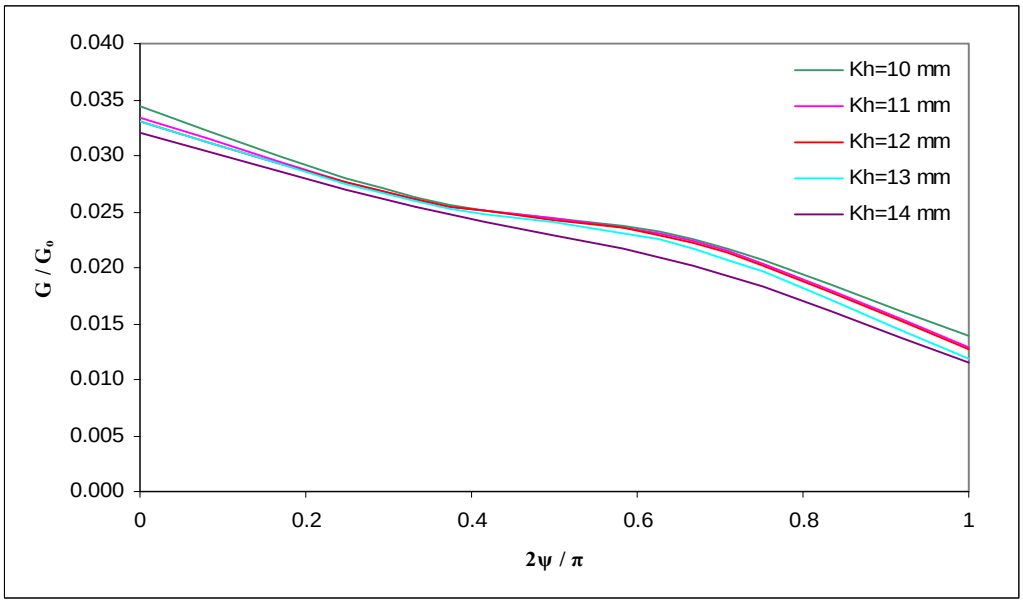

Figure 5.79 Normalized energy release rate versus crack angle parameter ψ for a surface crack, $\beta=\pi/6$, $a / t1=0.1$, $c / t1=0.3$, $K_v=12$ mm.

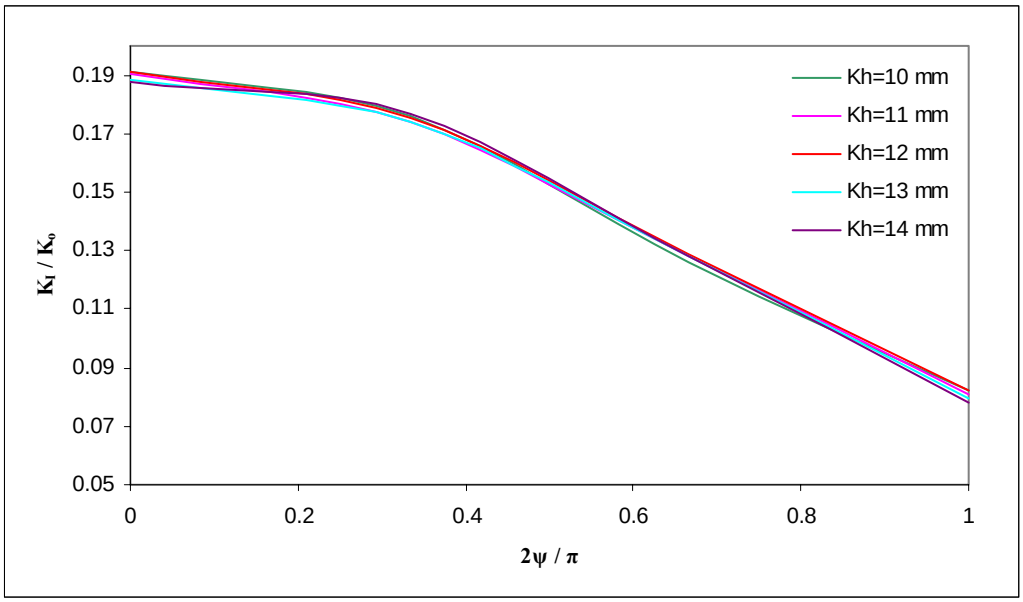

Figure 5.80 Normalized mode I SIF versus crack angle parameter ψ for a surface crack, $\beta=\pi/3$, $a / t1=0.1$, $c / t1=0.3$, $K_v=12$ mm.

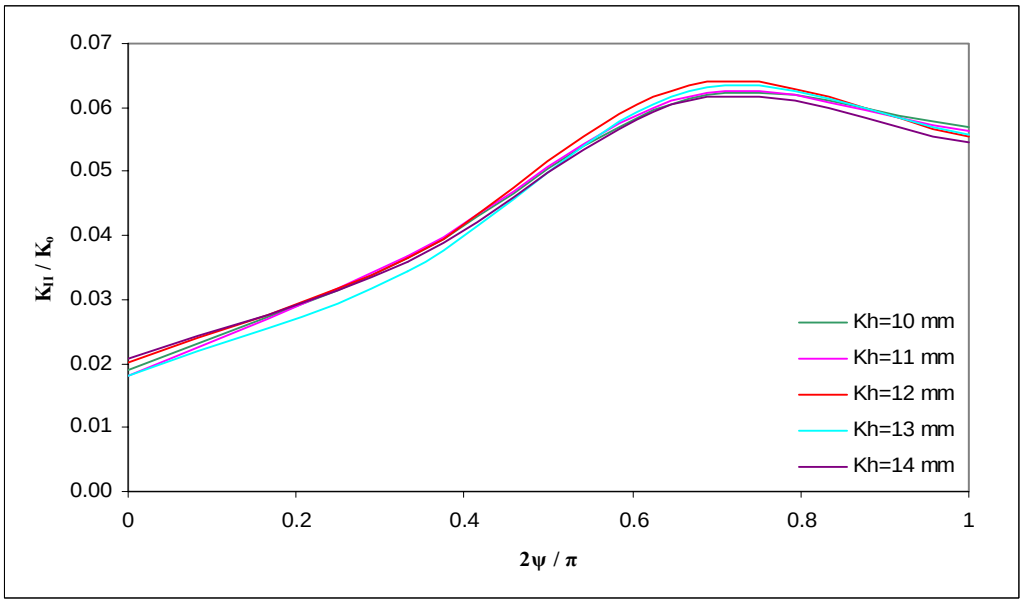

Figure 5.81 Normalized mode II SIF versus crack angle parameter ψ for a surface crack, $\beta=\pi/3$, $a / t1=0.1$, $c / t1=0.3$, $K_v=12$ mm.

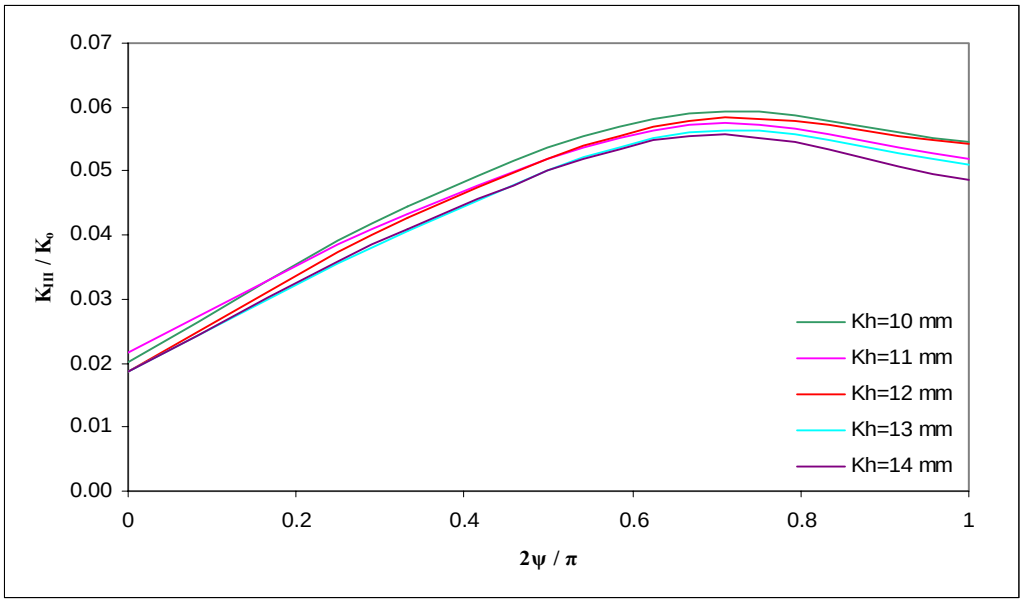

Figure 5.82 Normalized mode III SIF versus crack angle parameter ψ for a surface crack, $\beta=\pi/3$, $a / t1=0.1$, $c / t1=0.3$, $K_v=12$ mm.

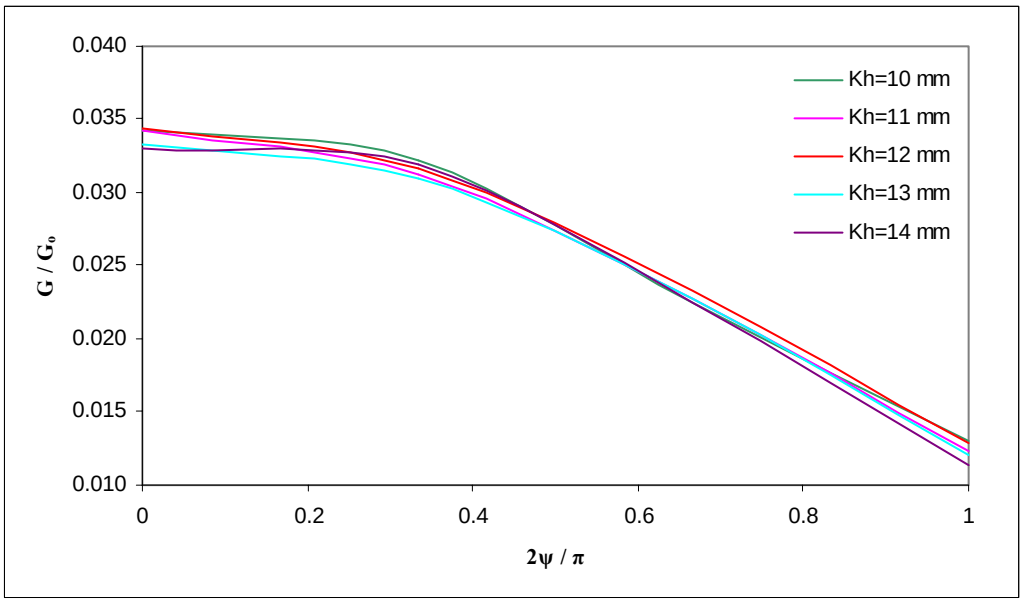

Figure 5.83 Normalized energy release rate versus crack angle parameter ψ for a surface crack, $\beta=\pi/3$, $a / t1=0.1$, $c / t1=0.3$, $K_v=12$ mm.

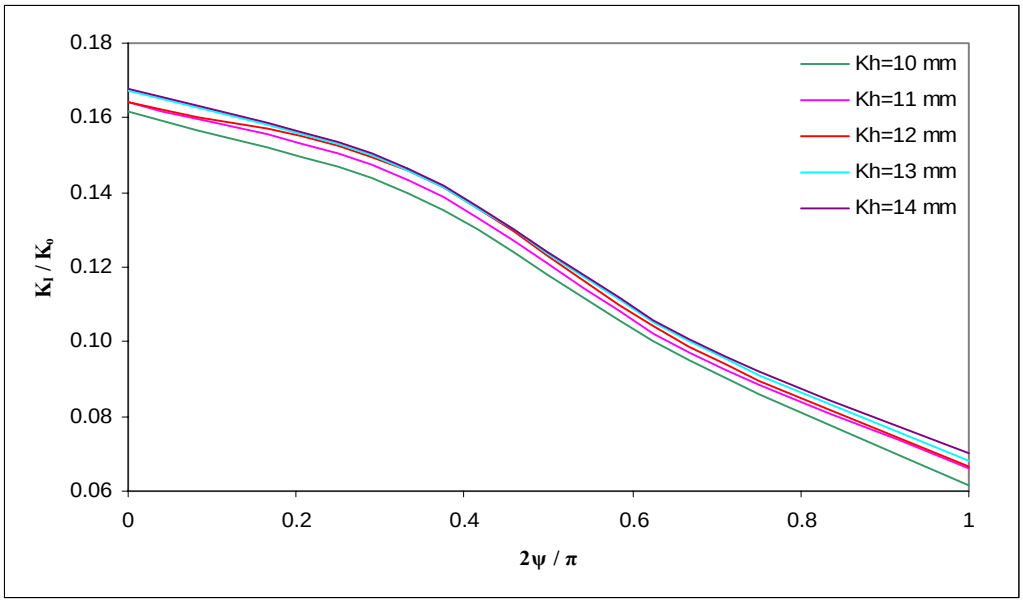

Figure 5.84 Normalized mode I SIF versus crack angle parameter ψ for a surface crack, $\beta=\pi/2$, $a / t1=0.1$, $c / t1=0.3$, $K_v=12$ mm.

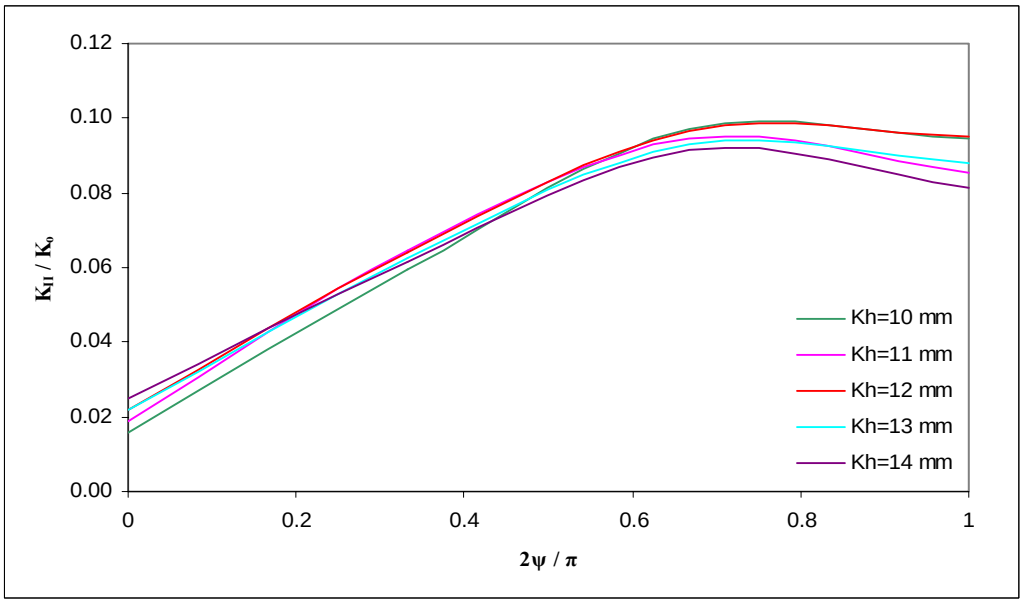

Figure 5.85 Normalized mode II SIF versus crack angle parameter ψ for a surface crack, $\beta=\pi/2$, $a / t1=0.1$, $c / t1=0.3$, $K_v=12$ mm.

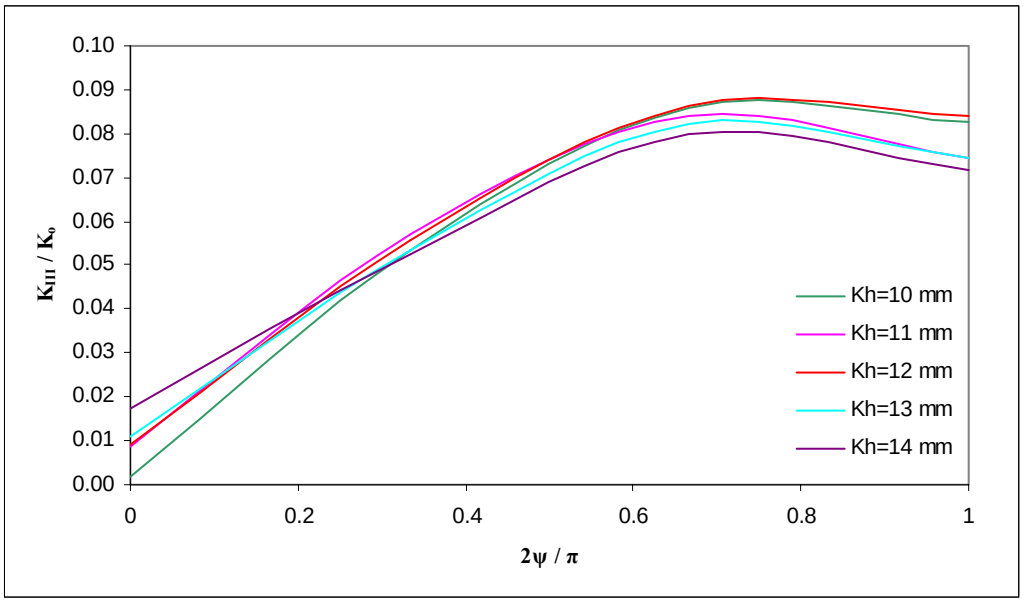

Figure 5.86 Normalized mode III SIF versus crack angle parameter ψ for a surface crack, $\beta=\pi/2$, $a / t1=0.1$, $c / t1=0.3$, $K_v=12$ mm.

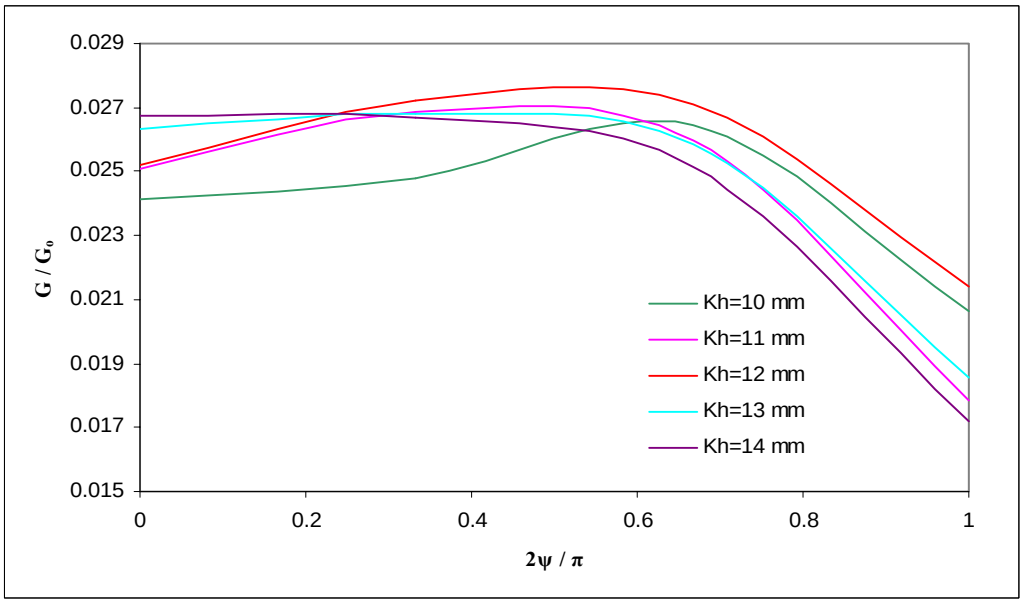

Figure 5.87 Normalized energy release rate versus crack angle parameter ψ for a surface crack, $\beta=\pi/2$, $a / t1=0.1$, $c / t1=0.3$, $K_v=12$ mm.

5.2.2.3 Loading of a Crack at the Side of the Weld Root for Various Crack Depth

In this section, a specimen with various crack geometry that is constructed with a crack at the side part of the weld root (Figure 5.37) is subjected to bending load. Crack dimensions are identified as parameters of the base sheet metal and the weld geometry is defined as K_v=12 mm and K_h=12 mm. The normalized K_I, K_{II}, K_{III} and G for four β are presented in the following figures 5.88 – 5.103.

In Figures 5.88-5.103, the variations of the normalized stress intensity factors and normalized energy release rate are plotted with respect to normalized crack angle, $2\psi/\pi$ for different crack geometry with respect to crack depth (a). In all these plots, it can be seen that the normalized energy release rate becomes higher for all β except $\beta = \pi/2$ as the crack deepens. At $\beta = \pi/2$, the contrary behavior is observed with respect to the normalized energy release rate. For higher crack depth values, the changes in the normalized K_I, K_{II}, K_{III} and G are much more remarkable. The normalized mode II and mode III stress intensity factors reach the maximum point at nearly half of the crack angle. The maximum values of the normalized K_I, K_{II}, K_{III} and G are seen at various β and ψ, not in the free ends of the specimen. However, for $\beta = \pi/6$, normalized K_{II} rises up from zero point and reaches its maximum value at $2\psi/\pi=0$, unlikely (see figure 5.86). Crack closure is observed for specimen at $\beta=\pi/6$, $\beta=\pi/3$, $\beta=\pi/2$ (see figures 5.85, 5.89, 5.93). For these parameters, the normalized mode I stress intensity factor is below zero. Actually, if the stress intensity factor has a minus sign, energy release rate is not computed at this point. This means that crack closure occurs and the crack surfaces seem to contact each other.

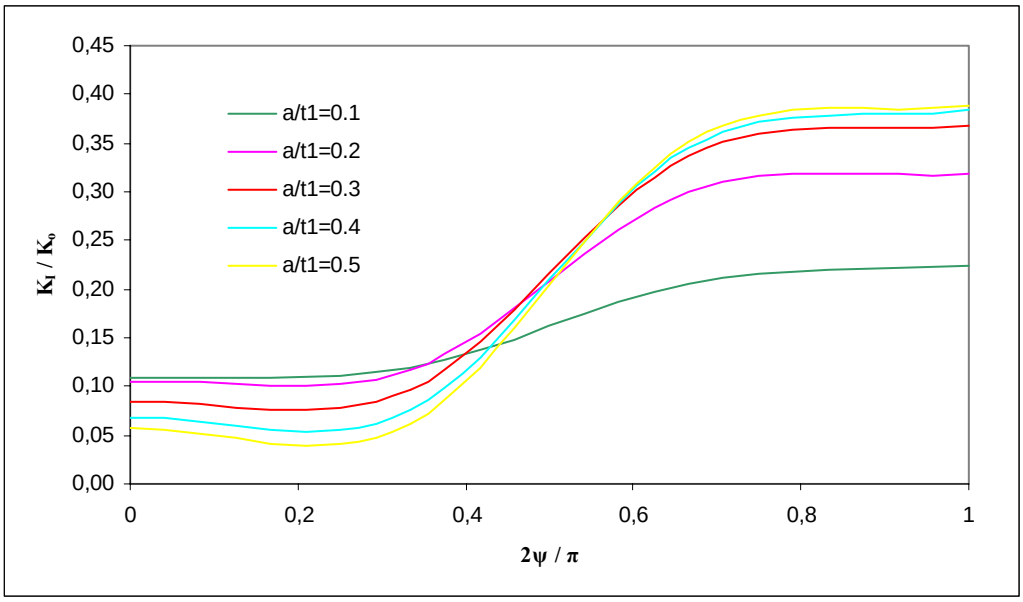

Figure 5.88 Normalized mode I SIF versus crack angle parameter ψ for a surface crack, β=0, c / $t1$=0.3, K_v=12 mm, K_h=12 mm.

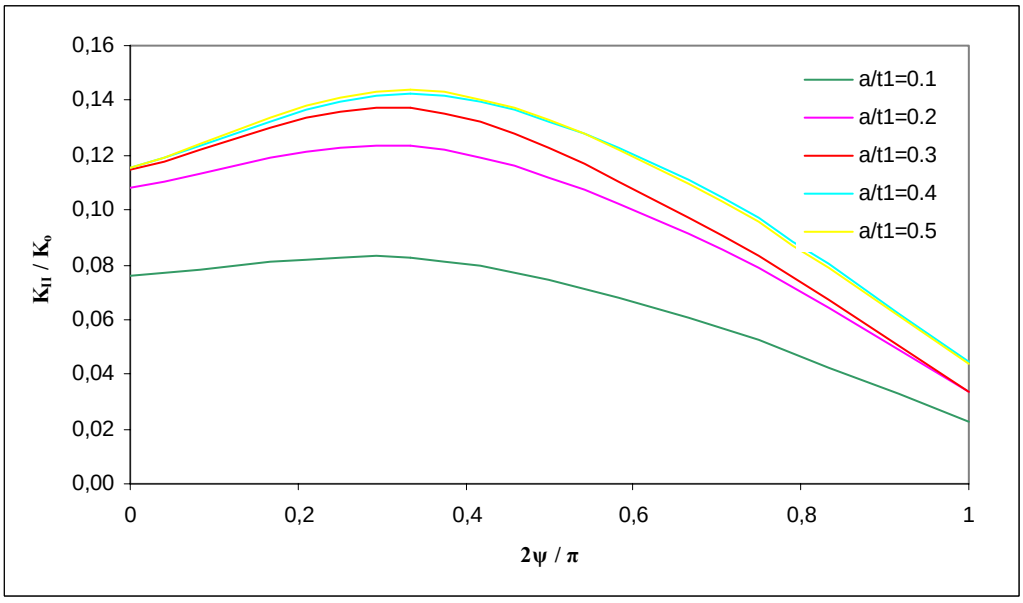

Figure 5.89 Normalized mode II SIF versus crack angle parameter ψ for a surface crack, β=0, c / $t1$=0.3, K_v=12 mm, K_h=12 mm.

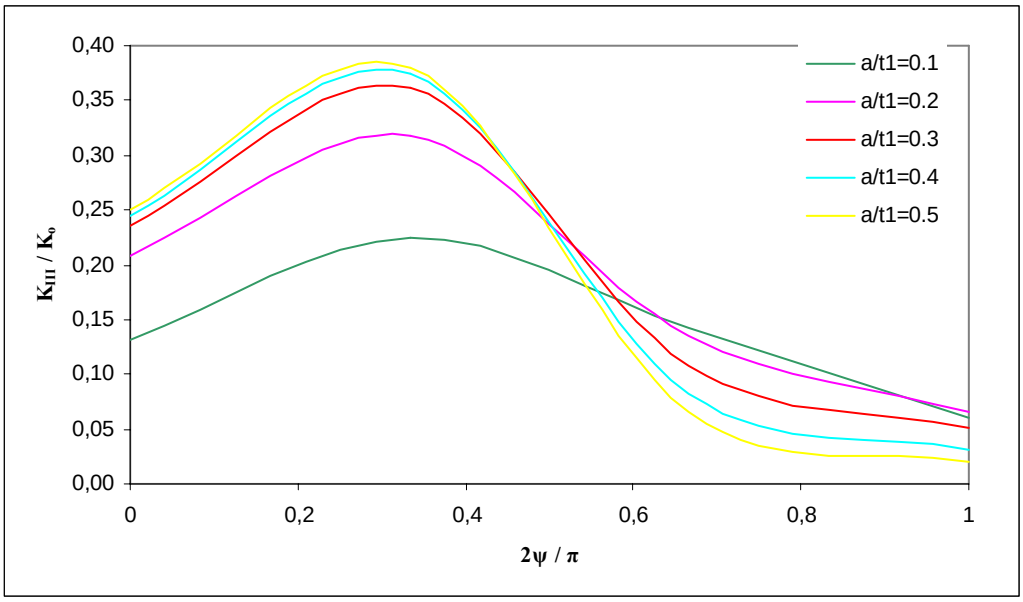

Figure 5.90 Normalized mode III SIF versus crack angle parameter ψ for a surface crack, β=0, $c / t1$=0.3, K_v=12 mm, K_h=12 mm.

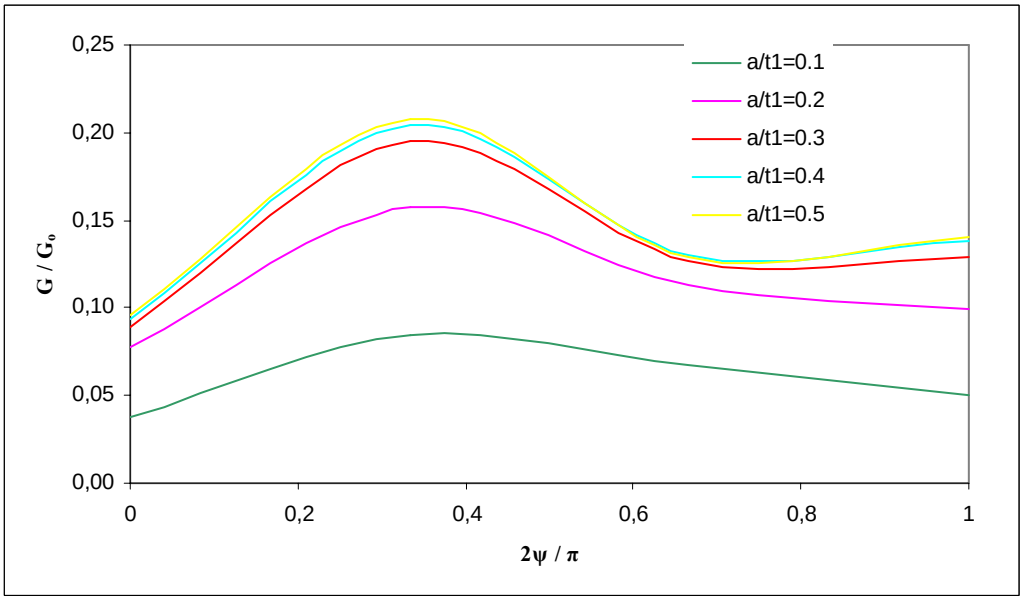

Figure 5.91 Normalized energy release rate versus crack angle parameter ψ for a surface crack, β=0, $c / t1$=0.3, K_v=12 mm, K_h=12 mm.

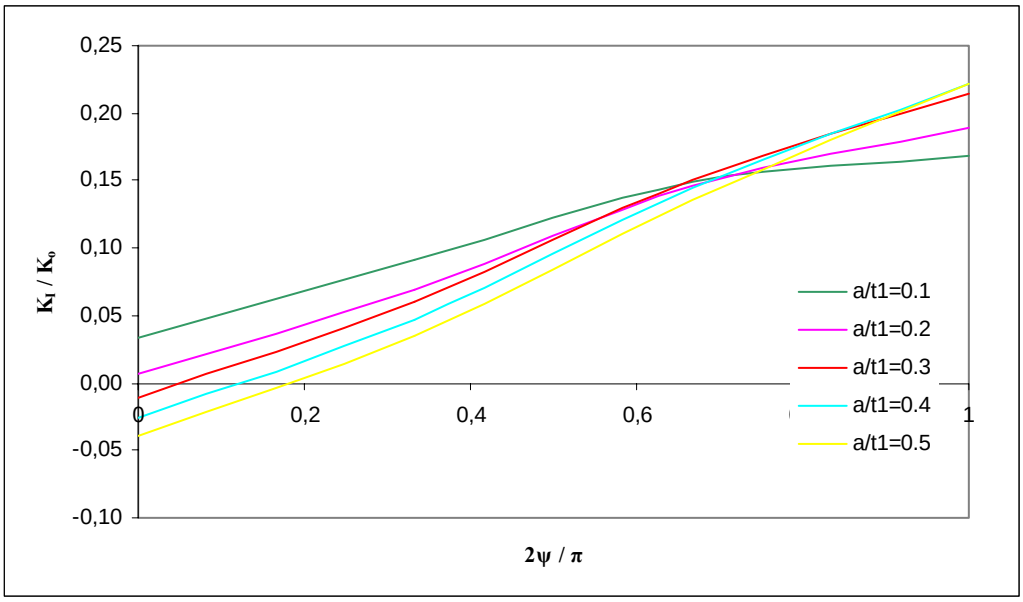

Figure 5.92 Normalized mode I SIF versus crack angle parameter ψ for a surface crack, $\beta=\pi/6$, $c / t1=0.3$, $K_v=12$ mm, $K_h=12$ mm.

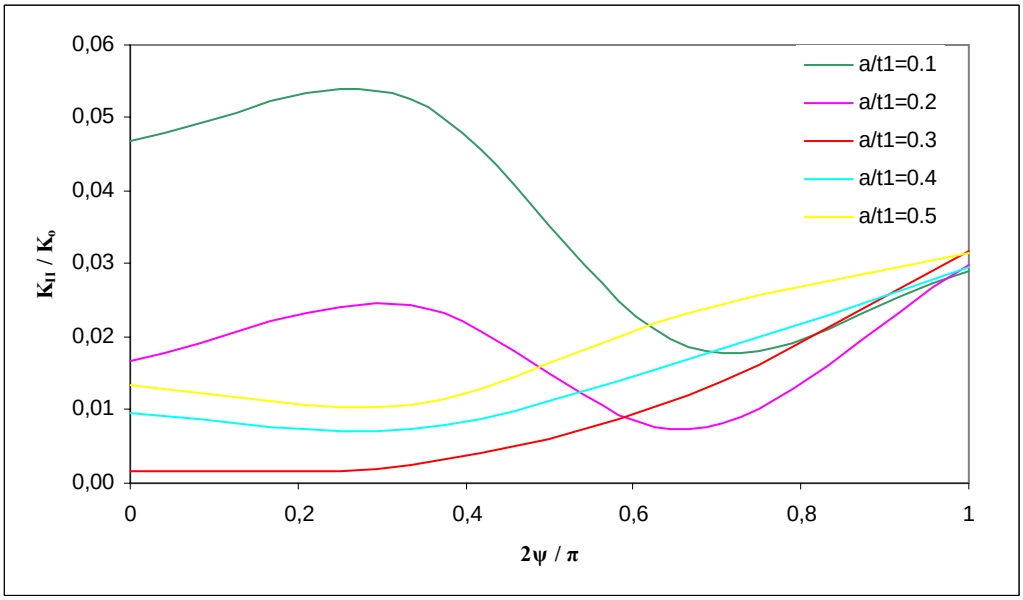

Figure 5.93 Normalized mode II SIF versus crack angle parameter ψ for a surface crack, $\beta=\pi/6$, $c / t1=0.3$, $K_v=12$ mm, $K_h=12$ mm.

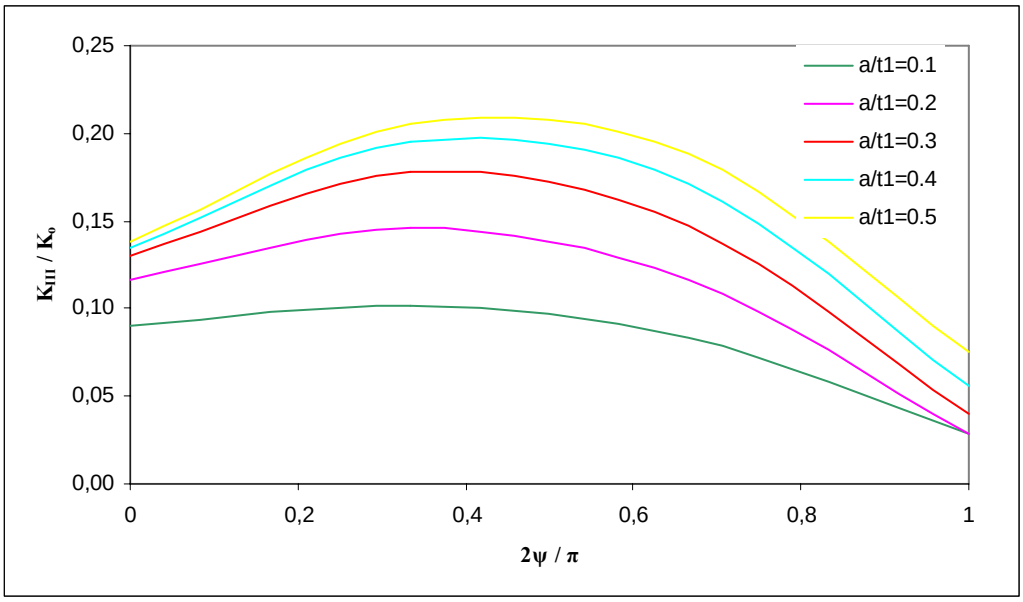

Figure 5.94 Normalized mode III SIF versus crack angle parameter ψ for a surface crack, $\beta=\pi/6$, $c / t1=0.3$, $K_v=12$ mm, $K_h=12$ mm.

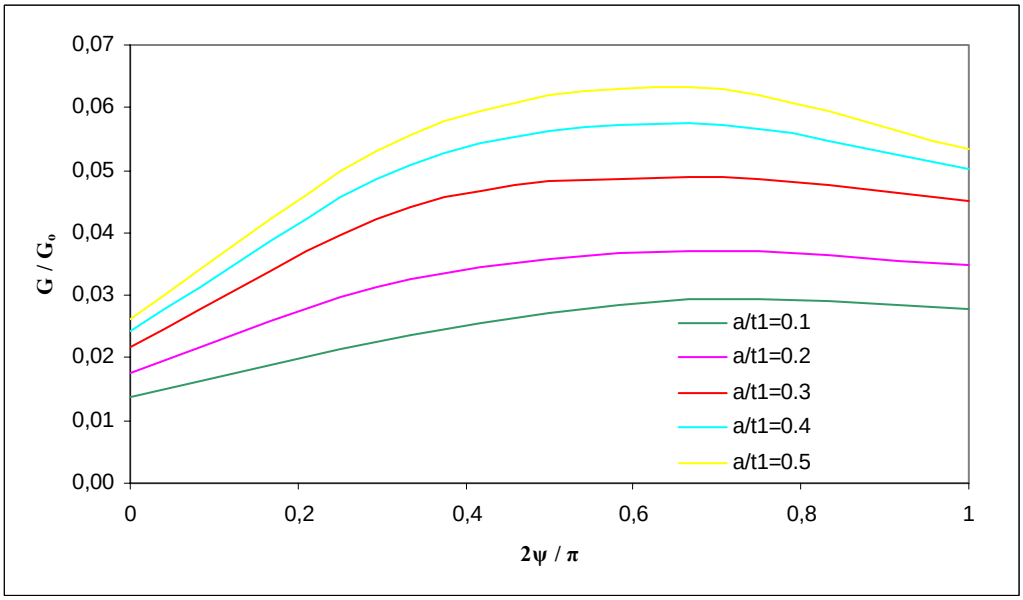

Figure 5.95 Normalized energy release rate versus crack angle parameter ψ for a surface crack, $\beta=\pi/6$, $c / t1=0.3$, $K_v=12$ mm, $K_h=12$ mm.

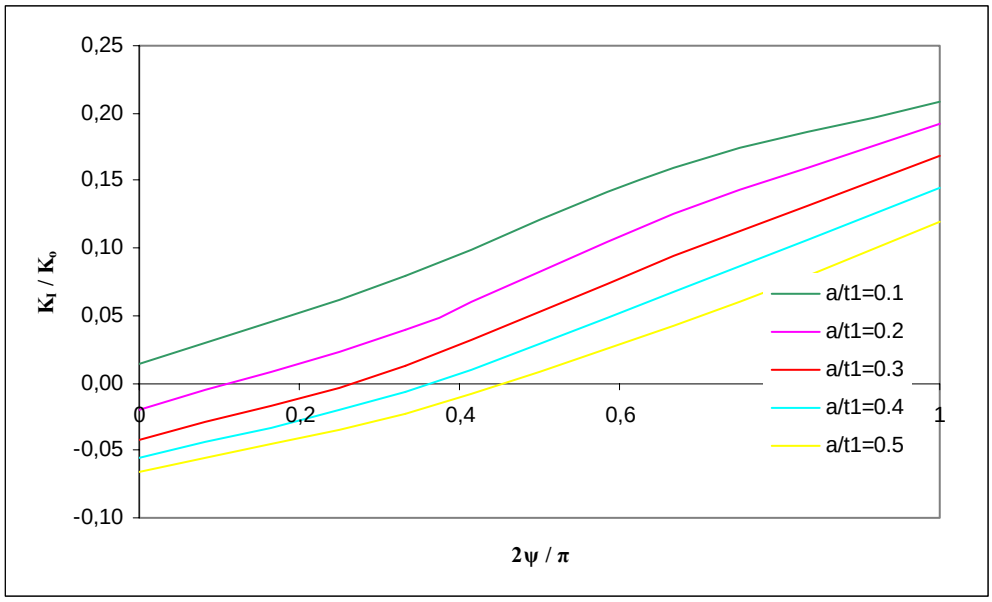

Figure 5.96 Normalized mode I SIF versus crack angle parameter ψ for a surface crack, $\beta=\pi/3$, $c / t1=0.3$, $K_v=12$ mm, $K_h=12$ mm.

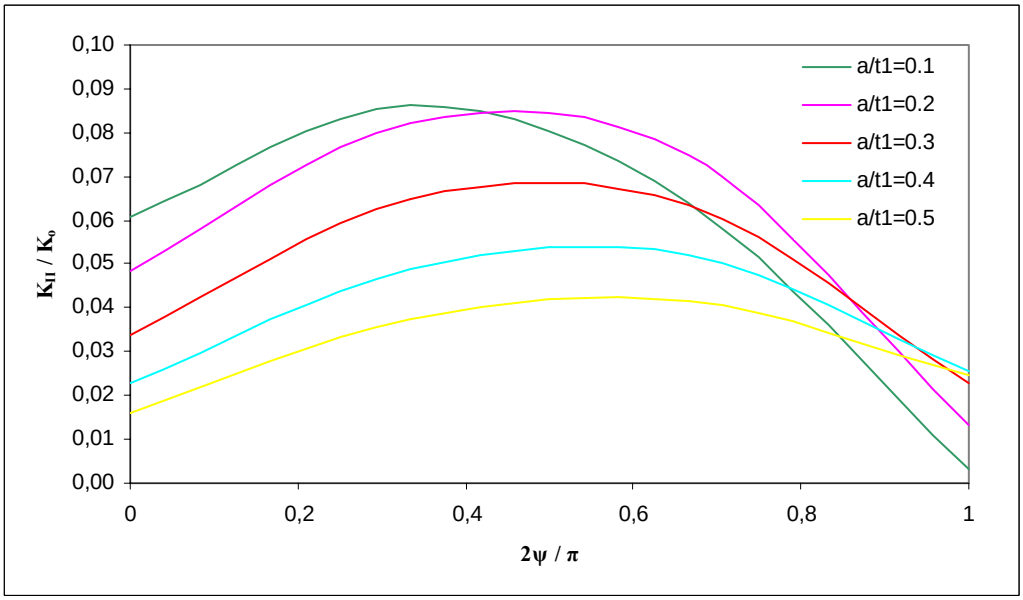

Figure 5.97 Normalized mode II SIF versus crack angle parameter ψ for a surface crack, $\beta=\pi/3$, $c / t1=0.3$, $K_v=12$ mm, $K_h=12$ mm.

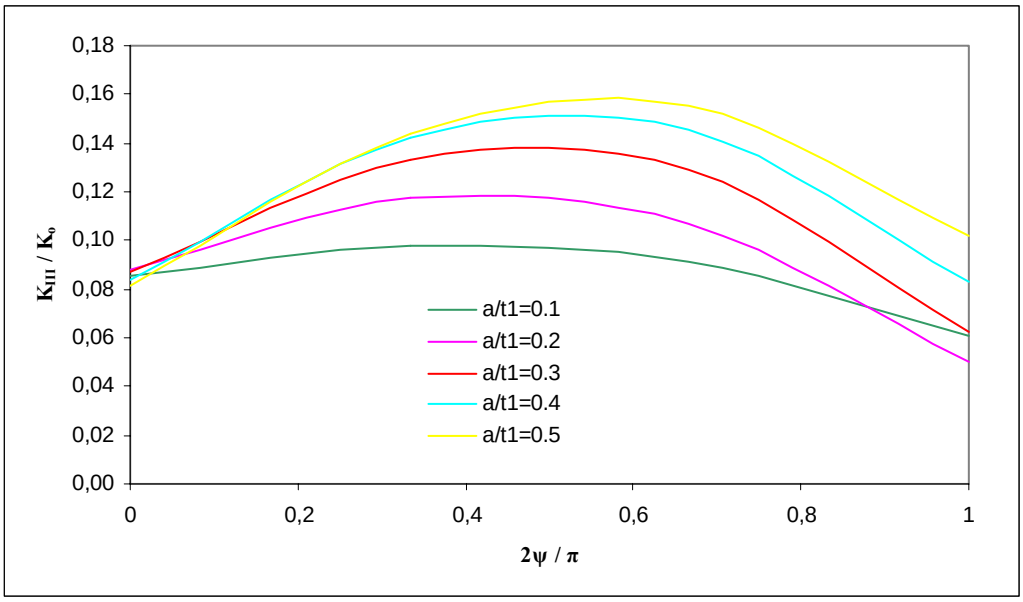

Figure 5.98 Normalized mode III SIF versus crack angle parameter ψ for a surface crack, $\beta=\pi/3$, $c / t1=0.3$, $K_v=12$ mm, $K_h=12$ mm.

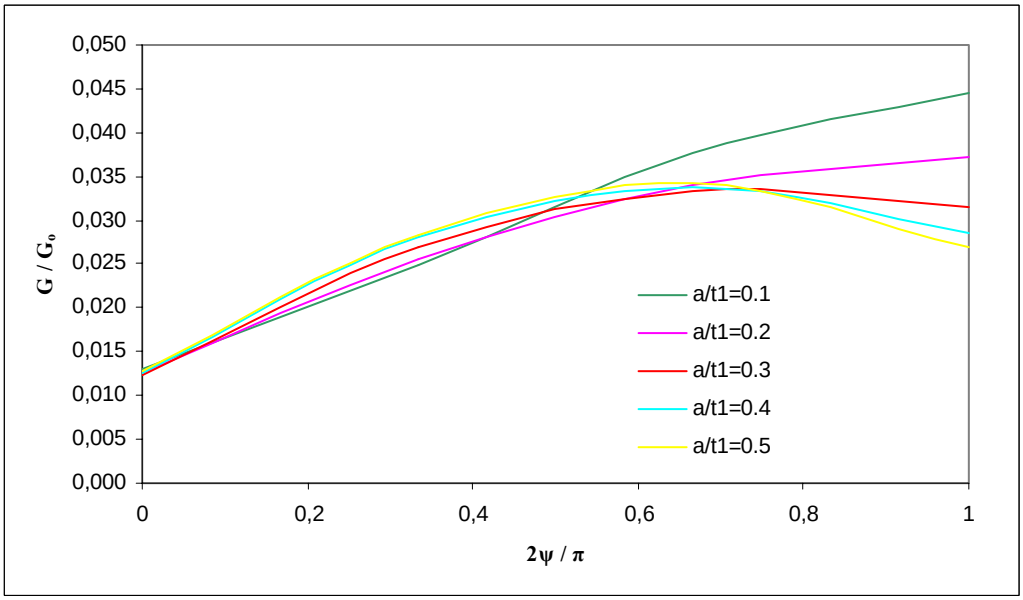

Figure 5.99 Normalized energy release rate versus crack angle parameter ψ for a surface crack, $\beta=\pi/3$, $c / t1=0.3$, $K_v=12$ mm, $K_h=12$ mm.

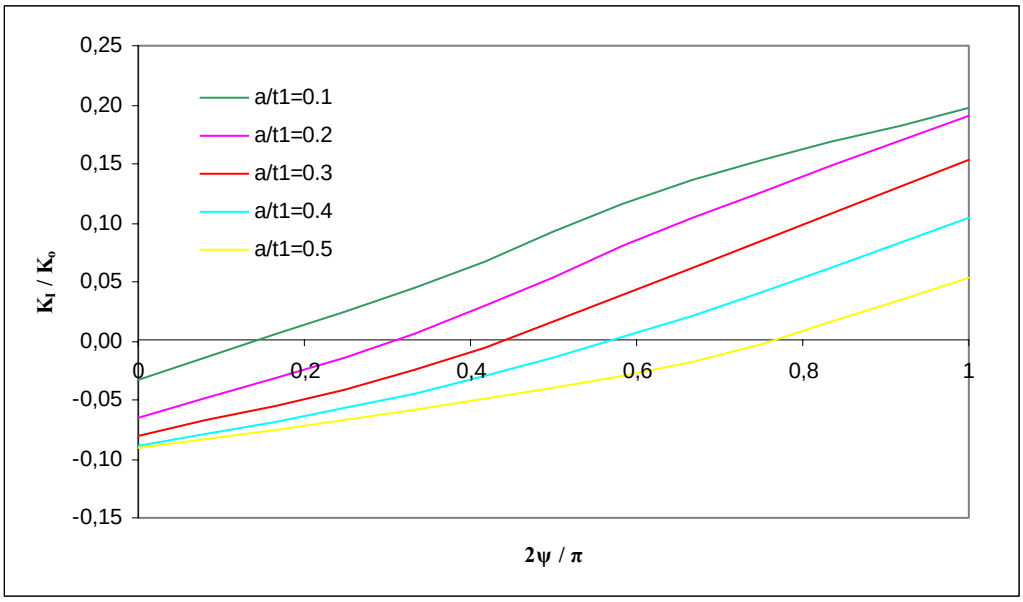

Figure 5.100 Normalized mode I SIF versus crack angle parameter ψ for a surface crack, $\beta=\pi/2$, $c / t1=0.3$, $K_v=12$ mm, $K_h=12$ mm.

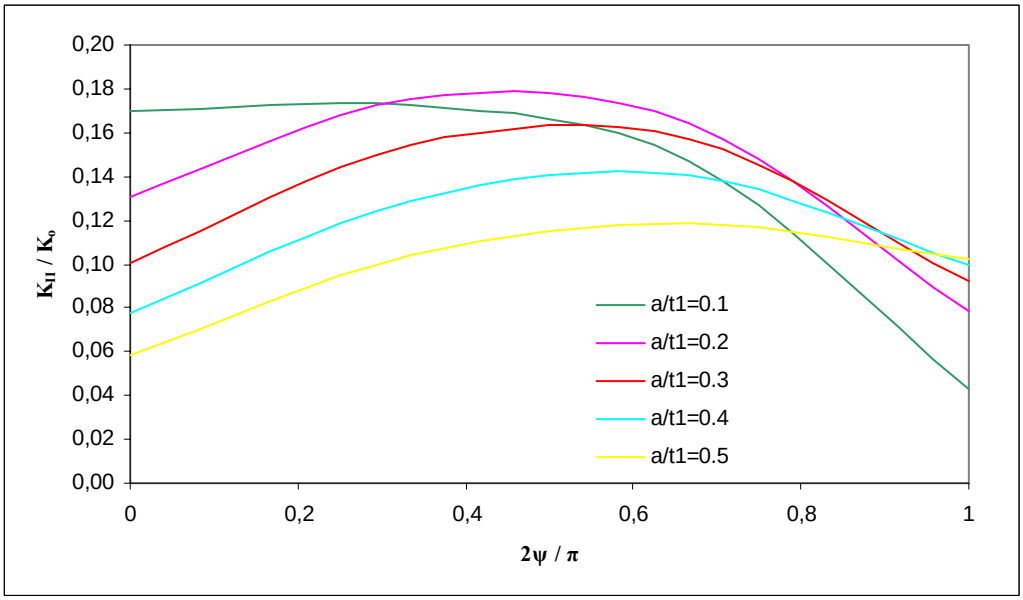

Figure 5.101 Normalized mode II SIF versus crack angle parameter ψ for a surface crack, $\beta=\pi/2$, $c / t1=0.3$, $K_v=12$ mm, $K_h=12$ mm.

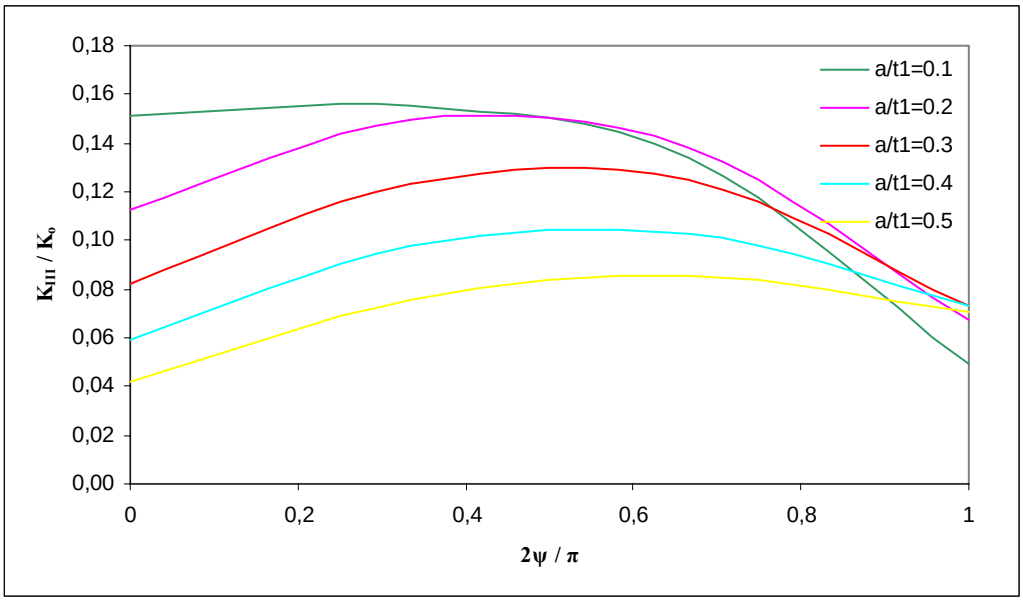

Figure 5.102 Normalized mode III SIF versus crack angle parameter ψ for a surface crack, $\beta=\pi/2$, $c / t1=0.3$, $K_v=12$ mm, $K_h=12$ mm.

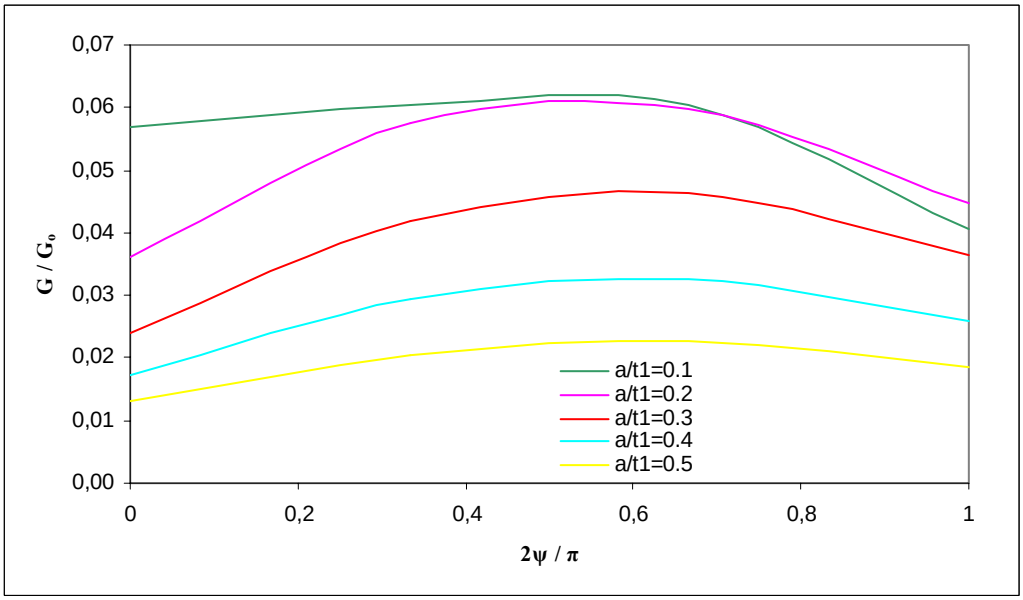

Figure 5.103 Normalized energy release rate versus crack angle parameter ψ for a surface crack, $\beta=\pi/2$, $c / t1=0.3$, $K_v=12$ mm, $K_h=12$ mm.

CHAPTER 6

CONCLUSIONS

In this study, three dimensional surface crack problems in fillet welds are analyzed under mechanical loading and the models are built up by three dimensional finite elements. An interface, which is capable of creating a finite element model of t-shaped weld specimen by using a set of design parameters, has been developed and 3D finite element models are developed by using the finite element analysis software MSC. MARC MENTAT R3. By using the developed interface, SIF CALCULATOR, the mixed modes I, II, III stress intensity factors and the energy release rate can be calculated around the crack front using displacement correlation technique for a surface crack. The surface crack is considered to occur at two regions; one at the weld root and the other at the weld toe, and it is assumed to have a quarter – elliptical crack front profile. Around the crack front, strain singularity is taken into account by using degenerated 20 – node quarter – point solid elements.

Firstly, the performance and the accuracy of the displacement correlation technique in mixed modes stress intensity factors are analyzed under mechanical loading, uniform tension. Stress intensity factors obtained by using MARC MENTAT are verified by making comparisons to the results given by Sneddon [27], Irwin [38] and Noda et al [37]. In these comparisons, the maximum difference is found 2 % for mode I problems, around circular and quarter-elliptic crack front, and 5 % for mixed mode problems in which

the inclination angle between surface and the crack plane is smaller than 45°. From these results, it can be said that displacement correlation technique is sufficient to find out the mixed modes I, II, III stress intensity factors unless the inclination angle is above 45°. In addition to these, surface effects are much more remarkable in stress intensity factor calculations and calculated stress intensity factors are not accurate near the free surfaces. However, these values are still useful for comparing the effects of the parameters, such as the geometry.

In the analyses of t-shaped weld specimen, three different parameters are taken into account during the case study. First one is about the weld option, whether it is double-sided or one-sided weld. The second one is about the weld geometry. For this case study, everything is kept fixed but the horizontal leg of the weld. The last case study is about the effect of the crack depth on the mixed modes stress intensity factors and also energy release rate.

In all the computation carried out for the first case study, it is observed that the normalized mode I, II and III stress intensity factors and the normalized energy release rate are not drastically influenced by the weld option. However, by the comparison, it can be said that one-sided weld option is seen more useful than the double-sided one. In the second case study, it is observed that as the K_h value becomes higher, the normalized energy release rate drastically drops. Nevertheless, the normalized mode I, II and III stress intensity factors shows various characteristics for two different types of loading. Most of them have the same behavior with the normalized energy release rates. For the last case study, as it is expected, the higher the (*a / t1)* ratio, the larger the normalized energy release rate is observed. However, it is seen that crack closure occurs when bending load is applied and the actual crack surfaces seem to contact each other. Therefore, the normalized energy release rate is unreliable for the bending load condition.

Fatigue failure of the welded structures is an important issue. Nevertheless, fatigue life prediction of the weldments is not considered in this study. By means of sub-modeling, a crack can be placed in a structure of the earth-moving machines, such as excavator, backhoe loader. Also, the effects of the heat affected zone, the mechanical properties of the weld material and heat treatment are not taken into account. These parameters have influence on the fatigue life of the welded structures. These parameters can be defined and the behavior of the specimen can be observed. In addition to these, the verification of this study by means of experimental results and the observation of the t-shaped welded specimen behavior under mechanical loading can be thought as a future work, as well.

REFERENCES

[1] Tanttari J., Saarinen K., “Noise Control of Vehicle Cabins”, Proceedings of INTERNOISE 93, 1993.

[2] Kainuma S., Mori T., “A Fatigue Strength Evaluation Method for Load-Carrying Fillet Welded Cruciform Joints”, International Journal of Fatigue, Vol.28, 864-872, 2006.

[3] Singh P. J., Guha B., Achar D. R. G., “Fatigue Life Prediction Using Two Stage Model for AISI 304L Cruciform Joints, with Different Fillet Geometry, Failing at Toe”, Science and Technology of Welding and Joining, Vol.8, 69-75, 2003.

[4] Motarjemi A. K., Kokabi A. H., Burdekin F. M., “Comparison of Fatigue Life for T and Cruciform Welded Joints with Different Combinations of Geometrical Parameters”, Engineering Fracture Mechanics, Vol.67, 313-328, 2003.

[5] Singh P. J., Guha B., Achar D. R. G., “Fatigue Life Prediction of GTA Welded AISI 304L Cruciform Joints with Lack of Penetration Using Local-Stress Approach”, Engineering Failure Analysis, Vol.10, 25-36, 2003.

[6] Solanki K., Daniewicz S. R., Newman J. J. C., “A New Methodology for Computing Crack Opening Values from Finite Element Analysis”, Engineering Fracture Mechanics, Vol.71, 1165-1175, 2004.

[7] Sethuraman R., Redy G. S. S., Ilango I. T., “Finite Element Based Evaluation of Stress Intensity Factors for Interactive Semi-Elliptic Surface Cracks”, Int. Journal of Pressure Vessels and Piping, Vol.80, 843-859, 2003.

[8] Ayhan A. O., “Mixed Mode Stress Intensity Factors for Deflected and Inclined Surface Cracks in Finite-Thickness Plates”, Engineering Fracture Mechanics, Vol.71, 1059-1079, 2004.

[9] Erdogan F., “Fracture Mechanics”, International Journal of Solids and Structures, Vol.37, 171-183, 2000.

[10] Inan O., “Three Dimensional Fracture Analysis of FGM Coatings”, Ms. Thesis Submitted to Middle East Technical University, Turkey, 2004.

[11] Gray L. J., Phan A. V., Paulino G. H., Kaplan T., “Improved Quarter-Point Crack Tip Element”, Engineering Fracture Mechanics, Vol.70, 269-283, 2003.

[12] Hou J., Goldstraw M., Maan S., Knop M., “An Evaluation of 3D Crack Growth Using ZENCRACK”, DSTO-TR-1158, 1-28, 2001.

[13] Guo K., Bell R., Wang X., “The Stress Intensity Factor Solutions for Edge Cracks in a Padded Plate Geometry under General Loading Conditions”, International Journal of Fatigue, Vol.29, 481-488, 2007.

[14] Kuok K. M., Kou K. P., “The SIF for Deep Semi-Elliptical Surface Crack in Finite Thickness Plates Determined by the Nodal Displacement Method”, 15th ASCE Engineering Mechanics Division Conference, 2002.

[15] Lee W. Y., Lee J. J., “Successive 3D FE Analysis Technique for characterization of Fatigue Crack Growth Behavior in Composite-Repaired Aluminum Plate”, Composite Structures, Vol.66, 513-520, 2004.

[16] Statnikov E. S., Muktepavel V. O., Trufyakov V. I., Mikheev P. P., Kuzmenko A. Z., Blomqvist A., “Efficiency Evaluation of Ultrasonic Impact Treatment (UIT) of Welded Joints in Weldox 420 Steel in accordance with the IIW Program”, IIW Doc. XIII-1817-00, 2000.

[17] Lahti K. E., Hanninen H., Niemi E., “Nominal Stress Range Fatigue of Stainless Steel Fillet Welds — the Effect of Weld Size”, Journal of Constructional Steel Research, Vol.54, 161-172, 2000.

[18] Fricke W., Doerk O., “Simplified Approach to Fatigue Strength Assessment of Fillet-Welded Attachment Ends”, International Journal of Fatigue, Vol.28, 141-150, 2006.

[19] Yuanqing W., Yanmin W., Yongjiu S., Jianjing J., “Three-Dimensional Stress and Stress Intensity for Tensioned Flat Plates with Edge Cracks”, Tsinghua Science and Technology, 131-136, 2006.

[20] Jia X. M., Dai F., “Three Dimensional Static and Dynamic Stress Intensity Factor Computations using ANSYS”, http://www.simwe.com/jour/cae/p001002.htm.

[21] Newman, J.C. and Raju, I.S., “An Empirical Stress – Intensity Factor Equation for the Surface Crack”, Engineering Fracture Mechanics, Vol.15, 185-192, 1981.

[22] Sabuncuoglu B., “Fatigue Crack Growth Analysis Models for FGM’s”, Ms. Thesis Submitted to Middle East Technical University, Turkey, 2006.

[23] Kadioglu S., Dag S., Yahsi S., “Crack Problem for a Functionally Graded Layer on an Elastic Foundation”, International Journal of Fracture, Vol.47, 533-545, 1991.

[24] Guo L.C., Wu L.Z., Zeng T., Ma L., “Mode I Crack Problem for a Functionally Graded Orthotropic Strip”, European Journal of Mechanics A/Solids, Vol. 23, 219-234, 2004.

[25] “ISO/DIS 14345: Fatigue testing of welded components”, 2001

[26] MSC. MARC User’s Guide Version 2005, MSC. Software Corporation, Santa Ana, ABD – 2005, last accessed 25.01.2007.

[27] Sanford R.J., “Principles of Fracture Mechanics”, Prentice Hall, 2003

[28] Online Dictionary, Definition: Butt Weld, http://dict.die.net/butt%20weld/, Last accessed 25.01.2007.

[29] “Lecture 11.2.1: Generalities on Welded Connections, Connection Design: Static Loading”, ESDEB WG3, http://www.kuleuven.ac.be/bwk/materials/Teaching/master/wg11/l0210.htm, Last accessed 25.01.2007.

[30] “Lecture 3.3: Principles of Welding, Fabrication and Erection”, ESDEB WG11,http://www.kuleuven.ac.be/bwk/materials/Teaching/master/wg03/l0300.htm, Last accessed 25.01.2007.

[31] Kelly Shawn M., “Fatigue”, http://www.sv.vt.edu/classes/MSE2094_NoteBook/97ClassProj/anal/kelly/fatigue.html, Last accessed 25.01.2007.

[32] Yener M., “Design of a Computer Interface for Automatic Finite Element Analysis of an Excavator Boom”, Ms. Thesis Submitted to Middle East Technical University, Turkey, 2005.

[33] Jefferson K., “Stress Intensity”, Term Project submitted to Virginia Tech Materials Science and Engineering, USA, 2000

[34] Yildirim B., Dag S., Erdogan F., “Three dimensional fracture analysis of FGM coatings under thermo-mechanical loading”, International Journal of Fracture, Vol.132, 369-395, 2005

[35] Cook Robert, “Finite Element Modeling for Stress Analysis”, John Wiley and Sons, 1995

[36] Zhenyu Huang, Suo Z., Guanghai Xu, Jun He, Prevost J.H., Sukumar N., “Initiation and Arrest of an Interfacial Crack in a Four-Point Bend Test”, Engineering Fracture Mechanics, Vol.72, 2005.

[37] Noda Nao-Aki, Kobayashi K., Yagishita M., “Variation of mixed modes stress intensity factors of an inclined semi-elliptical surface crack”, International Journal of Fracture, Vol.100, 207-225, 1999

[38] “Lecture 12.10: Basics of Fracture Mechanics”, ESDEB WG12, http://www.kuleuven.ac.be/bwk/materials/Teaching/master/wg12/l1000.htm, Last accessed 25.01.2007.

[39] “ME 583 Engineering Fracture Mechanics” http://www.me.metu.edu.tr/me583, Last accessed 25.01.2007.

[40] Jireh J. Yue, “Energy Concepts for Fracture” http://www.sv.vt.edu/classes/MSE2094_NoteBook/97ClassProj/anal/yue/energy.html, Last accessed 25.01.2007